



FRIEDRICH-SCHILLER-  
UNIVERSITÄT  
JENA

# **Large Scale Reevaluation of Influenza A Virus Classification based on Serotypes**

M A S T E R A R B E I T

zur Erlangung des akademischen Grades

Master of Science (M. Sc.)  
im Studiengang Bioinformatik

FRIEDRICH-SCHILLER-UNIVERSITÄT JENA  
Fakultät für Mathematik und Informatik

eingereicht von Alexander Henoch  
geb. am 02.02.1995 in Bremen

Betreuer: Prof. Dr. Manja Marz

Jena, den 14.07.2021



# **Zusammenfassung**

Hello, here is some text without a meaning. This text should show what a printed text will look like at this place. If you read this text, you will get no information. Really? Is there no information? Is there a difference between this text and some nonsense like “Huardest gefburn”? Kjift – not at all! A blind text like this gives you information about the selected font, how the letters are written and an impression of the look. This text should contain all letters of the alphabet and it should be written in of the original language. There is no need for special content, but the length of words should match the language.



# **Abstract**

Hello, here is some text without a meaning. This text should show what a printed text will look like at this place. If you read this text, you will get no information. Really? Is there no information? Is there a difference between this text and some nonsense like “Huardest gefburn”? Kjift – not at all! A blind text like this gives you information about the selected font, how the letters are written and an impression of the look. This text should contain all letters of the alphabet and it should be written in of the original language. There is no need for special content, but the length of words should match the language.



# **Danksagung**

Hello, here is some text without a meaning. This text should show what a printed text will look like at this place. If you read this text, you will get no information. Really? Is there no information? Is there a difference between this text and some nonsense like “Huardest gefburn”? Kjift – not at all! A blind text like this gives you information about the selected font, how the letters are written and an impression of the look. This text should contain all letters of the alphabet and it should be written in of the original language. There is no need for special content, but the length of words should match the language.



# Contents

<b>List of Abbreviations</b>	<b>3</b>	
<b>1</b>	<b>Introduction</b>	<b>5</b>
1.1	Zoonoses and the risks of pandemics . . . . .	5
1.2	Life-cycle and structure of the <i>Influenza A Virus</i> . . . . .	6
1.3	Evolution of the <i>Influenza A Virus</i> . . . . .	7
1.4	Vaccines design and the link to reassortment . . . . .	8
1.5	Secondary Structures of the <i>Influenza A Virus</i> . . . . .	8
1.6	Alignments and clustering . . . . .	9
1.7	WHO classification of <i>Influenza A Virus</i> . . . . .	9
1.8	The proposed project . . . . .	9
<b>2</b>	<b>Materials and Methods</b>	<b>11</b>
2.1	Data and Pipeline . . . . .	11
2.2	7-mer Frequency Calculation . . . . .	14
2.3	Dimension Reduction . . . . .	14
2.4	Hybrid Clustering . . . . .	15
2.5	Epsilon Selection . . . . .	19
2.6	Alignments and Vector Calculations . . . . .	20
<b>3</b>	<b>Results and Discussion</b>	<b>23</b>
3.1	Method Selection . . . . .	26
3.2	Database Annotation Errors . . . . .	31
3.3	K-mer Representation Quality . . . . .	34
3.4	Ground Truth for Clustering . . . . .	38
3.5	Differences in Dimension Reduction . . . . .	43
3.6	A New Classification . . . . .	46
<b>4</b>	<b>Conclusions &amp; Outlook</b>	<b>51</b>
<b>Bibliography</b>		<b>53</b>

<b>List of Figures</b>	<b>61</b>
<b>List of Tables</b>	<b>63</b>
<b>A Appendix</b>	<b>65</b>

# List of Abbreviations

## A

**AA** aminoacid

## D

**DBCV** density based cluster validity

## H

**HA** hemagglutinin

**HIV** human immunodeficiency viruses

## I

**IAV** *Influenza A Virus*

**IRD** Influenza Research Database

**IRES** internal ribosome entry site

## L

**LPAIV** low-pathogenic avian influenza virus

## M

**M1** matrix protein 1

**M2** M2 ion channel

**MERS** Middle East respiratory syndrome

**mRNA** viral messenger RNA

**MSA** multiple sequence alignment

**N**

**NA** neuraminidase

**NEP** nuclear export protein

**NP** nucleoprotein

**NPC** nuclear pore complex

**P**

**PA** polimerase acid protein

**PB1** polimerase basic protein 1

**PB2** polimerase basic protein 2

**R**

**RNP** viral ribonucleoprotein

**S**

**SARS** severe acute respiratory syndrome

**ssRNA(-)** negative-sense single stranded viral RNA

**U**

**UPGMA** unweighted pair group method with arithmetic mean

**W**

**WHO** world health organisation

# 1 Introduction

## 1.1 Zoonoses and the risks of pandemics

In times where infectious disease outbreaks become more frequent and sometimes even reach global appearance, unpredictable effects on humans, wildlife and whole ecosystems are inevitable [1]. Growing human population and persisting poverty has harmful impact on the biodiversity and results in degradation of natural habitats and more frequent human-wildlife contacts [1]. Therefore, increasing numbers of zoonoses, transfers of animal pathogens on humans, arise and are a major driving force in pathogen emergence on humans in recent decades [2]. Most of the human pathogens emerging lately are of animal origin, indeed, up to 75% [3]. Well-known examples of zoonoses are avian and swine flu human immunodeficiency viruses (HIV), ebola, Middle East respiratory syndrome (MERS) and severe acute respiratory syndrome (SARS) including the current circulating COVID-19 [4, 5, 6, 7].

While zoonoses can be of viral, bacterial and parasitic nature, emergences of higher magnitude, like the mentioned well-known examples, are often linked back to viral infections [3]. Harmfulness of viral infections can be diverse, ranging from mostly no sign of infection in the natural hosts to very severe symptoms or death in accidental hosts [8]. In contrast to natural hosts, humans, accidental hosts to, e. g. , the West Nile Virus, develop disease patterns upon infection and, thereby, are not able to support the virus life cycle [9]. High variety in host circulation and transmission ways from such natural or intermediate onto humans as accidental hosts, with long infectious periods without symptoms and high transmission pace have a high risk of pandemic events [10]. A prominent virus detected in a variety of hosts and known for reoccurring local and global outbreaks in the past is *Influenza A Virus* (IAV), member of the *Orthomyxoviridae* family and also commonly known as flu [8]. Analysis indicate a 1% chance of a pandemic with millions of deaths every year and is, therefore, the pathogen most likely to be responsible for a sudden severe pandemic [10].

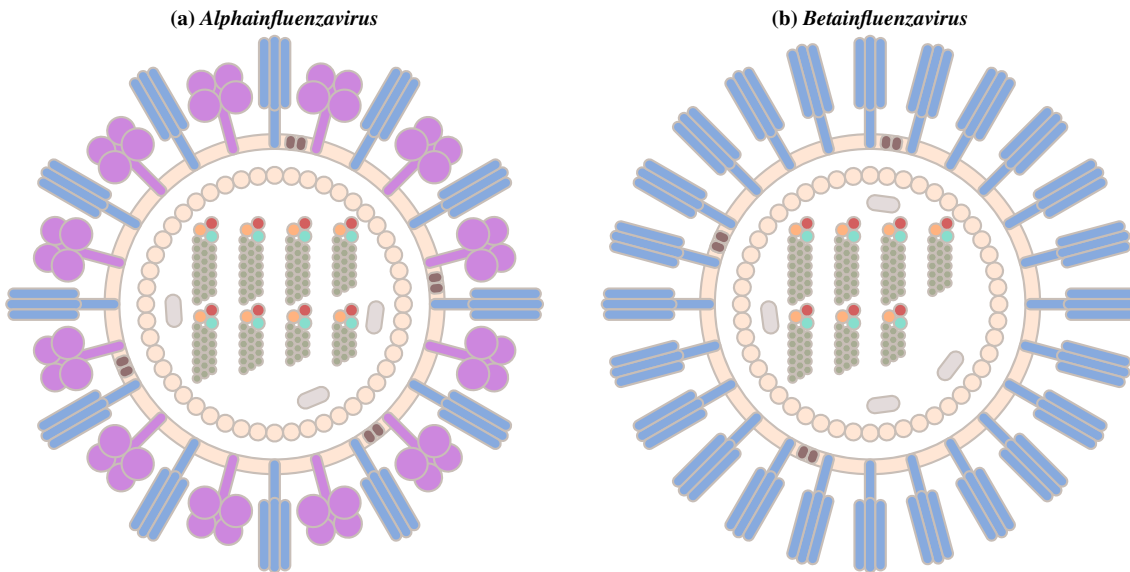


**Fig. 1.2.1** *Orthomyxoviridae*. .

## 1.2 Life-cycle and structure of the *Influenza A Virus*

In humans, infection by IAV affects the upper respiratory tract [11]. General symptoms like fever, cough and headache characterize the infection [11]. In some cases complications can occur, resulting in primary viral pneumonia or secondary bacterial pneumonia by bacterial infection [11]. The virus particles of IAV, called virions, are spherical in shape, 80–120nm in size and enveloped by the hosts cell membrane lipids [12, 13, 14]. These virions can sustain extensive forces in the hosts body and even survive deformation to around 33% of its total diameter [15]. Epithelial cells in the tissue of the respiratory tract, are the main infection area of the virions [12]. The IAV virions attach themselves to the host cells with their surface glycoproteins, the tetrameric neuraminidase (NA) and the trimeric hemagglutinin (HA) and enter the cells by clathrin-mediated endocytosis (Fig. 1.2.1a) [16, 17, 2, 13]. Equilibration of pH in the process of endocytosis involve the transmembrane protein M2 ion channel (M2) of IAV [18]. The surface glycoprotein tails are also connected to the second layer in the IAV virions, the matrix protein 1 (M1) [19]. Following the endocytosis the viral ribonucleoprotein (RNP) complexes are carried to the hosts cells nucleus by nuclear pore complex (NPC) for virus replication [20]. These RNP complexes contain the viral negative-sense single stranded viral RNA (ssRNA(-)), holding the genetic information, bound to multiple nucleoproteins (NPs) and the polymerase complex [20]. The trimeric polymerase complex including the polymerase basic protein 1 (PB1), polymerase basic protein 2 (PB2) and polymerase acid protein (PA) is essential for viral replication in the hosts nucleus [21, 20]. IAV is a segmented virus, one virion of IAV contains eight different short ssRNA(-)s, called segments, encoding in total

14 viral proteins [20]. In the nucleus the eight ssRNA(-)s are replicated and transcribed to viral messenger RNAs (mRNAs) with the latter translated to the virions proteins in the cytoplasm [20]. The translated nuclear export protein (NEP), M1, NP and proteins of the polymerase complex are imported by the NPC to build new RNP s with the replicated genomes and enable the nuclear exit [20]. By budding through the plasma membrane with the translated M2, while incorporating the translated HA and NA into the surface, new virions are released [20].

### 1.3 Evolution of the *Influenza A Virus*

Present day research, indicate mallards (*Anas platyrhynchos*) as main reservoir and natural host of low-pathogenic avian influenza viruses (LPAIVs) [22]. Studies on Pekin ducks, descended from mallards, have shown minor immune responses and antibody production to the infection with IAV strains and the possibility of a reinfection after two months with the same strain [23]. Strains are lines of IAV related to a specific location and time point [14]. Less dangerous strains of IAV, called LPAIVs, seem to repeatedly circulate in duck species and may evolve into human pathogenic strains by zoonoses [22]. Simple transmission over species is not enough to start a pandemic though, therefore, better understanding of the mostly unknown genetic changes vital for zoonotic events is required [4]. Circulation of these strains in aquatic bird species with continued evolution enable the transmission possibilities to humans, lower animals, and other birds [24]. The evolution occurs in all segments of the IAV but is most prominent in HA and NA [24]. Infection is mostly dependent on these surface glycoproteins, building the serotype, of the virus, as they are crucial for attachment to host cells [14]. Significant variation in the surface glycoproteins mostly occur by reassortment, also called genetic shift and point mutations, also called antigenic drift [24].

Point mutations in the segmented genome are very frequent, as the mutation rate in all RNA viruses is very high [25]. Present *poliovirus* research, indicate higher selection for faster replication and, therefore, acceptance of replication errors in favor of faster viral polymerases [26, 25]. This finding is in line with research indicating the short length or segmentation of RNA viruses and the high mutation rates as evolutionary trade-off [27, 28]. Thereby, creating a cloud of offsprings, called quasispecies, with 1-2 mutations in the genome each [27, 28]. The point mutations affect the offsprings surface proteins aminoacid (AA) composition in the translation process, by possible missense and nonsense errors or frameshifts [29, 24]. Reassortment is a more drastical change in the surface proteins and likely to be related to the pasts most horrible IAV pandemic, the spanish flu in 1918

[30]. For reassortment induced zoonoses, there has to be an intermediate host or „mixing vessel“, most likely pigs, able to be infected by IAVs of different hosts [31]. The host cells can then be co-infected by two different IAVs and create offsprings with mixed segments [32]. All segments can be exchanged, but, in case of surface proteins of different hosts, IAVs can occur that are able to do interspecies transmission [31]. Avian IAV strains can, thereby, evolve to human strains by co-infection of a pig with human transferable and avian originating IAV strains [31].

## 1.4 Vaccines design and the link to reassortment

No real cure to IAV infection is available and generation of vaccines is straining and not always as effective as expected [8, 33]. Furthermore, the efficacy of vaccines vary in specific populations and there are limitations to the manufacturing and the time frame of the production [33]. The strains most likely to circulate for the season are selected twice a year by the world health organisation (WHO), to be included in vaccines prepared for the winters in both hemispheres [34]. The seasonal used IAV vaccines target the highly mutable head domain of HA surface proteins to stimulate immune response [33, 35]. Therefore, the IAV vaccines efficiency vary depending on the similarity of the HA head domain of the strains used for the vaccines and the ones circulating in the season [35]. To manufacture the vaccines, reassortment of the selected strain with a master strain is induced in eggs [33]. The resulting hybrid strain contains the selected strains surface proteins and the master strains high-growth properties necessary for production of the vaccine in the short time frame [33]. Therefore enlarging the knowledge of IAV reassortment is important for predicting future pandemic strains, creation of vaccines by high-growth hybrid strains and the overall efficiency of the vaccines against the seasons circulating variable strains [33, 36]. For better understanding of IAVs reassortment, the secondary structure of the genome segments and their interaction mechanisms have to be discovered [36].

## 1.5 Secondary Structures of the *Influenza A Virus*

The eight IAV ssRNA(-) segments are single-stranded chains of nucleotides, by inter- and intra-molecular base-pairing various complex arrangements with different stabilities can be build [37, 36]. Negative single-stranded RNA viruses can use secondary structures on the ssRNA(-) as well as on the transcribed positive mRNA for different mechanisms, like the initiation of the translation on the mRNA by the internal ribosome entry site (IRES) or inter-molecular binding of different ssRNA(-) segments to each other [38, 39,

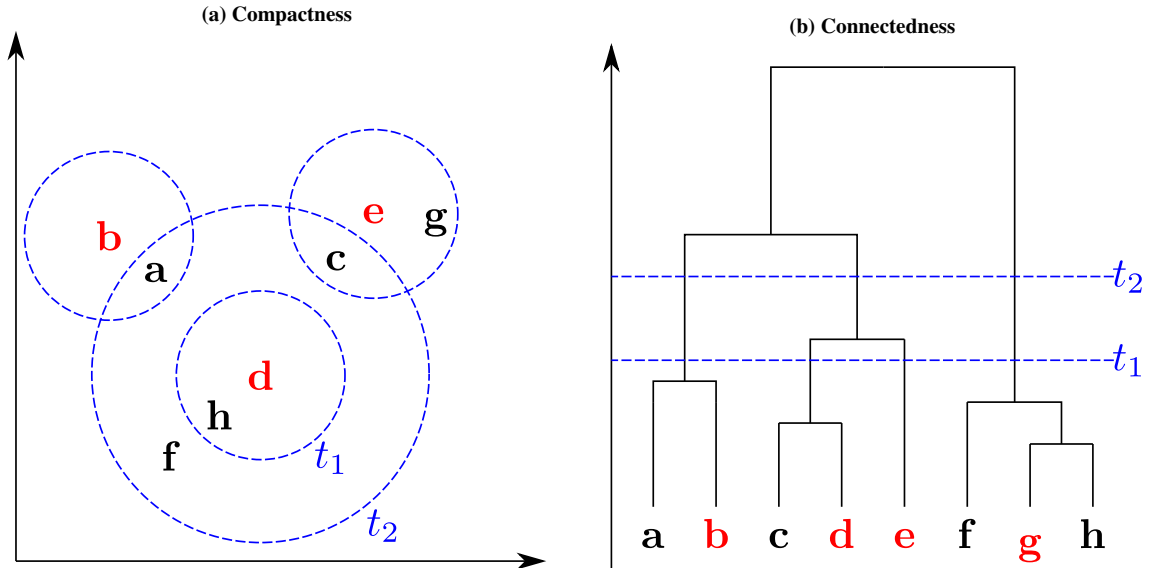


**Fig. 1.6.2 Clustering methods. .**

36]. Prediction of these viral secondary structures is possible by lab methods *in virio* and *in vitro* or *in silico*, with the latter only based on thermodynamic calculations alone [39, 36]. *In virio* methods involve modification inside a virion and *in vitro* methods involve modification on transcribed RNA in a probe, both can be used e. g., with SHAPE-MaP [40, 36]. Therefore, both methods can only be used to analyze secondary structure folding on single viruses, but reveal structures at single-nucleotide resolution [36]. *In silico* methods that are used without support by experiments are not limited by prediction on single viruses, only require prior sequenced genomes [39, 36]. Since *in silico* methods can be used on more than one virus, secondary structures can be predicted all together to find conserved equal folding regions in the sequenced genomes with alignments [39].

## 1.6 Alignments and clustering

## 1.7 WHO classification of *Influenza A Virus*

The present day classification of IAV is based on the serotype of the virus

## 1.8 The proposed project



## 2 Materials and Methods

### 2.1 Data and Pipeline

The tools listed in Table 2.1.1 were installed using the Conda package distribution system version 2-2.4.0 [41]. A configuration file for recreation of the used environment is present in the projects GitHub repository<sup>1</sup>

**Table 2.1.1 Pipeline tools.** All packages used in the project are listed here.

Name	Version	Purpose	Source
BioPython	1.78	alignments and tree construction	[42]
ETE3	3.1.2	tree plotting and labeling	[43]
HDBSCAN	0.8.26	hybrid vector clustering	[44]
kneed	0.7.0	Kneedle Algorithm implementation	[45]
MAFFT	7.475	multiple sequence alignment	[46]
numpy	1.19.5	matrix and vector calculations	[47]
pandas	1.2.2	dataframe creation and management	[48]
seaborn	0.11.1	plotting and data visualization	[49]
scikit-learn	0.24.1	PCA and vector normalization	[50]
SciPy	1.6.0	vector distance calculations	[51]
UMAP	0.4.6	UMAP dimension reduction	[52]

Since its file size exceeds the limits of GitHub, the FASTA file containing all the sequences of the *Influenza A Virus* (IAV), that are used in this project is only present on the attached USB stick, also containing a copy of the projects repository. The FASTA file can be manually retrieved from the Influenza Research Database (IRD)<sup>2</sup> using the settings in Table 2.1.2 for nucleotide sequence search. The header of the FASTA file has to be formatted as Accession Number, Strain Name, Segment, Protein Symbol, Type, SubType, Date, Host Species, Curation Flag in the given order before downloading from IRD for the tool to work as expected.

The version used for the proposed results was acquired at 08/11/2020<sup>3</sup>. Newer versions<sup>4</sup> might change the results slightly.

<sup>1</sup><https://github.com/ahenoch/Masterthesis.git>

<sup>2</sup><https://www.fludb.org/brc/home.spg?decorator=influenza>

<sup>3</sup>GenBank Genome Sequence/Annotation Update <= 11/2020

<sup>4</sup>GenBank Genome Sequence/Annotation Update >= 05/2021

**Table 2.1.2 Search parameter.** The parameters to use on the nucleotide sequence search interface of the IRD.

Field	Parameter
Data Type	Genome Segments
Virus Type	A
Complete Genome	Complete Genome Only
Select Segments	All
Complete	All

**Table 2.1.3 Summary of the clustering methods.** For easier separation the different settings were listed. Method PCA/DBCV and PCA/Knee use Fig. 2.1.1 pathway **1** followed by Fig. 2.1.2 pathway **3** for method PCA/DBCV and **4** for PCA/Knee. Method UMAP/DBCV and UMAP/Knee differ only by the first part using Fig. 2.1.1 pathway **2** instead of **1**.

Abbreviation	Method	100 Components	30 Components	Exploration
PB	PCA/DBCV	—	PCA	DBCV
PK	PCA/Knee	—	PCA	Kneedle Algorithm
UD	UMAP/DBCV	PCA	UMAP	DBCV
UK	UMAP/Knee	PCA	UMAP	Kneedle Algorithm

In this project four different ways to cluster the segments of IAV are described and discussed (Table 2.1.3). The methods are compared to each other and analyzed for their capability of IAV clustering. Abbreviations of the four methods were used in the following as indicated in Table 2.1.3.

A combined version of the pipelines in Fig. 2.1.1, Fig. 2.1.2 and Fig. 2.1.3 is available in the projects GitHub repository<sup>5</sup> as a novel clustering tool for IAV genomes. The tool contains the method elaborated as best suitable for IAV clustering and is intended to be used for future research (Sec. 3.6).

Execution of the tool on the FASTA file containing 449462 sequences takes around one and a half hours. The sequences are, thereby, clustered segment-wise based on their 7-mer frequencies. The output consists of database ready CSV files holding the cluster assignment of every sequence, analysis graphics and a labeled cluster tree of each used segment.

The method is based on the one proposed by Viehweger et al. [53]. Instead of using the tool `nanotext` as proposed in Viehweger et al. [54], a simple 7-mer frequency calculation was implemented and used as described in Sec. 2.2. Similar to Viehweger et al. [53], the calculated vectors were clustered using `HDBSCAN` with custom settings described in the Sec. 2.4. Since `nanotext` was not used in this project, different types of

<sup>5</sup><https://github.com/ahenoch/Masterthesis.git>

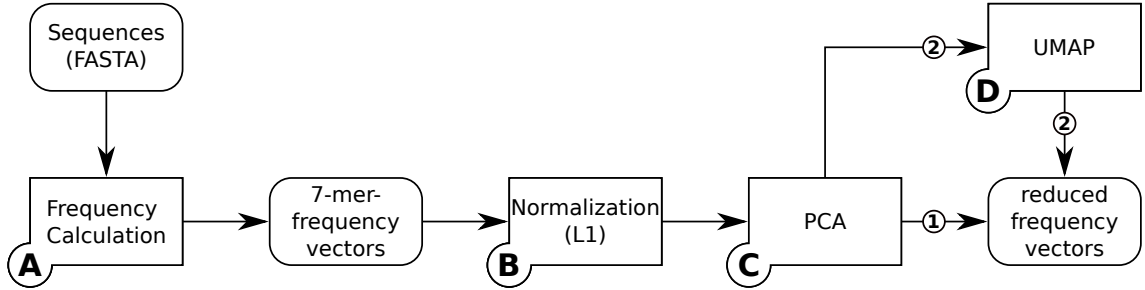


**Fig. 2.1.1 Preprocessing pipeline.** To create high-quality vectors representing the sequences, the FASTA file was translated to normalized vectors containing the 7-mer frequencies of the specific sequences (**A** and **B**). By pathway **1**, a low complexity representation of the vectors is obtained for clustering only using PCA (**C**). Pathway **2** describes additional execution of UMAP that can be used after PCA as intermediate instead of final step (**D**). Reduction with pathway **1** or **2** results in reduced frequency vectors with 30 components.

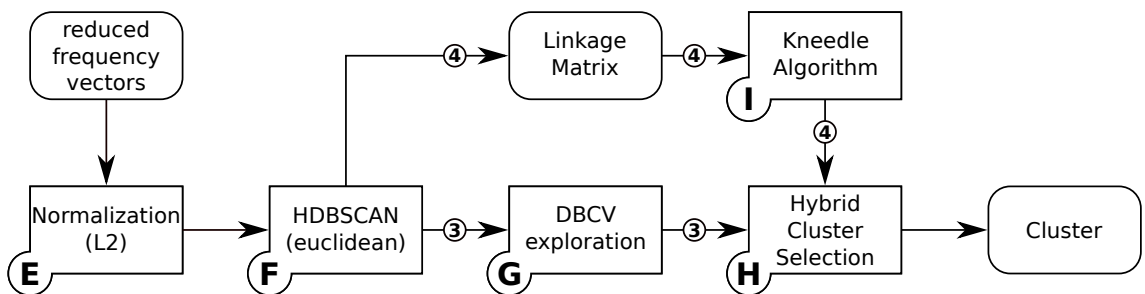


**Fig. 2.1.2 Clustering pipeline.** Following the preprocessing pipeline (Fig. 2.1.1) normalization is used again with L2-norm as preparation for HDBSCAN (**E**). Initial HDBSCAN clustering (**F**) is performed in preparation to the  $\varepsilon$  exploration using either pathway **3** or **4**. Final hybrid clustering (**H**) is then executed on the results of the  $\varepsilon$  exploration using the Kneedle Algorithm (**I** and pathway **4** or DBCV (pathway **3** and **G**).

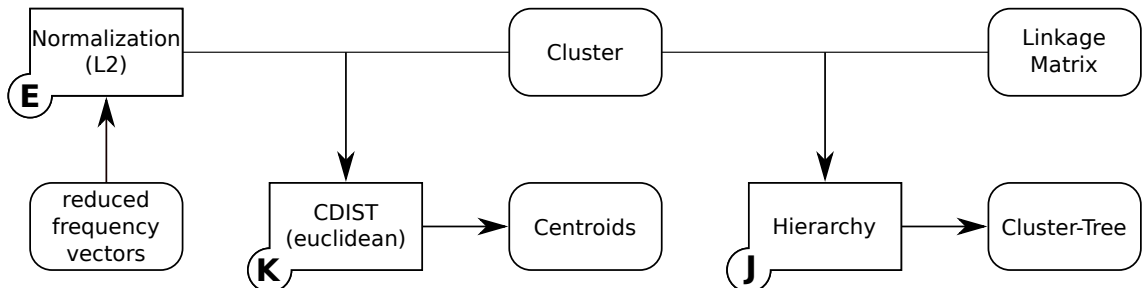


**Fig. 2.1.3 Postprocessing pipeline.** Following the clustering pipeline (Fig. 2.1.2) the cluster-tree is build by BioPython and visualized by ETE3 (**J**). For every cluster the vectors with the smallest distance to the other cluster members are calculated and determined as the clusters centroids (**K**).

dimension reduction were performed and compared, as described in Sec. 2.3 and discussed in Sec. 3.1. With reference to the use of cosine similarity  $s_{\cos}(x, y)$  as measurement for genomic similarity in **nanotext**, the use of the complementary cosine distance  $d_{\cos}(x, y)$

in HDBSCAN was targeted (Eq. 2.1.1) [54].

$$d_{\cos}(\mathbf{x}, \mathbf{y}) = 1 - s_{\cos}(\mathbf{x}, \mathbf{y}) \quad (2.1.1)$$

## 2.2 7-mer Frequency Calculation

The FASTA file containing the genomes of IAV for clustering, was converted to vectors to enable clustering in high dimension by counting their 7-mer frequency (Fig. 2.1.1 **A**).  $4^7$  possible constellations of the nucleotides A,C,G,T with length 7 exist. Therefore, taking every constellation into consideration, the vector of every sequence has  $4^7$  components. The numbers in the vector components are the number of occurrences of the related 7-mer in the sequence. The first constellation of the  $4^7$  possible ones with length 7 is AAAAAAA, given a example sequence of the FASTA contains this 7-mer 10 times, the first component of the sequences vector would be 10. Fig. 2.2.4 illustrates the calculation using 3-mers instead of 7-mers.

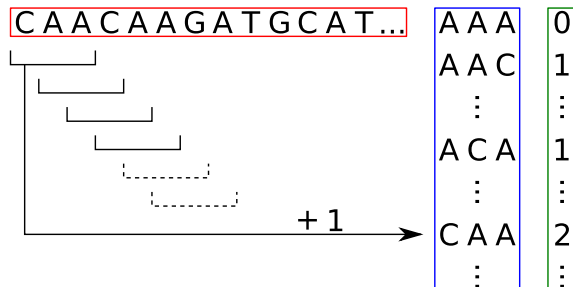


**Fig. 2.2.4 K-mer vector creation.** An example genomic sequence (red box) is splitted into 3-mers. The sequences 3-mers are then compared to the list of all  $4^3$  possible 3-mer constellations (blue box). Based on the occurrence number of the lists 3-mers in the sequence a vector with  $4^3$  components is created (green box).

To gain the frequency of the 7-mers all the vectors were normalized to a vector sum of 1, according to L1-norm (Eq. 2.2.2 and Fig. 2.1.1 **B**).

$$\hat{\mathbf{x}} = \frac{\mathbf{x}}{\|\mathbf{x}\|_1} \quad (2.2.2)$$

## 2.3 Dimension Reduction

PCA was used to handle the complexity of the vectors by simplification with the least loss of information possible (Fig. 2.1.1 **C**) [55] [50].

Without posterior use of UMAP 30 components were extracted by the PCA (Fig. 2.1.1 pathway **1**) and otherwise 100 (Fig. 2.1.1 pathway **2**). Extraction of 30 or 100 components out of 4<sup>7</sup> in total equals  $\approx 0.18\%$  or  $\approx 0.61\%$ . The size limit of the PCA function for calculation with default setting `svd_solver='auto'` is 500 different vectors with 500 components and at least 80% of the components to extract. Since every maximum for standard settings was exceeded, `svd_solver='randomized'` setting was used automatically.

UMAP was used for dimension reduction similar to PCA, aiming to better preserve the global structure of the data (Fig. 2.1.1 **D** and pathway **2**) [52]. It is similar to the well-known t-SNE with better run time performance and better structure preservation in the lower dimension and less restrictions [56, 52].

The used parameters of UMAP match most of the ones listed in the manual under section „UMAP enhanced clustering“<sup>6</sup>. The settings are proposed to be used with UMAP prior to HDBSCAN clustering. Since the goal was clustering, not plotting 30 components was used instead of the proposed 2. The neighbors number was also changed. It is recommended to be set in a range of 1 to 100. Based on the high number of sequences used e. g., 56617 for segment 4, the highest recommended setting of 100 was used to better preserve the global picture of the data. Also based on the input size `n_epochs=200` setting was used automatically.

UMAP was used posterior to dimension reduction with PCA, because of the similarity to t-SNE. As explained in the manual of t-SNE<sup>7</sup>, the dimension should be reduced to a reasonable amount prior to execution to reduce noise. In in section „What is the difference between PCA / UMAP / VAEs?“ of the UMAP manual<sup>8</sup> a pipeline is proposed, to reduce from high dimension with PCA, continue with reduction by UMAP and cluster with HDBSCAN and is, therefore, used as reference. Reduction with UMAP to 30 components posterior to PCA with 100 components also provided a comfortable balancing of computational effort of both methods, while preserving  $\approx 85\%$  explained variance with PCA [52].

## 2.4 Hybrid Clustering

HDBSCAN was used to cluster the reduced vectors. It is an clustering algorithm proposed by Campello et al. [57] as a novel version of the well-known DBSCAN [58]. Execution of HDBSCAN involves varying values of  $\varepsilon$ , thus, not one specific threshold is used to define the clusters, but instead clusters of varying densities are extracted based on their stability [44].

---

<sup>6</sup><https://umap-learn.readthedocs.io/en/latest/clustering.html> (accessed 07/01/2020)

<sup>7</sup><https://scikit-learn.org/stable/modules/generated/sklearn.manifold.TSNE.html> (accessed 07/01/2020)

<sup>8</sup><https://umap-learn.readthedocs.io/en/latest/faq.html> (accessed 07/01/2020)

HDBSCAN was used with hybrid clustering setting as proposed in Malzer and Baum [59], combining HDBSCAN it with DBSCAN. Thereby, some of the disadvantages of using either of these methods can be avoided [44, 60]. Since DBSCAN is a hierarchical clustering tool, it is dependent on a strict threshold  $\varepsilon$  for clustering. Vectors not surrounded by  $k$  other vectors in a radius defined by this threshold value  $\varepsilon$  are omitted as single vector clusters or noise [61, 62]. Standard HDBSCAN, on the other hand, tend to create unwanted micro-clusters in areas of high density [44]. Using the hybrid HDBSCAN proposed in [59], a threshold value  $\varepsilon$  can be used to extract these high density areas as single clusters with DBSCAN, but still use the standard HDBSCAN for the otherwise omitted vectors (Fig. 2.4.5 and Fig. 2.1.2 **H**). Hybrid HDBSCAN is, thus, clustering with DBSCAN, resulting in a **raw** cluster number containing finished clusters and omitted single vector clusters, and subsequent standard HDBSCAN, reducing the **final** cluster number by clustering the omitted vectors.

This method is useful when having a small cluster size value, while still aiming to cluster high-density areas together exactly suitable for the proposed clustering. Specific strains of IAV are sequenced a lot more, thereby probably creating high-density areas that should be clustered together with DBSCAN. The small cluster size is, thereby, used to find small clusters of rare sequenced variants by HDBSCAN, with possibly important mutations in low-density areas [59]. As explained, the smallest minimum cluster size of 2 was used to capture, in the best case, even genomes with rare appearing mutations, in their own clusters. To declare as least vectors as possible as noise, the minimum samples value  $k$  was also set to the minimum 1. Standard HDBSCAN was once performed without the hybrid setting, in preparation of  $\varepsilon$  exploration as described in Sec. 2.5 Fig. 2.1.2 **F**). Hybrid HDBSCAN clustering was used with the same settings plus respective  $\varepsilon$  value Fig. 2.1.2 **H**).

Distance calculations by HDBSCAN were performed with the euclidean distance setting due to an open issue in the GitHub Repository of HDBSCAN<sup>10</sup>. In the issue the inability to use cosine distance metric with HDBSCAN and the approximation of it by chord distance metric, is described. Given that chord distance metric is also not available firsthand, the possibility to use normalization of the vectors with L2-norm, prior to clustering with euclidean metric setting is also mentioned Fig. 2.1.2 **E**).

$$\hat{\mathbf{x}} = \frac{\mathbf{x}}{\|\mathbf{x}\|_2} \quad (2.4.3)$$

Calculation of chord distance  $d_{\text{chord}}$  is possible when having two vectors, here as an example named as **a** and **b** with the same L2-norm equal to a radius  $r$  of a sphere centered

<sup>9</sup>[https://hdbSCAN.readthedocs.io/en/latest/how\\_to\\_use\\_epsilon.html](https://hdbSCAN.readthedocs.io/en/latest/how_to_use_epsilon.html)

<sup>10</sup><https://github.com/scikit-learn-contrib/hdbSCAN/issues/69> (accessed 06/02/21)

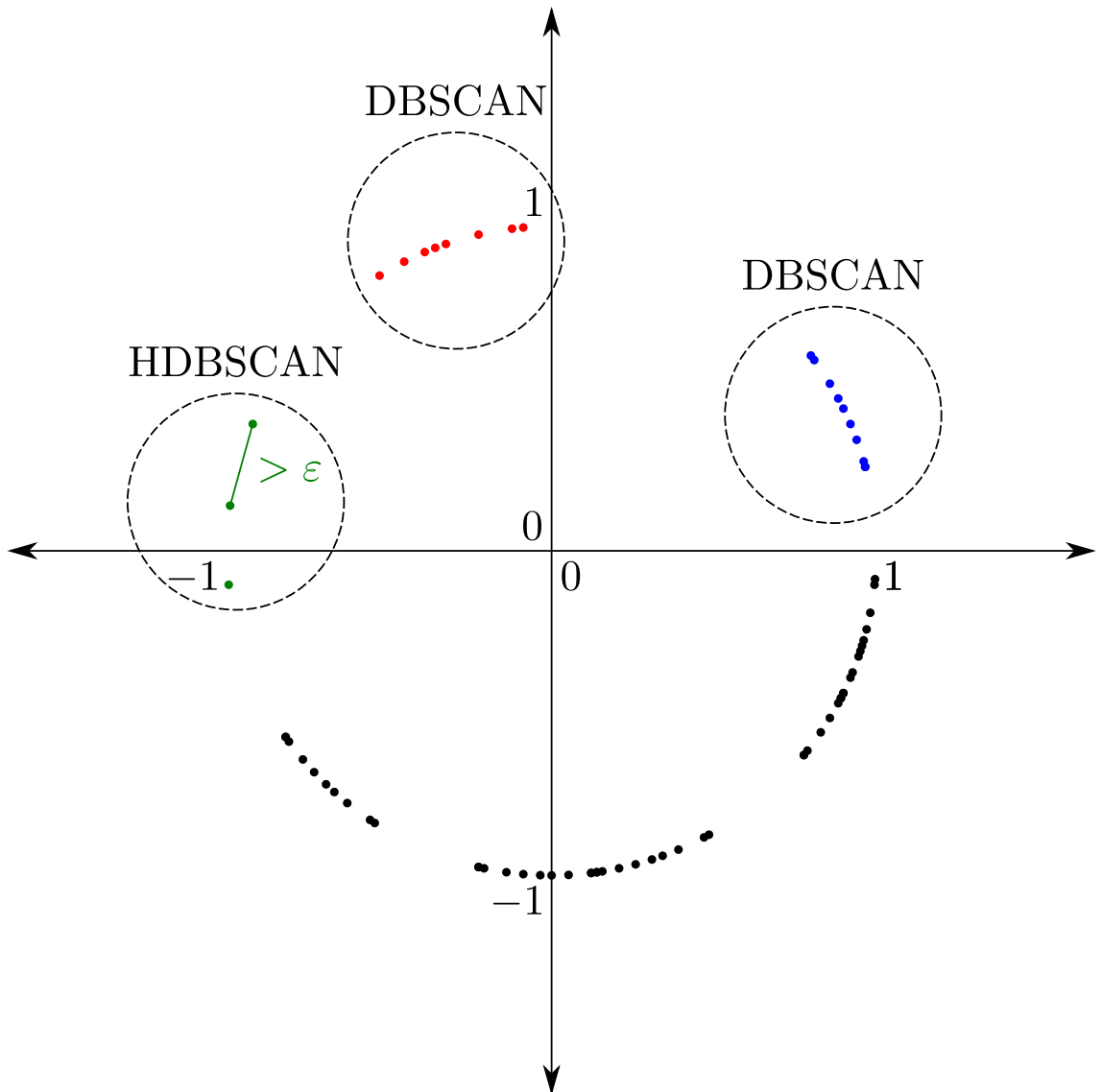


**Fig. 2.4.5 Hybrid clustering threshold.** The hybrid clustering HDBSCAN differentiates between clusters where vectors are connected by distances smaller and larger than  $\varepsilon$ . When the distance is smaller, the DBSCAN algorithm is used and clusters are generated based on this threshold value  $\varepsilon$  by combining vectors with smaller distance. Omitted vectors, not having a given number of  $k = 1$  vectors in reachable distance of  $\varepsilon$  and are, therefore, impossible to be clustered by DBSCAN are subsequently clustered with HDBSCAN building clusters with higher threshold if appropriate. The graphic is based on „Combining HDBSCAN\* with DBSCAN“ in the manual<sup>9</sup> and adapted to the calculations in this project, as a two dimensional example.

to the origin of the coordinate system and an angle of  $\Theta$  (Eq. 2.4.4 and Fig. 2.4.6a) [63]. The Euclidean distance  $d_{\text{eucl}}$  is equal to the chord distance for the same vectors.

$$\|\mathbf{a}\|_2 = \|\mathbf{b}\|_2 = r \Rightarrow d_{\text{chord}}(\mathbf{a}, \mathbf{b}) = 2 \cdot r \sin\left(\frac{\Theta}{2}\right) = d_{\text{eucl}}(\mathbf{a}, \mathbf{b}) \quad (2.4.4)$$

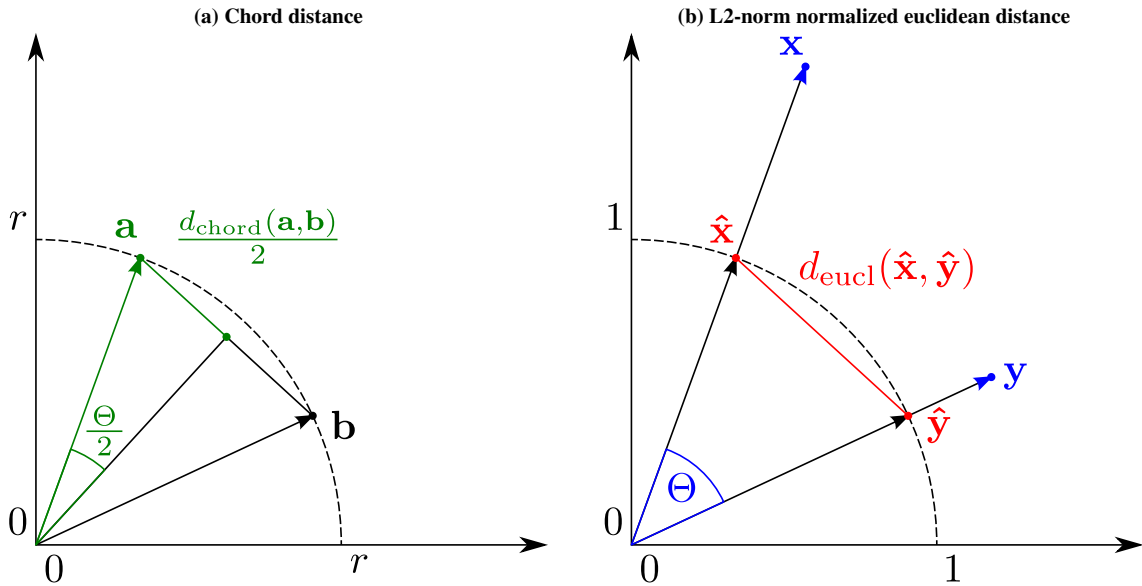


**Fig. 2.4.6 Chord calculation background.** The chord can be calculated with the radius similar for both vectors and the information of the angle of two vectors to the origin of the coordinate system. Since this information is not always available or sometimes expensive to calculate for a high number of vectors, the euclidean distance can be used with a L2-norm of both vectors equal to  $r$  for similar results instead. To approximate cosine distance, the same calculation of euclidean distance is used with L2-norm equal to 1. To always obtain similar values of L2-norm equal to 1, L2-norm normalization is used on every vector.

Thus, in this project, chord distance can be calculated with the euclidean distance metric, posterior to the normalization with the L2-norm, which scales the vectors to the unit sphere Fig. 2.4.6b.

$$\|\hat{x}\|_2 = \|\hat{y}\|_2 = 1 \Rightarrow d_{\text{chord}}(\hat{x}, \hat{y}) = d_{\text{eucl}}(\hat{x}, \hat{y}) = \|\hat{x} - \hat{y}\|_2 \quad (2.4.5)$$

The calculation of the chord distance, by L2-norm normalized vectors euclidean distance, is, thereby, integrated into the mutual reachability distance calculation of HDBSCAN. The mutual reachability distance is the maximum of the chord distance and the core distances of two vectors (Eq. 2.4.6). The core distance is the minimum radius necessary to include 5 other vectors around a given vector [44]. Threshold  $\varepsilon$  is used on the mutual reachability distances between the vectors Fig. 2.4.5.

$$d_{\text{mreach-}k}(\hat{x}, \hat{y}) = \max\{\text{core}_k(\hat{x}), \text{core}_k(\hat{y}), d_{\text{eucl}}(\hat{x}, \hat{y})\} \quad (2.4.6)$$

The used chord distance is proportional with the initially intended to use cosine distance as shown in Eq. 2.4.7. Dividing the squared chord distance by 2 results in the cosine

distance of the vectors Fig. 3.0.2.

$$\begin{aligned}
 d_{\text{chord}}(\hat{\mathbf{x}}, \hat{\mathbf{y}})^2 &= \|\hat{\mathbf{x}} - \hat{\mathbf{y}}\|_2^2 \\
 &= (\hat{\mathbf{x}} - \hat{\mathbf{y}})^\top (\hat{\mathbf{x}} - \hat{\mathbf{y}}) \\
 &= \hat{\mathbf{x}}^\top \hat{\mathbf{x}} - 2\hat{\mathbf{x}}^\top \hat{\mathbf{y}} + \hat{\mathbf{y}}^\top \hat{\mathbf{y}} \\
 \|\hat{\mathbf{x}}\|_2 = \|\hat{\mathbf{y}}\|_2 = 1 \Rightarrow &= 2 - 2\hat{\mathbf{x}}^\top \hat{\mathbf{y}} \\
 &= 2 - 2\cos(\Theta) \\
 &= 2 \cdot (1 - \cos(\Theta)) \\
 &= 2 \cdot d_{\cos}(\hat{\mathbf{x}}, \hat{\mathbf{y}})
 \end{aligned} \tag{2.4.7}$$

## 2.5 Epsilon Selection

To find an appropriate value for  $\varepsilon$ , two different methods were used and compared (Fig. 2.1.2 pathway **3** and **4**). The first method, the density based cluster validity (DBCV) exploration in Fig. 2.1.2 **G**, is based on repeated execution of hybrid HDBSCAN with different settings for  $\varepsilon$  and comparison by the DBCV. The DBCV is a calculation based on the minimum spanning tree to estimate overall cluster density [60]. To enable the calculation hybrid HDBSCAN was performed with `gen_min_span_tree=True` setting.

Second method for  $\varepsilon$  exploration was performed using the Kneedle Algorithm on the linkage matrix created by the initially performed of standard HDBSCAN clustering (Fig. 2.1.2 **F** and **I**) [45]. With increasing cluster number, the distance threshold  $\varepsilon$  of hierarchical clustering decreases. This describes a decreasing curve of convex type with distance threshold on the y- and cluster number on the x-axis. The knee is the number of clusters at the point in the polynomial representation of the curve with maximal acceleration. Polynomial representation was used to find the maximum acceleration of the smoothed curve. Therefore the settings `curve='concave'`, `direction='increasing'` and `interp_method='interp1d'` were used to find the optimal number of clusters. The optimal number of clusters was converted to the respective  $\varepsilon$  threshold.

Knee point selection was restricted to a given area between one and a maximum value of 500. The maximum was chosen to include the area with the highest expected differences. The best Knee point was expected to be less than 100, a higher value was used to prevent forcing the number of clusters to be maximal 100.

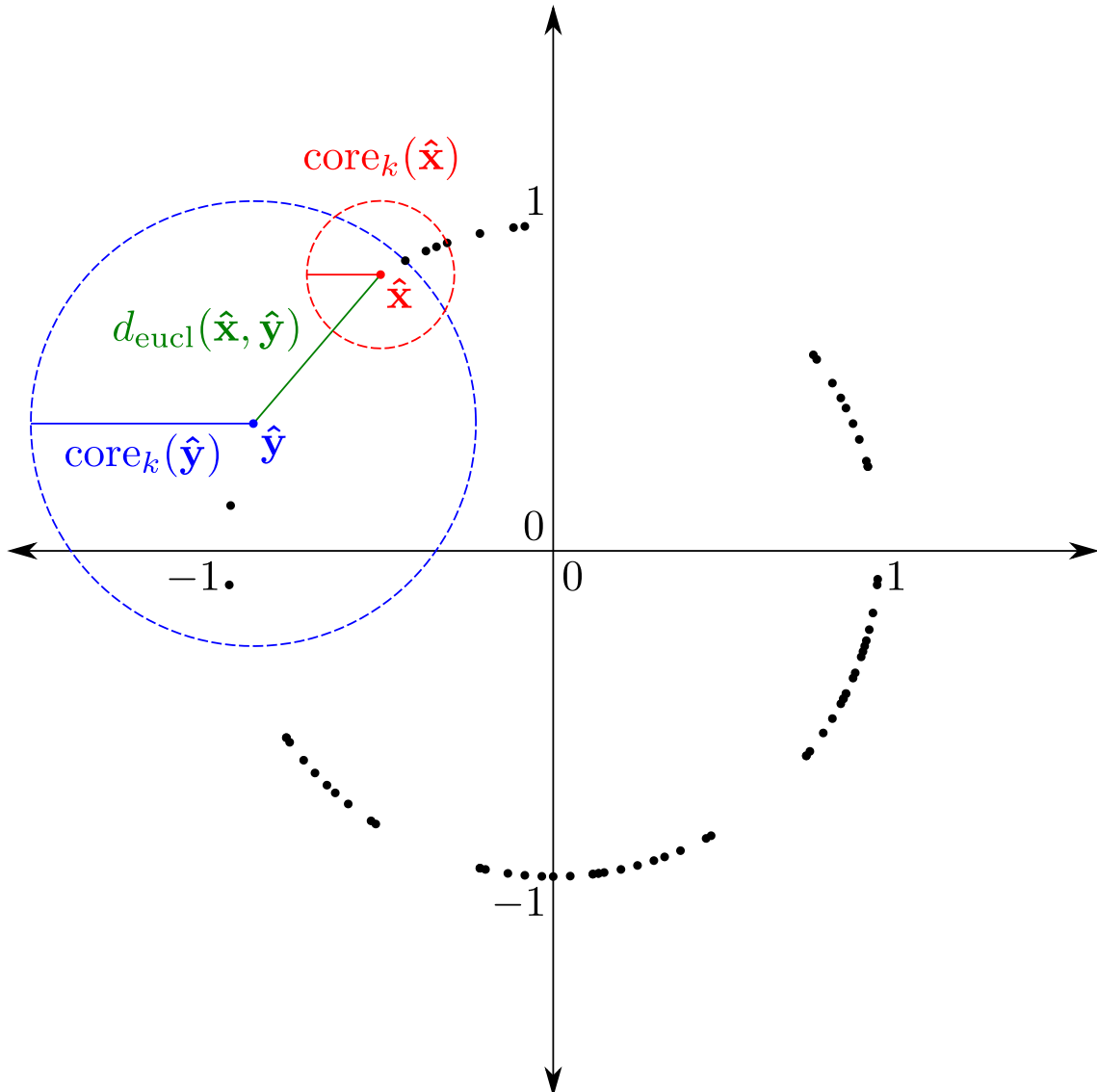


**Fig. 2.4.7 Mutual reachability calculation.** A low dimension representation of the calculation HDBSCAN performed in this project. To calculate the mutual reachability distance, the smallest radius is calculated to include exactly  $k$  vectors. This example should demonstrate the calculation for vector  $\mathbf{x}$  in blue and  $\mathbf{y}$  in red, with a  $k$  of 5. The euclidean distance between these vectors is then calculated and compared to the radii. The maximum of both radii and the euclidean distance is the mutual reachability distance (Eq. 2.4.6).

## 2.6 Alignments and Vector Calculations

The labeled cluster trees were created by ETE3 with a newick file, generated according to a feature request, proposed for the SciPy<sup>11</sup> (Fig. 2.1.3 **J**) [43]. Clusters centroid vectors were selected by calculating euclidean distance between all the vectors of a cluster to each other. The vector with the smallest mean distance was declared as centroid (Fig. 2.1.3 **K**). The precalculated trees were created using cosine distance calculation on the L1-norm

<sup>11</sup><https://github.com/scipy/scipy/issues/8274> (accessed 06/02/21)

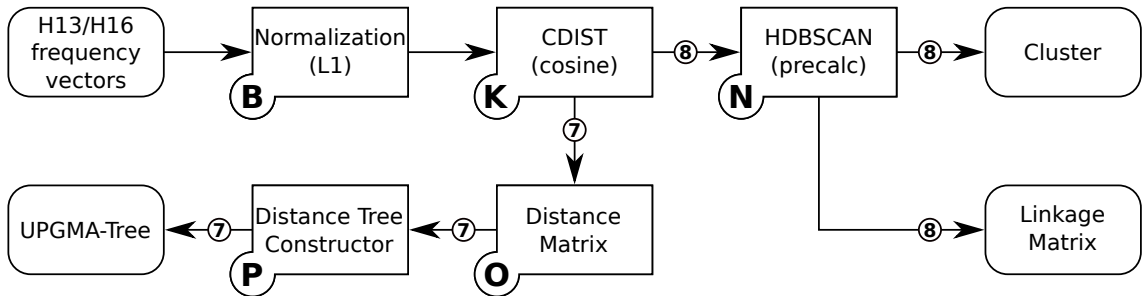


**Fig. 2.6.8 Precalculation pipeline.** For the precalculated trees the L1-normalized 7-mer vectors distances were calculated and used for clustering by HDBSCAN (**B**, **K**, **N** and pathway **7**) and on the other hand processed with BioPython for unweighted pair group method with arithmetic mean (UPGMA) tree creation and visualization by ETE3 (**N** and **8**).

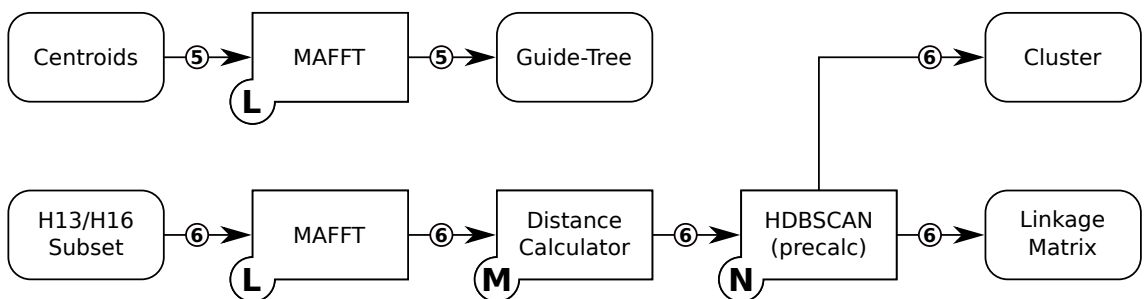


**Fig. 2.6.9 Alignment pipeline.** The sequences related to the centroid vectors were aligned using MAFFT resulting in the output as guide-tree visualized by ETE3 (**L** and pathway **5**). A small FASTA subset of H13/H16 was also aligned by MAFFT prior to evolutionary distance calculation with BioPython and clustering with HDBSCAN (**L**, **M**, **N** and pathway **6**).

normalized 7-mer frequency vectors of the segment 4 H13 and H16 sequences of the FASTA (Fig. 2.6.8 **F**). The calculated distances were used for UPGMA tree building with BioPython (Fig. 2.6.9 **O** and **P**). The vectors were also clustered by HDBSCAN using the calculated distances with `metric='precalculated'`. Other settings were used as described in Sec. 2.4 without hybrid clustering.

MAFFT was used for multiple sequence alignments (MSAs) and guide tree creation with `treeout=True` on the centroid sequences and on the FASTA subset containing H13 and H16 sequences of segment 4 (Fig. 2.6.9 **L**) [46]. The MSA of the FASTA subset was converted to evolutionary distances with BioPython and clustered by HDBSCAN (Fig. 2.6.9 **M** and **N**). Pairwise alignments in Sec. 3.6 were performed using BioPython.



## 3 Results and Discussion

For a basic overview of the sequences in the FASTA file (Chap. 2), the number of sequences of a segment related to specific subtypes was counted and visualized (Fig. 3.0.1). Hereby, the high number of segment 4 sequences of subtype H1 and H3 in Fig. 3.0.1a and segment 6 sequences of N1 and N2 in Fig. 3.0.1b was noticeable. Furthermore, the similarity of the number of sequences of segment 4 subtype H1 and N1 as well as of segment 6 H3 and N2 was also remarkable. The similarity seems to be most likely due to the frequency of subtype combinations H1N1 and H3N2 of the full genomes, which was also in line with the most prominent subtypes of *Influenza A Virus* (IAV) mentioned in Deng et al. [64]. In addition to the most frequent subtypes a, high number of not classified sequences named „none“ is present in the data. These unclassified strains were possibly sequenced without prior subtype testing or are in fact sequences that do not belong to either of the known subtypes and, thereby, no antibody antigen reaction was observable [65].

As described in Chap. 2, the clustering was performed multiple times to compare different methods for their quality and efficiency of IAV clustering. The four methods are compared directly to each other in the following. For better separation, the four methods were called by their abbreviation, to be found in Table 2.1.3. As a short reminder, PD uses direct reduction to 30 components with PCA following  $\varepsilon$  exploration using the density based cluster validity (DBCV) and PK using the same reduction but exploration with the Kneedle Algorithm instead. Method UD and UK are performed in a similar way but using reduction to 100 components by PCA and to 30 afterwards by UMAP instead. The numbered pathways in Fig. 2.1.1, Fig. 2.1.2 and Fig. 2.1.3 represent the different to be compared methods.

To choose a reasonable number of components for the PCA mentioned in Sec. 2.3, the 7-mer frequency vectors of segment 4 (Fig. 2.1.1) were reduced by running PCA with different settings. The sum of explained variance for every setting were calculated and listed in Table 3.0.1. Because of the high increase of explained variance from 10 to 20 components with 58.7% to 68.7% and likewise to 30 components with 73.9% explained variance, a value of 30 was used as default in this project. A fairly small value was used, due to increasing computational effort of the PCA implementation and also to preserve the

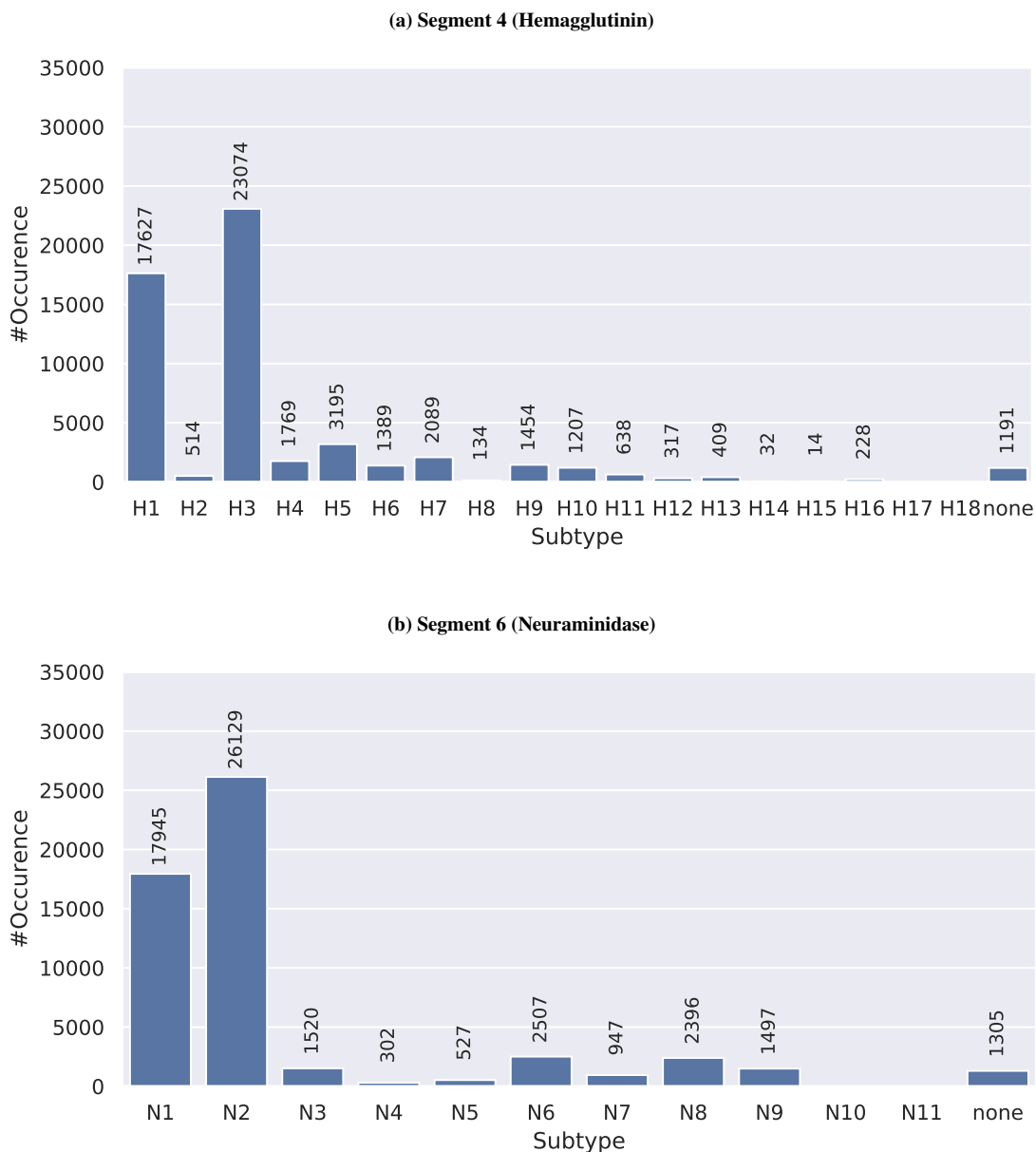


**Fig. 3.0.1 Antigen subtype frequency.** The number of occurrences of segment 4 and segment 6 sequences related to antigen subtypes is visualized. Sequences related to subtypes H1 and H3 are the most frequent ones from segment 4 with a total number of 17627 and 23074. Subtype H5 is also slightly over-represented with 3195 sequences. 1191 sequences from segment 4 in the data have no classification and are listed as „none“. Sequences related to subtypes N1 and N2 are the most frequent ones from segment 6 with a total number of 17945 and 26129. 1305 sequences from segment 6 in the data have no classification and are also listed as „none“.

usability of spanning tree calculation with HDBSCAN. Calculation of the spanning tree is with HDBSCAN and the preferred settings, only possible to less than 60 components. For better comparison of the methods, the number of final components for UMAP reduction in UD and UK was also set to 30. Therefore, clustering is with all used methods was performed on vectors with 30 components.

**Table 3.0.1 Explained variance by different PCA settings.** The explained variance of specific PCA settings used on the 7-mer frequency vectors of segment 4. A result of 0.587 as for 10 components represents 58.7% of the variance is explained by the first 10 components of the vector. The more components are extracted the lower the increase in additional explained variance [55].

#Components	Var( $X$ )
10	0.587
20	0.687
30	0.739
40	0.771
50	0.793
60	0.809
70	0.821
80	0.831
90	0.839
100	0.846

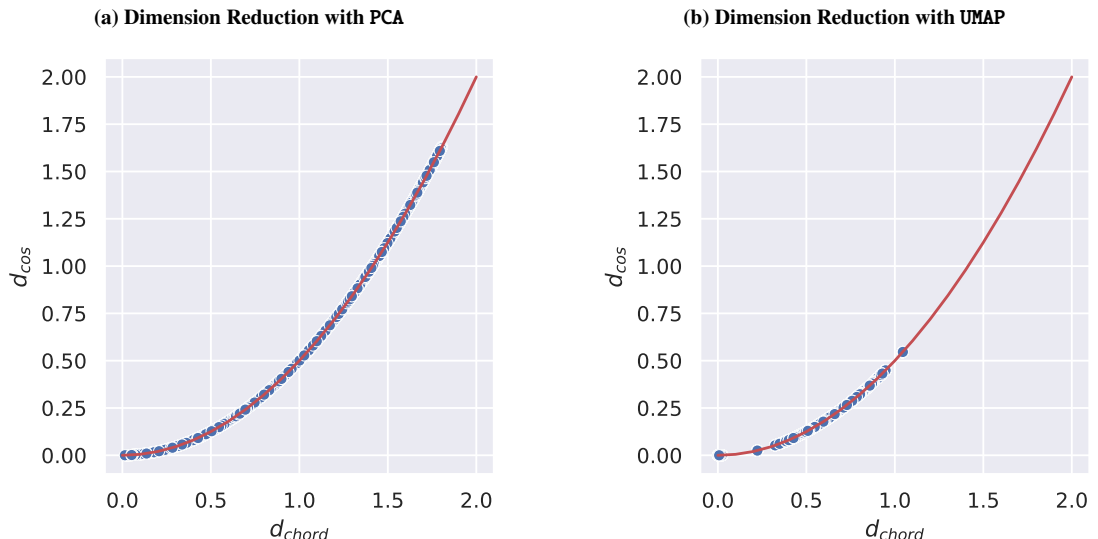


**Fig. 3.0.2 Cosine distance approximation.** Calculations for the chord and the cosine distances were performed on subsets for both pipelines and compared. In both cases the difference is exactly matching the proportional increase of squared chord distance divided by two equals the cosine distance as described in Sec. 2.4. Crowding of the points in the right graph representing reduction with UMAP is explained by the embedding mechanism of the tool further reduction the distance of similar vectors [52].

For a graphical comparison of the demonstrated mathematical proof of the proportional increase of the chord distance to the cosine distance (Sec. 2.4), subsets of the real data were used. In Fig. 3.0.2a, a subset of 100 7-mer frequency vectors of segment 4 were reduced by PCA and compared to each other by chord and cosine distance as described in Sec. 2.4 and Sec. 2.3. All the calculated distances for chord distance were then plotted against the equivalent cosine distances. The red line indicates the proportional increase as calculated in Sec. 2.4. All the points are arranged exactly along the red line which

confirms the calculation and proportionality of the used method to cosine distance that was intended to be used. The same was repeated for the settings with the use of the UMAP pipeline resulting in the same graphical confirmation (Fig. 3.0.2b). In Fig. 3.0.2b, all the points are crowded much more to a dense area of the curve. This is reasoned by the embedding behavior of UMAP and will be discussed in the following sections.

### 3.1 Method Selection

Clustering with each of the four methods, resulted in tables containing the used settings and a summary of the clustering. The tables are combined based on the exploration method. Table 3.1.2 contains the results of the two methods using the Kneedle Algorithm and Table 3.1.3 the results based on using the DBCV. Every segment of IAV was clustered by each method. By result comparison of methods using  $\varepsilon$  exploration by the Kneedle Algorithm (PK and UK) in Table 3.1.2, a major difference in the number of raw clusters stood out. Hybrid HDBSCAN clustering of the only PCA reduced 7-mer vectors resulted in around 60 to 70 raw clusters (DBSCAN part) and 40 to 50 final clusters (standard HDBSCAN part) per segment. The number of final clusters is relative close to the state of the art subtype classification with 18 hemagglutinin (HA) and 11 neuraminidase (NA) antibody subtypes [65]. The UK method results in a way higher number of clusters with no difference of raw and final cluster number. Therefore, the hybrid HDBSCAN clustering only used the DBSCAN part. This can be explained by the overall higher  $\varepsilon$  threshold compared to the PCA version (PK). By a higher  $\varepsilon$  more points are included in the DBSCAN part of the hybrid clustering. With the UMAP reduction method (UK) in comparison to the one using PCA all vectors of every segment could be clustered with no unclustered vectors. The approach using PCA alone is unable to cluster the vectors of around 10 to 30 sequences per segment. However the number of unclustered for, e. g., segment 4 is 6 of 56617 used sequences and, therefore, neglectable  $\approx 0.01\%$ . As a comparison, 1191 sequences segment 4 are declared unclassified by the current subtype convention making  $\approx 2\%$ . Comparing the methods to the ones using the DBCV for  $\varepsilon$  exploration instead of the Kneedle Algorithm (Table 3.1.3 did not result in much difference for the UMAP reduction with DBCV exploration method (UD). The number of clusters found was a little higher compared to the results found with the Kneedle Algorithm exploration. Using DBCV to find the optimal  $\varepsilon$  with the PCA pipeline (PD) on the other hand changes the results drastically. The number of final clusters was between 9000 and 12000 depending on the segment, with the exception of segment 4. The raw cluster number was equivalent to the total number of sequences for the given segment. Also the number of unclustered sequences was increased by a major amount to around 20% for some segments, making

**Table 3.1.2 Clustering results with the Kneedle Algorithm.** The results of the clustering methods using the Kneedle Algorithm (PK and UK). Listed is every used segment with the number of raw clusters and the final cluster number after hybrid clustering with the given value of  $\varepsilon$ . The numbers of mixed cluster numbers of H and N denotes number of clusters containing vectors related to more than one subtype. The variance is calculated as the sum of the explained variance by the PCA.

Method	Segment	#Cluster			#Mixed		#Unclustered	$\varepsilon$	Var( $X$ )
		Final	Raw	Normalized	H	N			
PK	1	29	65	0.128	20	21	30	0.258	0.773
	2	39	63	0.124	18	18	21	0.285	0.756
	3	42	72	0.142	20	20	20	0.310	0.777
	4	56	67	0.132	2	41	6	0.191	0.739
	5	32	71	0.140	18	20	27	0.277	0.800
	6	44	58	0.114	30	3	9	0.215	0.754
	7	41	72	0.142	20	21	22	0.348	0.822
	8	37	61	0.120	18	19	20	0.311	0.826
UK	1	255	255	0.509	103	107	0	0.064	0.859
	2	222	222	0.443	88	89	0	0.066	0.849
	3	268	268	0.535	92	94	0	0.055	0.865
	4	266	266	0.531	2	104	0	0.043	0.846
	5	309	309	0.617	94	95	0	0.056	0.882
	6	271	271	0.541	90	4	0	0.035	0.855
	7	437	437	0.874	100	112	0	0.093	0.903
	8	360	360	0.719	111	111	0	0.089	0.899

the method in any case unusable for IAV clustering. Only the clustering of segment 4 with DBCV  $\varepsilon$  exploration (PD) seemed to be as stable as with the Kneedle Algorithm (PK). The number of clusters for the other segments was higher, because the DBCV method was searching for the  $\varepsilon$  value setting that results in the best DBCV. In all the segments except 4 this resulted in a value of zero. Hybrid clustering with a  $\varepsilon$  value of zero results in standard HDBSCAN clustering only and is, considering the amount of unclustered sequences, not suited for IAV clustering without the hybrid setting. Based on the results in Table 3.1.2 and Table 3.1.3, the best method for IAV clustering seemed to be the combination of PCA and the Kneedle Algorithm (PK). It resulted in an appropriate number of clusters and was the only combination using all the benefits of the hybrid HDBSCAN clustering.

To backup this assumption, the results were visualized for better understanding and analysis. Since investigation of all segments would overfill this section, only the methods PK, UK and UD and their clustering behavior on segment 4 were discussed in detail. As described, the PCA method in combination with the DBCV (PD) used only standard HDBSCAN, resulting in a very high number of clusters and 20% unclustered sequences. Therefore, the method is already rejected and not included in the following discussions. Nevertheless, all graphics for the other segments with all used method can be found in the Appendix A.

**Table 3.1.3 Clustering results with the DBCV.** The results of the clustering methods using the DBCV (PD and UD). Listed is every used segment with the number of raw clusters and the final cluster number after hybrid clustering with the given value of  $\varepsilon$ . The numbers of mixed cluster numbers of H and N denotes number of clusters containing vectors related to more than one subtype. The variance is calculated as the sum of the explained variance by the PCA.

Method	Segment	#Cluster		#Mixed		#Unclustered	$\varepsilon$	DBCV	Var( $X$ )
		Final	Raw	H	N				
PD	1	11,599	55,436	1,152	1,225	13,548	0.000	0.404	0.773
	2	11,596	55,292	1,067	1,169	13,457	0.000	0.417	0.756
	3	11,521	55,351	1,080	1,168	13,017	0.000	0.422	0.777
	4	51	58	2	38	4	0.200	0.572	0.739
	5	10,717	32,818	1,074	1,158	11,478	0.000	0.479	0.800
	6	11,143	34,600	713	3	12,065	0.000	0.455	0.754
	7	8,866	55,620	1,119	1,227	8,753	0.000	0.513	0.822
	8	9,189	55,563	1,125	1,225	9,794	0.000	0.493	0.826
UD	1	279	279	110	116	0	0.041	0.860	0.859
	2	242	242	92	93	0	0.052	0.838	0.849
	3	265	265	92	94	0	0.060	0.897	0.865
	4	261	261	2	103	0	0.049	0.891	0.846
	5	283	283	87	88	0	0.094	0.868	0.882
	6	255	255	85	4	0	0.061	0.919	0.855
	7	462	463	103	115	0	0.050	0.869	0.903
	8	364	364	111	111	0	0.079	0.868	0.899

A big difference in the cluster size distribution stand out, when comparing the method with PCA (PK) to the ones with UMAP (UK and UD). Only the method using PCA and the Kneedle Algorithm created clusters with more than 10000 vectors (Fig. 3.1.3c). The different cluster sizes using UMAP are spreaded more equally with no cluster of 3000 vectors or more (Fig. A.0.2c and Fig. A.0.3c). Since the UMAP methods also use prior PCA reduction, the major difference is the additional use of UMAP (Sec. 3.5). Therefore, the difference in cluster size distribution was most likely caused by UMAP. UMAP not only reduces the dimension of the data but also changes the position of the vectors in the embedded dimension according to the used settings. The `n_neighbors=100` setting seems to be most likely the cause of a change of this magnitude. By increasing the number of neighbors the vectors were more crowded in groups to support the bigger picture of the data and, therefore, seemed to build more crowded clusters of equal sizes.

With the distribution of segment 4 sequences in the data in Fig. 3.0.1a in mind, it was expected that a distribution of cluster sizes in segment 4 clustering would in fact approximate the distribution of the sequences in the former one. Therefore, a clustering with PCA in combination with Kneedle Algorithm exploration seemed to give the expected results and appears again as the best method for IAV clustering. Taking also the relation of the cluster number and the distance into consideration Fig. 3.1.3b indicated continuous merging of

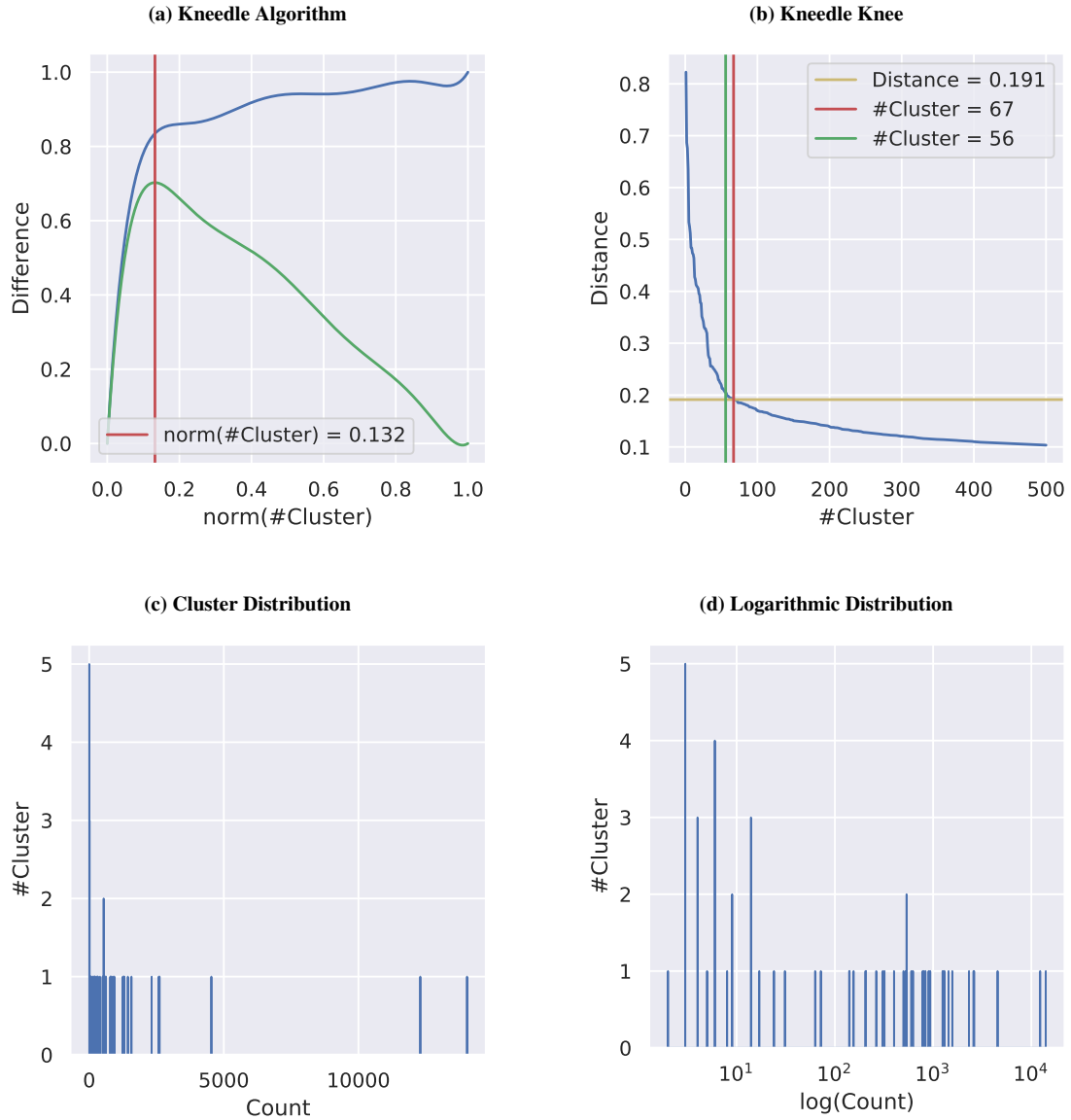


**Fig. 3.1.3 Clustering of segment 4 with PK.** Segment 4 clustering, using the combination of PCA and the Kneedle Algorithm (PK) results in the given figure. The green curve in the top left sub figure describes the change of the distance in the single linkage tree with increasing normalized cluster number and, therefore, the location of the knee, at the maximum, highlighted by the red line. The blue line is the inverse polynomial representation of the blue line in top right sub figure. The top right sub figure shows the absolute relation of the distance in the single linkage tree to the total number of clusters as the blue line. The red line, indicates the number of raw clusters, by the DBSCAN part of the hybrid HDBSCAN clustering and the final cluster number in green. The yellow line describes the threshold, extracted from the knee and, therefore, the  $\varepsilon$  value used to perform the hybrid clustering. The normalized cluster number in the red line in the top left sub figure is equivalent to the raw cluster number in the top right sub figure. The bottom sub figures give information about the distribution of the clusters sizes in continuous and logarithmic scale.

clusters with decreasing cluster number in the linkage tree and easily distinguishable knee point. The behavior is not present in Fig. A.0.3b and Fig. A.0.2b in a similar degree.

The results of the method using PCA in combination with the Kneedle Algorithm (PK)

were visualized by the cluster tree Fig. 3.1.4. Labeling of the tree was performed based on the HA antibody subtype as shown in Fig. 3.0.1a. Therefore, clusters only containing sequences of a given subtype are labeled as such. If a cluster only contained sequences of one subtype, plus some not classified sequences, the not classified sequences were declared as the subtype too. That way, a clear presentation of the subtype distribution by labeling was possible, since the not classified sequences were very likely to actually belong to an existing subtype when clustered that way. If they actually did not belong to a existing subtype, a cluster only containing these not classified sequences would most likely have occurred, which is not the case. Furthermore, the chance to eventually break the classification of subtypes by declaring not classified sequences to a existing subtype is not given. The clusters are not based on subtypes in any way and the visualization is only for guidance and not possible for any segments other than 4 and 6 anyway. Also, without this assignment of the not classified sequences, no presentation would be possible since they are distributed over mostly all clusters.

If a cluster contains sequences of more than one subtype plus some not classified sequences, no labeling was performed, since the cluster was not homogeneous for one subtype and a declaration of the unclassified was not possible. In the following the term vector is mostly replaced by sequence to aid the discussion in terms of tree placement and subtype relation. Since the vectors represent the sequences, the terms are linked to each other and used as synonyms.

The prime example of the not classified sequence annotation is the yellow colored cluster 29 of subtype H9 (Fig. 3.1.4 **A**). While the vectors of all sequences of subtype H9 are accumulated in this single cluster, the cluster size of 1569 is bigger than the number of H9 sequences in Fig. 3.0.1a with 1454. This is justified by the presence of 115 not classified sequences in the cluster which are declared as H9, since only H9 and unclassified sequences are present in the cluster. The declaration of the unclassified sequences to be the H9 sequences is supported by the very small evolutionary distance values for the unclassified sequences in comparison to a sample of H9 sequences from the same cluster (Table 3.1.4). The sequences were also compared to unclassified sequences from other clusters to prove the smaller evolutionary distance to H9 sequences. This comparison was performed to prove that, even when only used for visualization reasons, the annotation of not classified sequences in that way is most likely true.

The number of clusters for a given subtype of HA antibody seems to correspond roughly to the overview of sequences in Fig. 3.0.1a. Clusters of very low represented subtypes, like H15, contain mostly all the subtypes sequences, while the high represented subtypes sequences, like H1 and H3, are spreaded over more clusters.

**Table 3.1.4 Unclassified sequences in segment 4 cluster 29 with PK.** The multiple sequence alignments (MSAs) mean distance of the given sequences in comparison to a sample of H9 sequences of the same cluster and a sample of unclassified sequences present in other clusters. Only the first 20 columns are presented here, the full table can be found in the projects GitHub Repository<sup>1</sup>.

Accession	H9	unclassified
>CY125733	0.167	0.499
>KP286620	0.104	0.509
>KP286635	0.105	0.510
>CY206227	0.166	0.499
>MG042357	0.140	0.500
>MG957616	0.139	0.501
>MG957513	0.138	0.501
>MG957519	0.139	0.500
>MH791733	0.141	0.501
>MN209446	0.145	0.501
>MN209378	0.145	0.502
>KP416339	0.104	0.509
>KP416375	0.104	0.510
>KP416404	0.104	0.509
>KP415847	0.104	0.510
>KP416464	0.105	0.511
>KP415453	0.106	0.509
>KP286584	0.112	0.503
>KP414685	0.113	0.506
>KP415520	0.105	0.511
...	...	...

Striking anomalies divergent from the expected nearly uniform allocation of the subtypes in Fig. 3.1.3 are noted by **B**, **C** and **D** and are discussed in the following. For final acceptance of the method PK as the prime IAV clustering method proposed in this project, the cluster tree was compared to a similar one created on the results from method UK (Fig. A.0.4). While the labeling of the cluster tree of method PK resemble the subtype classification of IAV very closely, no recognizable subtype separation is present in the cluster tree of UK.

## 3.2 Database Annotation Errors

To evaluate the anomalies in Fig. 3.1.3 **B** and **C**, an evolutionary distance was calculated by MSA for every eventually misplaced sequence (Sec. 2.6). Therefore, the eventually misplaced sequence was compared to ten other sequences. A sample of five sequences from the same cluster related to the dominant subtype of the cluster, and a sample of five sequences with subtype equal to the misplaced sequence but from other clusters. The mean of distances was then calculated for both cases to rate the assignment and reveal

<sup>1</sup><https://github.com/ahenoch/Masterthesis.git>

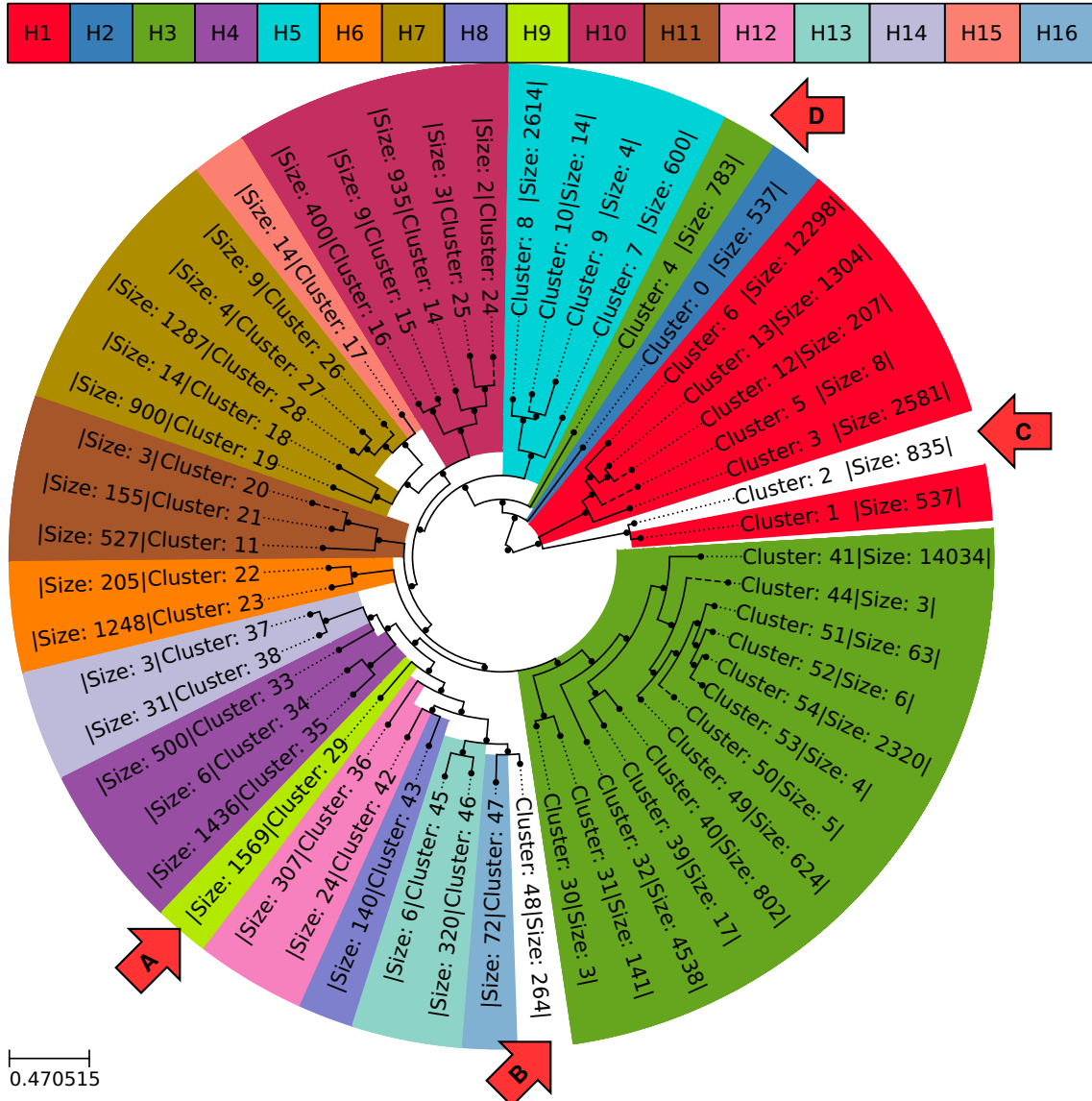


**Fig. 3.1.4 Clustering tree of segment 4 with PK.** The clustering tree of segment 4 clustering, using the combination of PCA and the Kneedle Algorithm (PK) (Fig. 3.1.3). The labeling of the clusters in the tree is based on the subtype of the contained sequences. Unclassified sequences of a cluster are reclassified as a given subtype if sequences of only this subtype are present in the cluster in addition to the unclassified ones. Unlabeled clusters contain sequences from at least two subtypes and zero or more unclassified sequences. Two clusters are mixed since containing sequences of more than one subtype (Table 3.1.2). These non homogeneous clusters are marked by **B** and **C**. The cluster 29 marked by **A** is an example for a cluster consisting of all sequences from a given subtype. The misplaced cluster from subtype H3 is marked by **D**. Dotted lines in the tree indicate the same host.

possible misannotations in the Influenza Research Database (IRD).

In case of Fig. 3.1.3 **C**, a single sequence with subtype H10 was classified as belonging to cluster 2 which other than that completely consists of H1 and unclassified sequences. By investigation on this possible misplacement, comparison with MSA was used. The results for this comparison in Table 3.2.5 points to the fact, that the as H10 annotated

**Table 3.2.5 Anomalies in segment 4 cluster 2 with PK.** The MSAs mean distance of the given sequences in comparison to a sample of H1 sequences of the same cluster and a sample of H10 sequences present in other clusters.

Accession	H1	H10
>MK237334	0.049	0.488

sequence with accession MK237334 is related to subtype H1. The mean of evolutionary distance based on MSAs with the sequence and a sample of cluster 0 H1 sequences was very low. Considering the large size of cluster 0 a higher difference was expected, pointing in direction of many very similar sequences in the cluster. Nevertheless, the evolutionary distance of the sequence in comparison to a sample of random H10 sequences was much higher (Table 3.2.5). Furthermore, only this sole sequence, annotated as subtype H10, was present in a cluster of over 900 sequences of H1 with a very low evolutionary distance to a sequence sample of the cluster, rendering the error most likely as a misannotation.

**Table 3.2.6 Anomalies in segment 4 cluster 48 with PK.** The MSAs mean distance of the given sequences in comparison to a sample of H16 sequences of the same cluster and a sample of H13 sequences present in another cluster. Only the first 20 columns are presented here, the full table can be found in the projects GitHub Repository<sup>2</sup>.

Accession	H16	H13
>MH498778	0.278	0.217
>MF682848	0.299	0.244
>KX979327	0.298	0.238
>KX978913	0.300	0.241
>KX979541	0.300	0.240
>KX978076	0.301	0.241
>KX978980	0.299	0.242
>KX979063	0.298	0.238
>KX978876	0.299	0.239
>KX979544	0.301	0.241
>KX979380	0.300	0.240
>MF682844	0.300	0.240
>KX978929	0.298	0.238
>MF575207	0.297	0.239
>KR087564	0.290	0.251
>MF147289	0.298	0.241
>MF147869	0.298	0.241
>CY185569	0.287	0.258
>CY185489	0.287	0.250
>MF461180	0.297	0.244
...	...	...

When comparing the distances for the same calculation performed on Fig. 3.1.3 C in

<sup>2</sup><https://github.com/ahenoch/Masterthesis.git>

Table 3.2.6, no decision for misannotation can be made. The dominant subtype in the cluster 48 is H16 but the sequences of subtype H13 that seem to be misplaced in the cluster have a smaller distance to the sample of sequences from subtype H13. The difference in distance to sample sequences of H13 as well as to sequences of H16 gave indeed no clear finding. Both results are quite similar and the misclustered sequences seem to share much sequence similarity with both subtypes. Maybe the misclustered sequences in cluster 48 point to a more complex classification. Cluster 48 remained a mixed cluster with many sequences from subtype H13 and H16 and, thus, was treated as clustering error. Therefore, subtype H13 and H16 are the focus of investigations of the clustering behavior in the following sections to reveal possible subdivisions responsible for the clustering error.

The last error involved cluster 4, that is homogeneous for subtype H3 but is split off the other H3 clusters by nearly all the non H3 clusters Fig. 3.1.3 **D**. By evaluation of the clusters relation with a MSA created guide tree generated from the centroid vectors sequences, the error persists (Fig. 3.2.5). Every of the 55 clusters have a sequence that should best represent the whole cluster, the centroid sequence, calculated as described in Sec. 2.6. When using the guide tree as comparison, the uniform color distribution stood out. Even the centroid of the mentioned cluster 4 is arranged in a line with all the centroids of clusters homogeneous for subtype H3. This subset of centroid sequences used for the guide tree might be too small for a sure proof, but still the centroid sequences should be the most meaningful ones representing the whole cluster and point to a clear subtype separation. Therefore cluster 4 and 48 (Fig. 3.1.3 **C** and **D**) remained as identified clustering mistakes and are further examined in the following.

### 3.3 K-mer Representation Quality

Investigation on the anomalies resulted in two persistent clustering errors (Fig. 3.1.3 **B** and **D**). To evaluate if the method is suitable for the clustering of IAV possible error sources are discussed.

By building a UPGMA tree with cosine distance calculation on the non-reduced segment 4 k-mer frequency vectors with  $4^7$  components of all the H13 and H16 sequences, the unbiased relation of sequences from these subtypes were analyzed (Fig. 2.6.8 pathway 7). These calculations require high computation power and are only possible due to the small amount of segment 4 H13 and H16 sequences. Since no component reduction was performed in this case the fundamental use of k-mer frequencies could be validated or rejected. The tree was labeled in a similar way to the previous ones. Therefore, aiding the visualization, unclassified sequences were declared as a given subtype based on the clusters

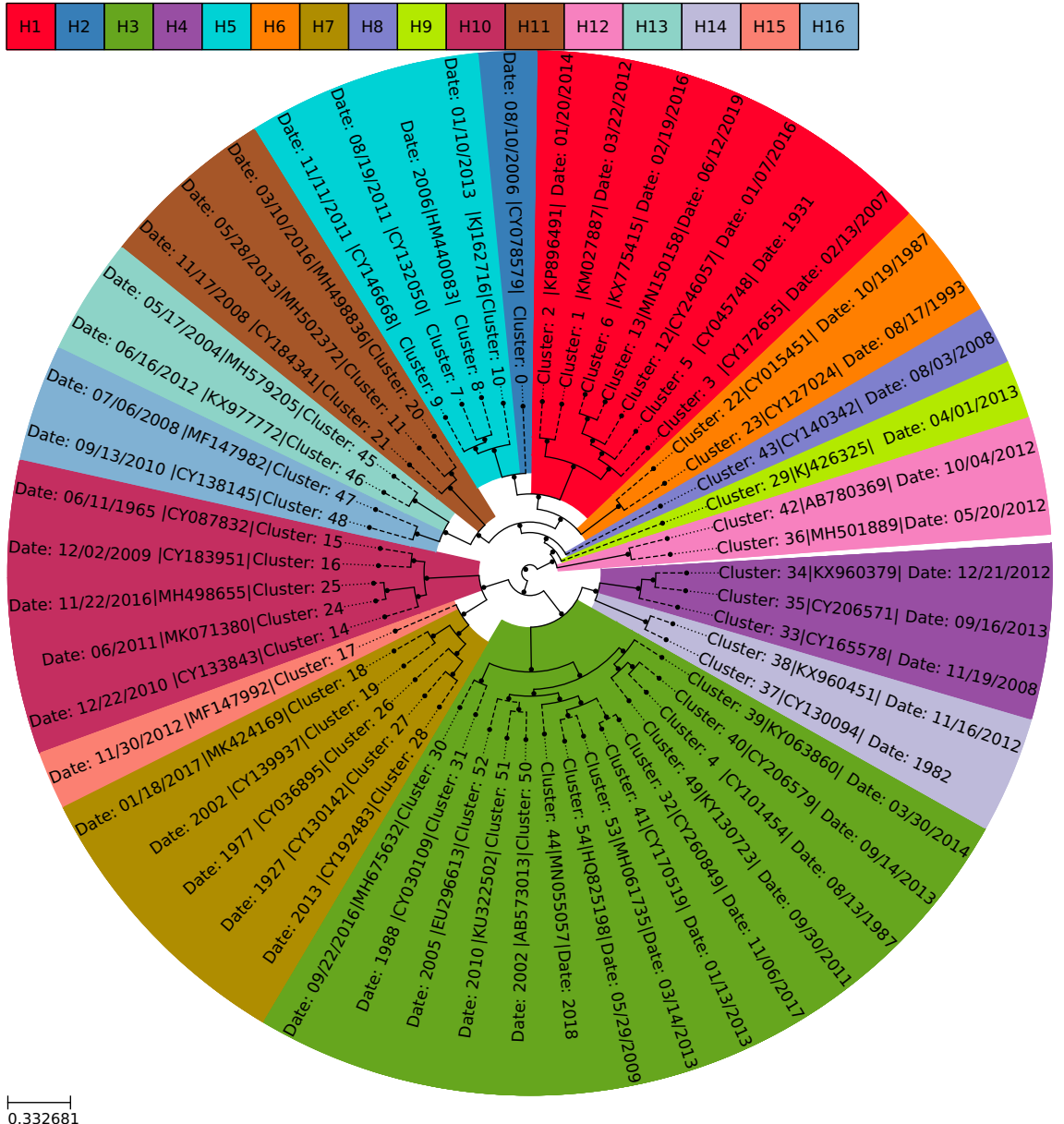


**Fig. 3.2.5 Centroid guidetree of segment 4 with PK.** The guide tree was created by building a MSA on the centroid sequences of clusters resulting from the PCA and Kneedle Algorithm (PK) pipeline. The coloring of the tree is based on the related subtype of the centroid sequence used for the MSA.

of Fig. 3.1.4 again. The small amount of not labeled sequences in the UPGMA tree are unclassified sequences, that also could not be assigned to a given subtype in the previous sections (not assigned sequences from mixed cluster 48). The labeling based on the clusters in Fig. 3.1.4 was used to better visualize the separation and also reversely evaluate the labeling too. Outstanding labeling mistakes breaking the uniform color separation would, thus, reject the assignment of not classified sequences, that was performed. All sequences in the UPGMA tree were also annotated by their cluster number in Fig. 3.1.4

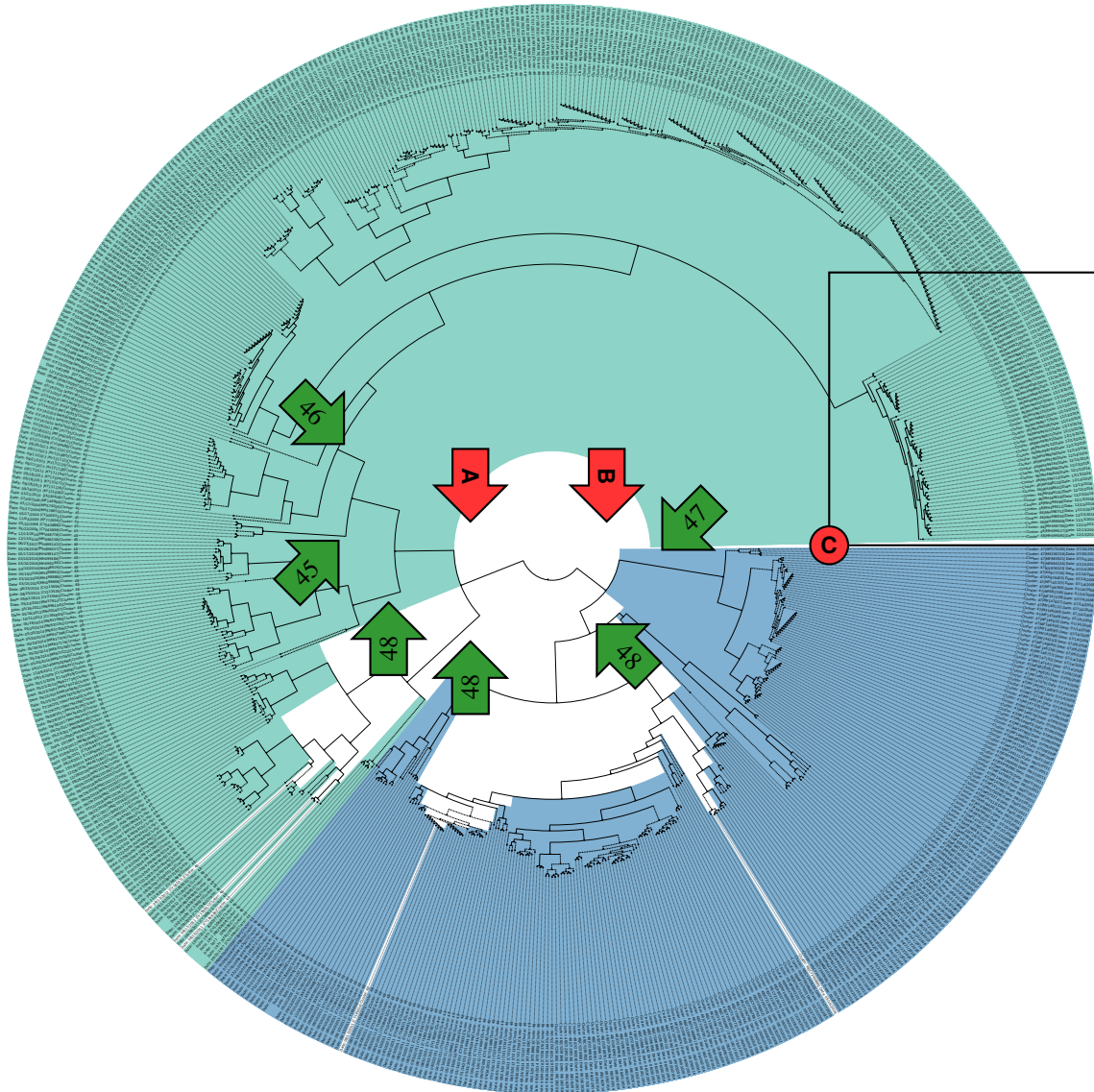


**Fig. 3.3.6 UPGMA tree of H13/H16 with cosine distance.** Calculated cosine distance between the k-mer frequency vectors of sequences related to subtype H13 and H16 clusters in Fig. 3.1.4 were used to build a unweighted pair group method with arithmetic mean (UPGMA) tree. The same coloring of the previous tree was used to clarify the difference between H13 and H16 sequences. Uncolored sequences are unclassified ones from the mixed cluster 48 and, thereby, not assigned to a single subtype. The numbers in the green arrows indicate the cluster number of the sub trees sequences in Fig. 3.1.4. The red arrows are used in the following to point to the trees division into H13 **A** and H16 **B**. Fig. 3.3.7 is an enlarged view on the highlighted square at **C**.

to enable better comparison. The green arrows indicate sub trees in the UPGMA tree containing the sequences assigned to a given cluster in the previous section. Sequences from cluster 46, 45 and 47 are contained in well separated sub trees, while the sequences of cluster 48 are spreaded over half the UPGMA tree. This finding is in line with Fig. 3.1.3 error **B** and Fig. 3.2.5 indicating the existence of a clear separation of both subtypes even when a degree of similarity might exists.

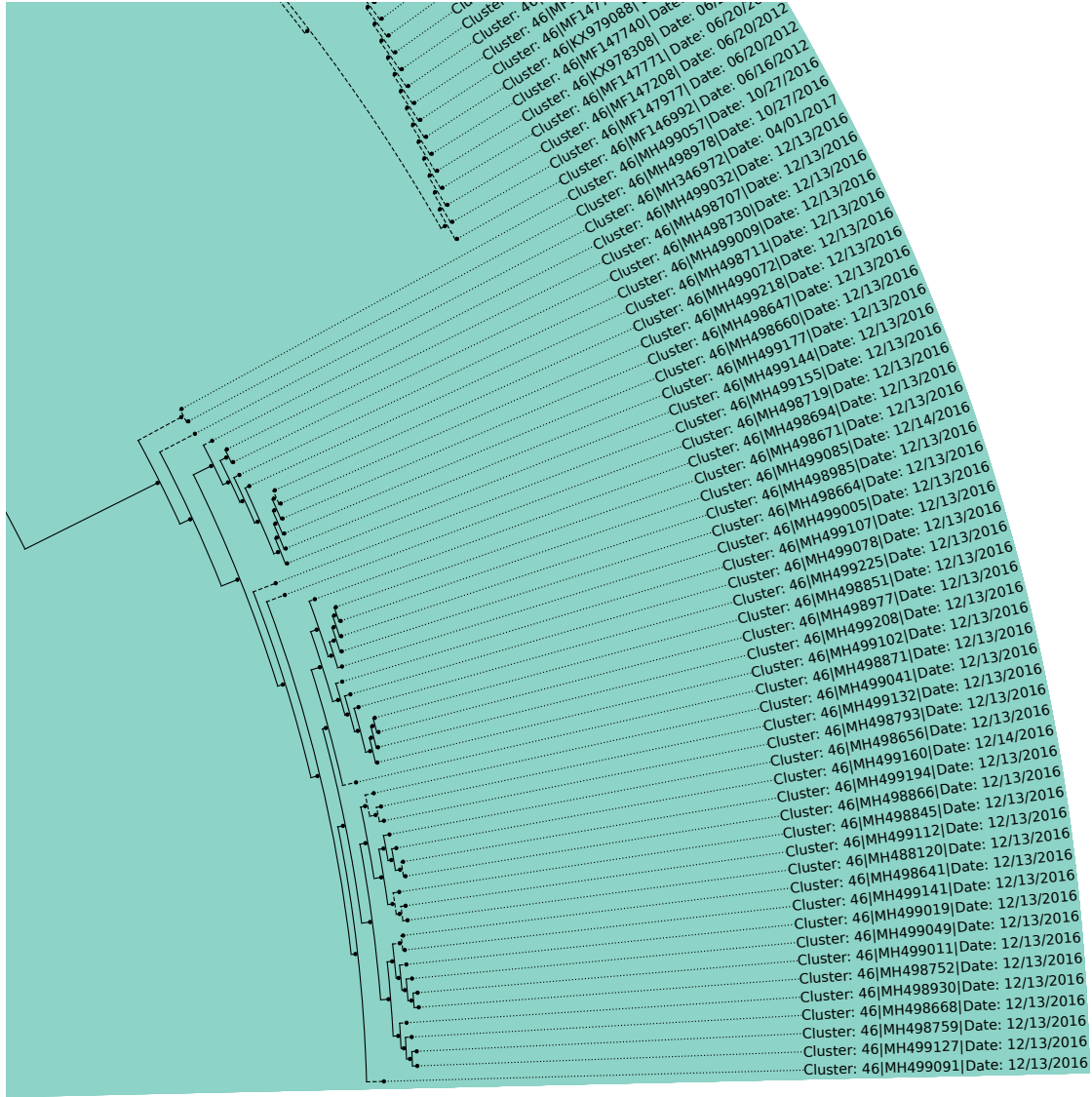


**Fig. 3.3.7 Relation of collection date and k-mer vector distance.** Enlarged view of the by **C** highlighted square in Fig. 3.3.6. The sequences were labeled according to their collection date to indicate the correlation of the close k-mer frequency vector distance in the tree with their sequences similarity. Labeling with the strain name could misleadingly point in a false direction, since the strain names indicate major difference while the sequences having very high similarity. Thereby the close distance of the vectors of sequences collected on the same date with high sequence similarity point to the precise representation by the k-mer frequency vectors.

While both subtypes in Fig. 3.3.6 are completely separated directly after the trees root, there are also subsequent subdivisions for both subtypes directly after that. This early subdivision can point to the existence of more subtle variations with major difference to each other than the existing subtype classification reveals. In this case it appears as if at least two subgroups for H13 and at least two or three subgroups for H16 exist. The threshold is difficult to define, as no clustering was performed here. Thereby, this statement is based only on the early subdivision in the UPGMA tree (Fig. 3.3.6 **A** and **B**). The exact

separation from the root is in line with the centroid guide tree based on MSA were both subtypes were completely separated too (Fig. 3.2.5). Since this is also in line with the subtype classification, the k-mer frequency approach seemed to work as expected in this project. Furthermore, when focusing on a portion of the UPGMA tree with very small distance in Fig. 3.3.6 **C**, the similar collection date of all these sequences (12/13/2016) stand out. The only sequences not from this collection date but, nevertheless, included in this sub tree are MH499057, MH498978, MH346972, MH499085, and MH499160. Two of the first three mentioned sequences are from the same collection date but some days prior to the rest, while the third was collected some days after the 12/13/2016. These three sequences are the last linked sequences in the sub tree with the highest distance in comparison to the rest and their collection date is nearly the same as for the rest. The other two sequences with different date MH499085 and MH499160 are in the middle of the sub tree but the collected just one day after the rest. This points in the direction that even small differences are noticed by the k-mer approach. The collection date was used as comparison here because many of the sequences in the sub tree have very different strain names but are almost or completely similar and, thereby, usage of the strain name instead could cause a misinterpretation. MH499085 of strain A/environment/Chile/C20369/2016 and MH498671 of strain A/white\_backed\_stilt/Chile/C20090/2016 differ by their strain names, as the virus was collected apparently completely different but the sequenced genomes are in fact 100% the same. Around the tree in nearly every case similar collection dates have a small distance based on the k-mer frequency vectors, supporting the statement of the usability of k-mer frequencies for IAV clustering. Same calculation for the precalculated UPGMA tree was also repeated with euclidean distance (Fig. A.0.6) with the same result.

## 3.4 Ground Truth for Clustering

Since the use of k-mer frequencies proved to be valid for IAV clustering, further investigation on the source of the persisting errors Fig. 3.1.3 **B** and **D** was performed. For investigation standard HDBSCAN clustering was used without hybrid setting and  $\varepsilon$  exploration on the same small subset of H13 and H16 sequences used in the previous section. Standard HDBCSCAN was used for simplification and minimization of error sources. Two clustering runs with different input were compared to find a ground truth and subsequently compared to a clustering on the same subset with a simple version of the PK method. The first input was the non-reduced set of k-mer frequency vectors used in Sec. 3.3 as pre-calculated cosine distance matrix (Fig. 2.6.8 pathway **8**). HDBSCAN can use precalculated distances as input instead of vectors. Therefore, no distance calculation is performed by HDBSCAN. Precalculated distances on  $n$  vectors create matrices of size  $n \times n$ , therefore,

precalculation is very RAM intensive and not usable on a high number of sequences. Still, since this approach involves no dimension reduction and less calculation by the clustering tool, thereby less error sources, the resulting clustering can be used as ground truth. The result of the clustering was visualized as a cluster-tree (Fig. 3.4.8).

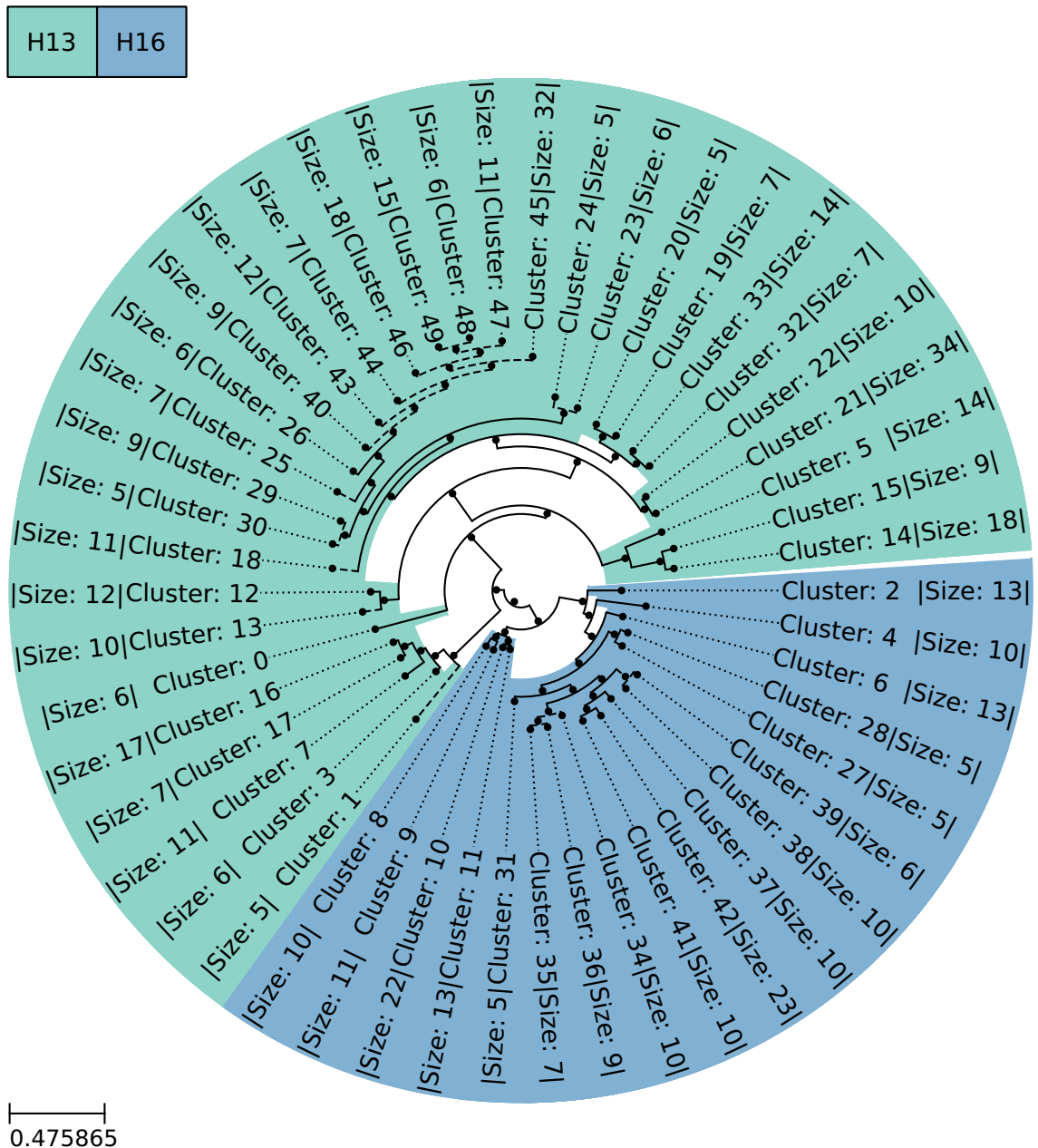


**Fig. 3.4.8 Simple clustering tree of H13/H16 with cosine distance.** Cluster tree, based on the clustering by simple HDBSCAN without any  $\varepsilon$  exploration and hybrid clustering. The matrix used contained precalculated cosine distances of all the k-mer frequency vectors to each other. The used vectors were calculated from the sequences, present in the H13 and H16 clusters in Fig. 3.1.4 without reduction with PCA or UMAP. Therefore, HDBSCAN was used with precalculation input instead of a distance metric.

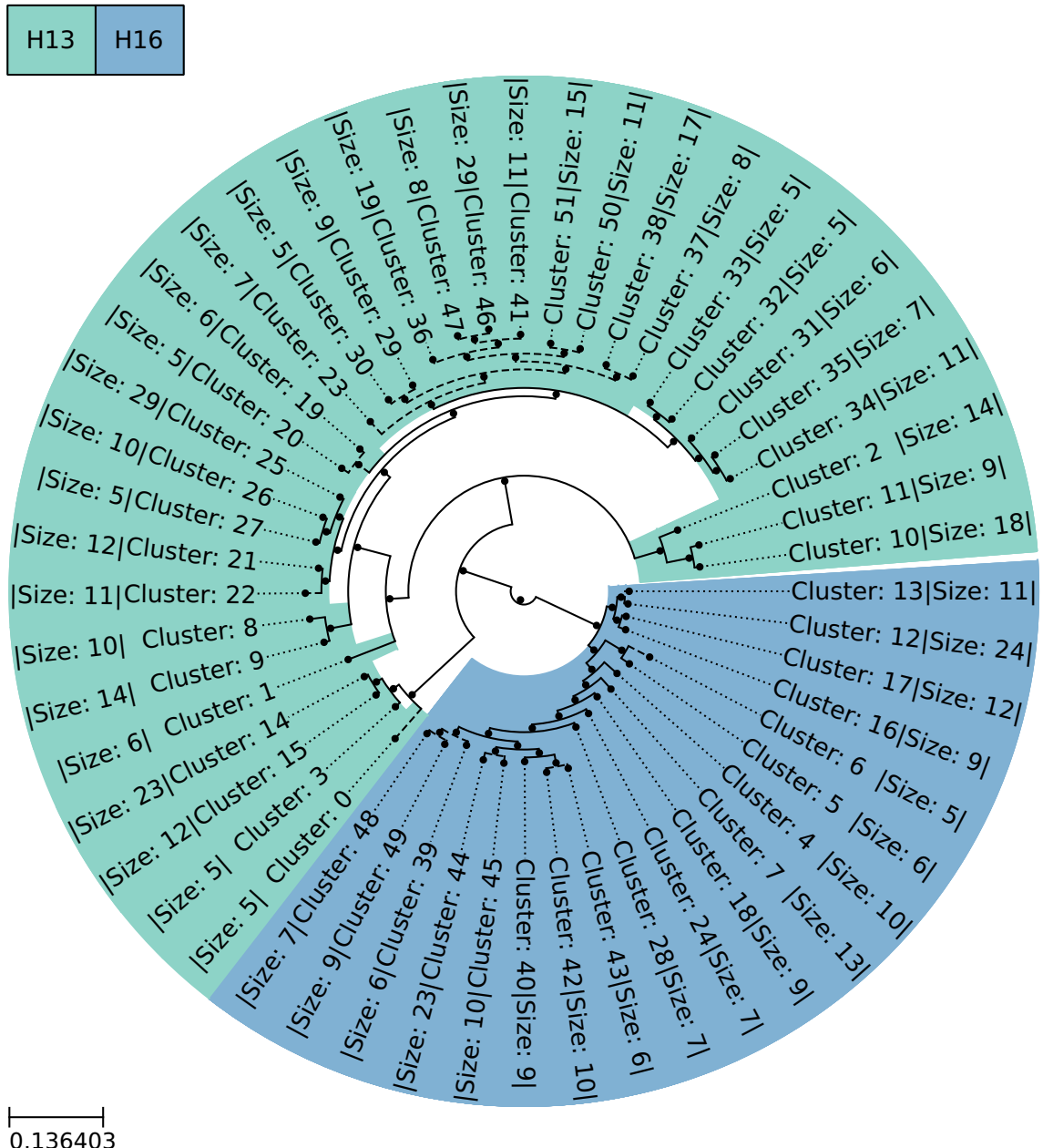


**Fig. 3.4.9 Simple clustering tree of H13/H16 with evolutionary distance.** Cluster tree, based on the clustering by simple HDBSCAN without any  $\varepsilon$  exploration and hybrid clustering. The matrix used contained precalculated MSA based distances of all the sequences to each other. The sequences, present in the H13 and H16 clusters in Fig. 3.1.4 were used for the MSA. Therefore, HDBSCAN was used with precalculation input instead of a distance metric.

In a similar manner to the precalculated UPGMA tree in Fig. 3.3.6, the subtypes are completely separated and split on both sides in two subgroups. This points to the fact, that the HDBSCAN clustering of the precalculated cosine distances of the k-mer frequencies are as usable as the k-mer frequencies itself and are able to draw a clear line to separate

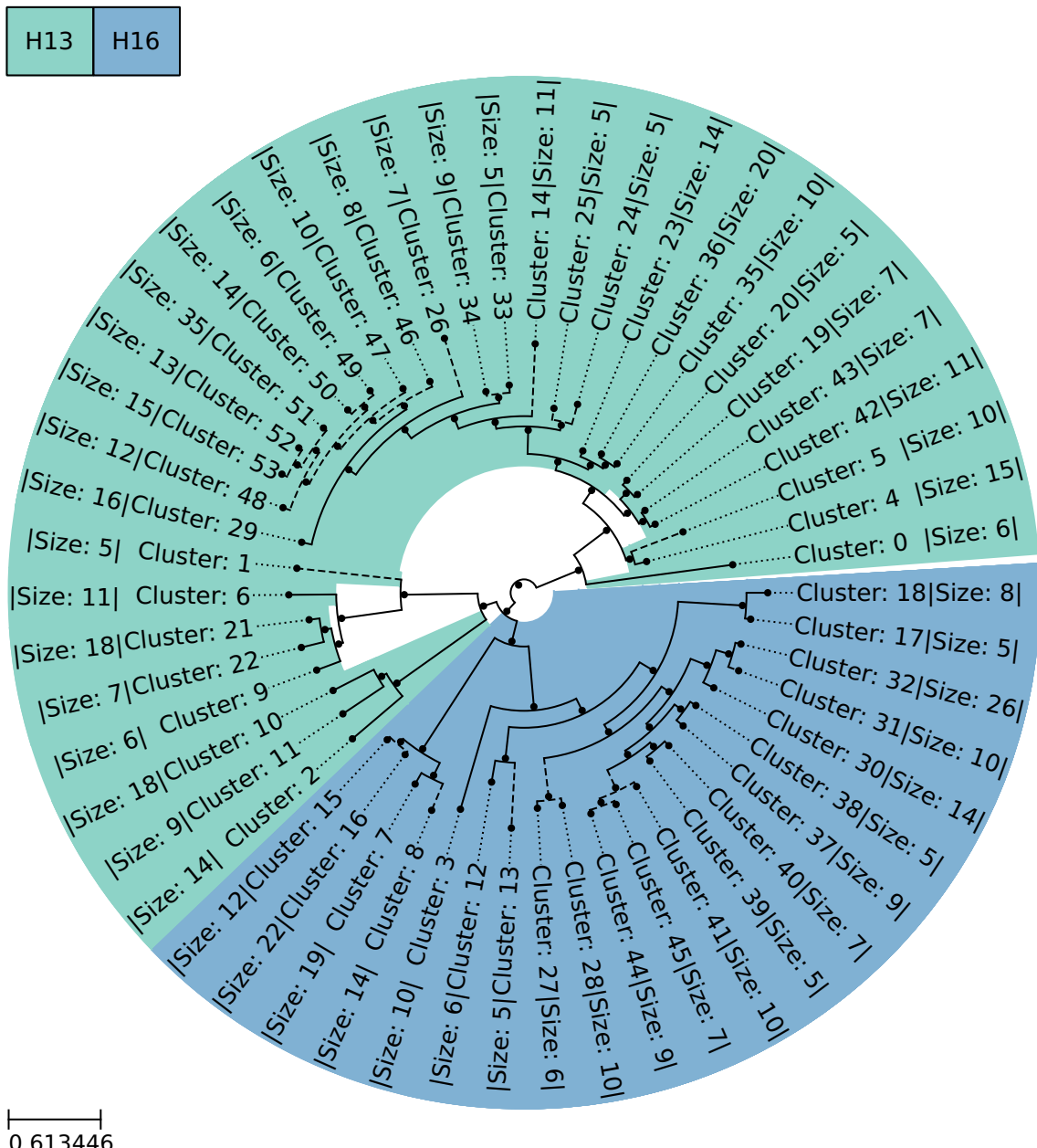


**Fig. 3.4.10 Simple clustering tree of H13/H16 with PCA.** Cluster tree, based on the clustering by simple HDBSCAN without any  $\varepsilon$  exploration and hybrid clustering. The used vectors were calculated from the sequences, present in the H13 and H16 clusters in Fig. 3.1.4 with prior PCA reduction to 30 dimensions.

the subtypes. This finding is in line with the second cluster tree based on similar clustering on the same sequences with evolutionary distances of a MSA instead (Fig. 2.6.9 pathway 6). The same separation is even more obvious, as the subtypes sub trees are farther away from the separation at the trees root. On the side of the H13 sequences, a subdivision is also clearly noticeable. Subgroups in the H16 sequences are, on the other hand, not that clear separated in Fig. 3.4.9. Maybe the different distances between the

subtypes and the subgroups on each side of the subtypes is different because evolutionary aspects like nucleotides that are more likely to change are involved in the MSA. In the k-mer frequencies, the pure constellation of nucleotides is used, evolutionary aspects are neglected. Still, the precalculated approach as well as the MSA evolutionary distances used the full information available from the sequences themselves, since no reduction with PCA or UMAP was performed and both indicate full subtype separation. Therefore these cluster trees (Fig. 3.4.8 and Fig. 3.4.9) are the only ground truth for H13/H16 clustering with HDBSCAN available. As already mentioned precalculated clustering with HDBSCAN, is a highly computationally expensive, as the matrices of size  $n \times n$  have to be calculated and saved to be used in HDBSCAN. The calculation is, therefore, not possible without the availability of major RAM space. When using HDBSCAN with the k-mer vectors posterior to reduction with PCA to 30 dimensions, only a matrix of size  $n \times 30$  has to be saved without the necessity of any distance precalculation. This is a **major** reduction of computational power necessary. A third clustering tree using reduced vectors on the same H13/H16 sequences should therefore represent the previous trees as best as possible. As described in Sec. 3.1 the method using PCA and the Kneedle Algorithm was declared as best method for IAV clustering (PK). In the comparison by standard HDBSCAN clustering without  $\varepsilon$  exploration, the sole reduction with PCA, representing simplified PK method should, match the ground truth (Fig. 3.4.10).

Unfortunately, some major differences between the clustering trees using PCA and the two trees using precalculated cosine distance MSA evolutionary distance stood out (Fig. 3.4.8, Fig. 3.4.9 and Fig. 3.4.10). The same clustering behavior as in the complete cluster tree in the previous section can be observed as no clear separation on the H13 and H16 clusters is present (Fig. 3.4.10 and Fig. 3.1.4 **B**). Since the distance calculation by HDBSCAN only used in the third tree is proportional to cosine precalculation (Fig. 3.5.11), the PCA or dimension reduction step seems to be the origin of the clustering error in Fig. 3.1.3 **B** and **D**.

As already mentioned, the precalculated cluster trees use the whole available amount of information given by the sequences. Either by direct use of the nucleotide comparisons with MSA (Fig. 3.4.9) or by using the k-mer frequency vectors without reducing the dimension (Fig. 3.4.8). Thus, the amount of information remaining in the vectors did not seem to suffice for the given task resulting in the differences in Fig. 3.4.10. The standard HDBSCAN clustering was also performed with the same subset of H13 and H16 sequences reduced with UMAP posterior to PCA (Fig. A.0.8) with results inferior to the sole use of PCA. In the appendix, a precalculated cluster tree using euclidean distance instead of cosine distance is also present, offering a similar result to the one using cosine distance

(Fig. A.0.7).

## 3.5 Differences in Dimension Reduction

To investigate the processing behavior prior to the clustering and, thereby, find explanations for the mentioned errors, the small H13 and H16 subset of segment 4 k-mer frequencies, were reduced by PCA and UMAP to two components for in detail visualization. Comparison to UMAP was done although the method was already declared as not appropriate, to validate this statement again and see the impact of different neighbor values.

The target of the reduction prior to the HDBSCAN clustering, was to find a representation of the data that is most suitable to be used for the clustering, by preserving the information with a lower complexity. As explained in Sec. 3.3 and Sec. 3.4 the optimal representation of the vectors should make a clear difference between H13 and H16 and is, thereby, also used as the ground truth in the following. Since the vectors are visualized in two dimensions, the term point instead of vector is used.

The visualization of the reduction by PCA is denoted as neighbors value -1 (Fig. 3.5.11). It shows five different accumulations of points. Labeling of these points is based on the original clustering example in Fig. 3.1.3. This is becoming apparent when focusing on the cluster 48 points containing H13 and H16 sequences. That way a fundamental distribution on the points of H13 and H16 can be reviewed as well.

The reduction with PCA on the subset results in easy separable accumulations of the cluster 46 and 48 points in Fig. 3.5.11 (neighbors = -1). The distribution of these points is basically in line with the result shown in Fig. 3.1.3, as their accumulations are well separated, building the two clusters with the same sequences in both figures. The major difference, however, is the distance between the accumulations of cluster 48 points to each other as well as to the ones of cluster 47. This would probably result in a imaginary clustering of unchanged cluster 46 and 45 and two or three clusters consisting of the cluster 48 points of which one also contains the points of cluster 47. It seems as if the distance of the cluster 47 points and the H13 cluster 48 points is largely affected by the reduction. The difference between cluster 46 and 45 in the Fig. 3.5.11 (neighbors = -1) picture is on the other hand preserved and would result in clustering similar to Fig. 3.1.3. In Fig. 3.1.3 cluster 47 and 48 are also relatively close related as they would be linked on the next higher tree-node.

In Fig. 3.5.11 (neighbors = -1) it appears as if the points of cluster 47 and 48 are possibly quite similar, which is not the case as the Fig. 3.3.6 sub trees clearly show the wanted

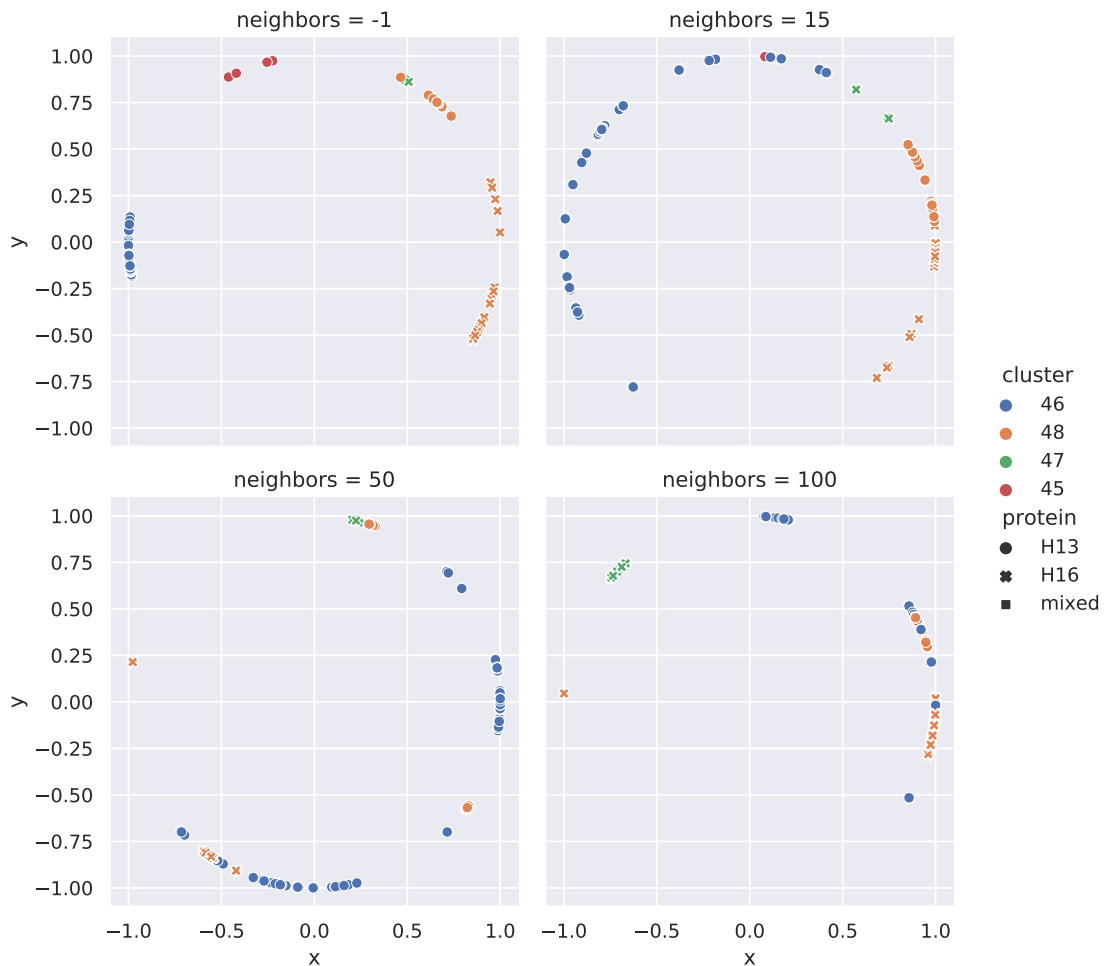


**Fig. 3.5.11 Comparison of H13/H16 component reductions.** The subset of sequences from the H13 and H16 cluster in Fig. 3.1.4 were reduced down to two dimensions enabling simple visualization. Cluster labeling was performed according to Fig. 3.1.4. Sole use of PCA (top left picture) as well as the combination with UMAP (other three pictures) was performed as described in Sec. 3.5 with the reduction to two components for visualization. For the combination of PCA and UMAP different values for the neighbors setting were used, the UMAP standard value 15, a average value 50 and the standard value of this project 100. The subtype of the sequences were labeled by different types of points.

separation of H13 and H16 in cluster 48 as well as the wanted distance to 47. Keeping the lower complexity in mind, the consequence of lowering the dimension by PCA to two dimension seems to preserve most of the information related to the difference of cluster 45 and 46. The difference of the subtype separation inside 48 as well as the overall difference to 47 seems on the other hand to be lost completely and cause the unwanted effects. Since the ground truth separation of Fig. 3.3.6 seems to be partially present in Fig. 3.1.3, by at least separating 47 completely from 48, the higher number of dimensions might be in direct connection to the correct separation of some part of H13 and H16. Therefore, the number of components should be increased to the maximum of 50, that still preserves all

functions of HDBSCAN for spanning-tree building.

Comparing these results to the use of UMAP with different settings of the neighbors value, the impact of this parameter becomes clear. The higher the value, the more crowded the points. This also explains the crowded behavior in Fig. 3.0.2b. Since a neighbors value of 100 was used as standard in this project, the values are overall crowded in groups of at least 100 points. The random subset for Fig. 3.0.2b was reduced by the same setting with UMAP despite the small sample size used there. The small random sample in addition to a high neighbors value resulted in a low number of overall distribution to clarify this behavior. Aside from the example in Fig. 3.0.2b the usage of a high neighbors value through the project was well reasoned and based on the huge size of the dataset used as described in Sec. 3.5. The same value as well as 15 and 50 neighbors was used on the subset of H13 and H16 segment 4 sequences to visualize the difference.

None of the settings results in a separation as good as with the sole use of PCA. With the UMAP standard neighbors value of 15 all the points are next to each other and there is no reasonable cluster building possible Fig. 3.5.11 (neighbors = 15). Furthermore, H13 points would be merged with H16 points before merging with others from H13, thereby breaking the subtype division similar to the PCA use. Aside from the fact that the other points, when using PCA, are well separated. Setting the neighbors value to 50 results in a spreading of the cluster 46 points and mixing with little islands of cluster 48 points Fig. 3.5.11 (neighbors = 50). With a neighbors value of 100 a separation into imaginary clusters is possible, when ignoring the cluster labeling and only taking the subtypes labeling into consideration. This is, therefore, the only setting with use of UMAP that would provide a more or less reasonable separation of the subtypes in imaginary clusters. However, clusters of different subtypes are closer than to similar subtypes, resulting also in no real subtype separation, even when ignoring the cluster 47 points that might be very sensible to the magnitude of preserved information.

In conclusion, the use of PCA gives the best results compared the ones with UMAP. Still there are challenges to overcome as could be seen with the position of the cluster 47 points. Maybe increasing the information preserved by the PCA would give clearer results as assumed. This project aimed to find high-quality representations of IAV genomes for the purpose of clustering in a extend that was never reached before. Therefore, the usability of hybrid HDBSCAN with parameters as good as possible was of higher importance than the use of UMAP at all costs. In the results of the project PCA performed better than UMAP but only with all the tested parameters. Thus, it might be possible to find parameters for UMAP not explored in this project to represent the genomes even better in a equal low-dimension

in the future. Also, change of UMAP in favor of t-SNE could be tested in terms of vector representation quality.

### 3.6 A New Classification



**Fig. 3.6.12 Clustering tree of segment 4.** The cluster tree of segment 4 clustering, using the combination of PCA and the Kneedle Algorithm (PK) with a reduction to 50 instead of 30 dimensions (Fig. 3.1.3). The coloring of the clusters in the tree is based on the subtype of the contained sequences. Unclassified sequences of a cluster are reclassified as a given subtype if sequences of only this subtype are present in the cluster in addition to the unclassified ones. Uncolored clusters contain sequences from at least two subtypes and zero or more unclassified sequences. Dotted lines in the tree indicate the same host.

Reannotation of the most likely false annotated sequence in Fig. 3.1.4 C as well as

increasing of the components in PCA successfully raised the accuracy of the pipeline. Thus, the clustering was performed according to the PK method, that proved to give the most stable results, with 50 components reduction instead of 30. Clustering errors found in the previous section were resolved successfully as H13 and H16 are now completely divided, with the mentioned small but still present difference between these subtypes. Also, all clusters of H3 are now present in direct connection to each other and no cluster not homogeneous for one subtype exist anymore.

Resulting from this improved clustering of segment 4 a new classification involving 57 groups instead of 18 subtypes is proposed (Fig. 3.6.12). By pairwise comparison of random 10 sequence samples of these groups the similarity inside these groups is described in Fig. 3.6.13. To avoid creating a bias, the result for accidental comparisons of sequences with the same accession are ignored and not considered in calculations of respective mean values. Samples of 10 sequences were used due to the high amount of computational power that is necessary for this calculation. For segment 4 calculation involves  $10^2$  pairwise alignments, for every of the 57 clusters to each other. Making  $57^2 \cdot 10^2$  calculations.

All clusters in Fig. 3.6.13 have the highest similarities with themselves and mostly high similarities with clusters of the same subtype. For instance cluster 0, share some degree of sequence identity with other clusters stemming from the same subtype H1, as shown in Fig. 3.6.13. However, the highest similarity of around 90% is only shared with other sequences of the cluster itself, which makes this cluster very self contained.

Exceptions for the relative high similarity to other clusters of the same subtypes are the subtypes H7 and H15 with the clusters 45 to 50, as well as H4 and H14 with clusters 35 to 38. There was no clear separation performed as the clusters merge with other subtypes in higher tree nodes, although other clusters of the same subtype are still available (Fig. 3.6.12). The similarities of these cluster, are also high compared to the other subtype and indicate a relation neglected by the current subtype classification. The almost uniform H7 subtree of clusters 45, 46, 48, 49, and 50 is divided by the one and only cluster of subtype H15 cluster 47. When comparing the sequence similarities in Fig. 3.6.13, the highest similarity persist inside the clusters themselves, but the cross similarities of cluster 45 and 46 to 47, 48, 49, and 50 are around 65% without big difference between subtype H7 and H15. Further pointing to more subtle but present differences between and inside of the current subtypes.

With this pipeline blueprint created by adjusting the clustering for segment 4 in the previous sections, all IAV segments could be clustered the same way, since no subtype information

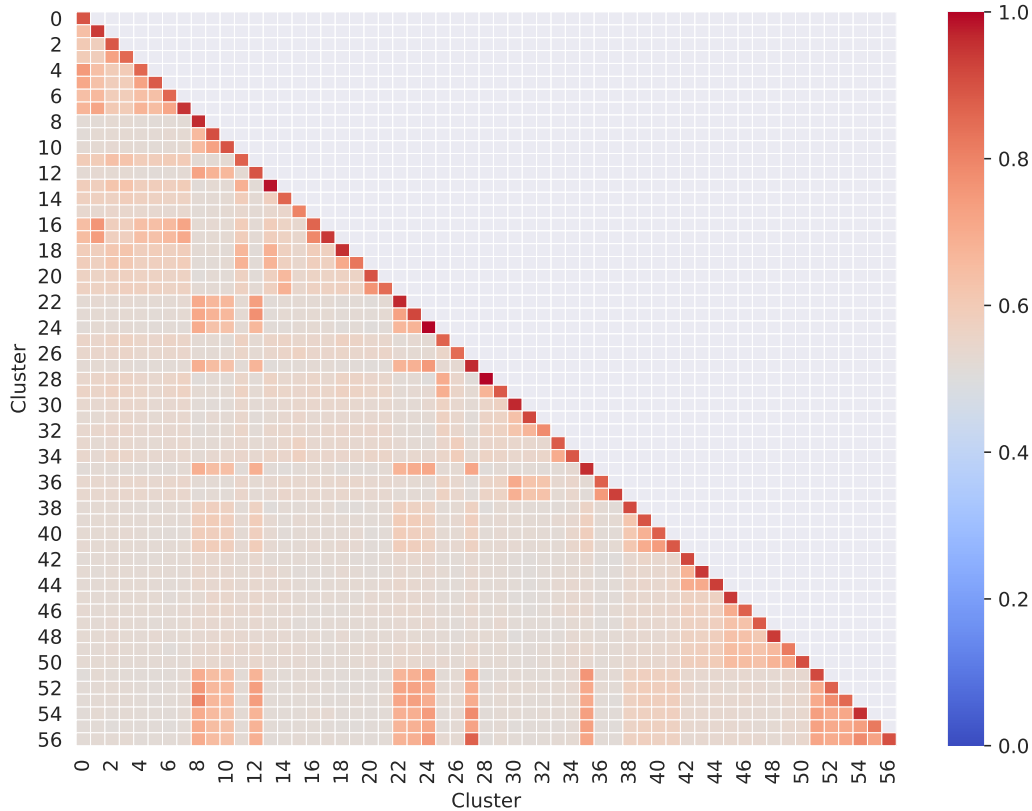


**Fig. 3.6.13 Similarity matrix of segment 4 clusters.** Random samples of up to 10 sequences of every cluster in Fig. 3.6.12 were compared by pairwise alignments with the samples of all other clusters. Less than 10 sequences were only used in clusters containing less than 10 sequences. The percentage of similarity was calculated for every alignment making a matrix of up to  $10 \times 10$  holding the similarity values of the samples comparisons. The mean of the matrix was then calculated and written as the given cluster interactions mean similarity. This was repeated for every possible cluster interaction resulting in the presented figure. Interactions of the same clusters were reduced to only different sequences, results of alignments with sequences having the same accession were removed, thereby, preventing bias creation. The mean of these up to 100 comparisons for every cluster interaction are colored according to their similarity from 1.0 or 100% similarity in red to 0.0 or 0% similarity in blue.

is necessary for the clustering. Coloring of the tree was performed as guideline and was the only part involving actual sequence position to subtype evaluation. Thereby, the clustering trees for other segments, except segment 6, are unlabeled. All other cluster trees and similarity matrix graphics, as well as tables containing sequence cluster assignment and the tables containing the values used to create the graphics are presented in the Appendix A. Hereby new classifications for all segments based on k-mer frequency vectors are proposed, containing 28 groups for segment 1, 28 for two, 29 for three, the shown 57 for segment 4, 26 for five, 40 for six, 30 for seven and 24 groups for segment 8.

The groups of the segments one to three, five, seven, and eight share by far more overall similarity, therefore, less clusters were created. Still, the similarity inside the clusters

themselves is higher than the cross similarity and, thereby, solid clustering by the proposed clustering method was possible despite the overall higher similarity (Appendix A). Higher similarity of the segments not encoding the surface protein is most likely reasoned by the lower evolutionary pressure. The higher pressure of the surface proteins is necessary to ensure infection of the host cells.

While the clusters of segment 4 seem to be very self contained and give a good representation on possible subdivisions inside the subtypes, the trees based on evolutionary distances increase the subtypes distance even more (Fig. 3.2.5 and Fig. 3.4.9). Present day research propose a phylogenetic tree of IAV that is split in four subtrees [35]. The subdivisions are mostly present in the clustering tree in Fig. 3.6.12. Still, there are some difference primarily the higher-ranking structure of the subtypes. In Wei et al. [35] subtype H3 is contained in a subtree alongside H4 and H14 and H9 in a subtree with H8 and H12. This relations are not present in Fig. 3.6.12. Though, other subtrees contain subtypes similar to the proposed phylogenetic tree in Wei et al. [35]. Aside from that, the order of the subtrees in Fig. 3.6.12 do not match the one from the phylogenetic tree.

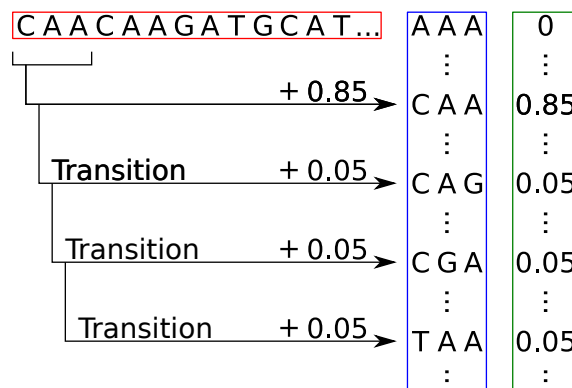


**Fig. 3.6.14 7-mer vector calculation involving transitions.** An example genomic sequence (red box) is splitted into 3-mers. The sequences 3-mers are then compared to the list of all  $4^3$  possible 3-mer constellations (blue box). Based on the occurrence number of the lists 3-mers in the sequence a vector with  $4^3$  components is created (green box).

As already mentioned the proposed method for IAV clustering did not acknowledge evolutionary distances. Transitions and transversion for example are handled as nucleotide differences without a higher or lower chance of change. When including mutation chances in the k-mer frequency clustering, the relation of whole subtypes subtrees might improve and give a result more similar to the one proposed in Wei et al. [35]. Because HDBCSCAN only uses existing distance metrics, when not using the precalculated option, which should be avoided at any case, the k-mer frequency vectors themselves have to be changed in some way. Therefore, Fig. 3.6.14 illustrate a possible option for inclusion of evolution inside k-mer frequency vectors, by considering all mutations of a given k-mer with low represen-

tation value. Vectors containing k-mers only apart with single mutations are, thus, closer to each other in the high-dimensional vector space. The magnitude of these values have to be considered wisely and should be subject of future research optimizing the proposed clustering even more.

## 4 Conclusions & Outlook

The existing classification of *Influenza A Virus* (IAV) is solely based on the surface proteins and gives, therefore, no insight on the differences of the other segments. While many publications exist, involving evolutionary research on these, as well as, the other segments, that propose subgroups or clusters, most are based on alignments for comparison [66, 30, 67]. Present day alignment methods offer accurate insight of sequence relation. Nevertheless, downsides of the use of multiple sequence alignments (MSAs) for the clustering of IAV is the high number of available sequences and, thus, the necessity of high nearly unfeasible computational power, when involving all of them. Even with the hardware available a threshold for usability at a given number of sequences still exist or a drop of alignment quality is unavoidable. The usage of precalculation on the non-reduced k-mer frequency vectors mentioned in this project is another method aside from MSA involving no dimension reduction methods. The exhibited results are, indeed, of mostly equal quality to the MSA as shown in Sec. 3.4 and drawing a similar clear line between subtypes. Still, similar downsides exist also, making scaling to the enormous number of existing IAV sequences nearly impossible and render both methods mostly usable on smaller subsets.

This project proposed a method scale-able to a much higher degree for clustering all segments of IAV, that is usable on multi-core computers with around 32Gb of RAM available. The fast execution time of the method makes it usable to even cluster novel sequenced IAV genomes with the existing ones to find associated well-known strains in short time. The dimension reduction with PCA proved to preserve the necessary amount of information for robust clustering and with the Kneedle Algorithm a solid threshold was defined. The present day version of the method already produced self contained clusters, with a higher order mostly in line with the current subtypes classification. Furthermore, increasing the amount of informations by reasonable subdivision in smaller subordinated groups. Still, there are options to fathom in the future to possibly produce even better results.

Including measurement possibilities for evolutionary distances by slight changes in the vector creation process as described in Sec. 3.6 could possibly improve the accuracy

in terms of comparison to MSAs. While PCA as tool for dimension reduction performed sufficient enough, the usage of a methods offering better low dimension representations and higher information preservation of the vectors could be beneficial. Therefore, repeating the comparisons to PCA with t-SNE instead of UMAP might be rewarding.

Still, the results point in the direction of a bioinformatical IAV classification with more subdivisions as the known subtypes classification can offer. Renewing the classification in that way and, thereby, including more subtle differences might considerably improve future large scale *in silico* secondary structure analyses. With better and more self contained subgroups of IAV searching for conserved structures and would make a step ahead and could offer new insight to the IAV.

# Bibliography

- [1] DS Schmeller, F Courchamp, and G Killeen. “Biodiversity loss, emerging pathogens and human health risks”. In: *Biodiversity and Conservation* 29.11 (2020), pp. 3095–3102. doi: 10.1007/s10531-020-02021-6.
- [2] KE Jones, NG Patel, MA Levy, A Storeygard, D Balk, JL Gittleman, and P Daszak. “Global trends in emerging infectious diseases”. In: *Nature* 451.7181 (2008), pp. 990–993. doi: 10.1038/nature06536.
- [3] LH Taylor, SM Latham, and ME woolhouse. “Risk factors for human disease emergence”. In: *Philosophical Transactions of the Royal Society of London. Series B: Biological Sciences* 356.1411 (2001). Ed. by MEJ Woolhouse and C Dye, pp. 983–989. doi: 10.1098/rstb.2001.0888.
- [4] K Van Reeth. “Avian and swine influenza viruses: our current understanding of the zoonotic risk”. In: *Veterinary Research* 38.2 (2007), pp. 243–260. doi: 10.1051/vetres:2006062.
- [5] PM Sharp and BH Hahn. “Origins of HIV and the AIDS Pandemic”. In: *Cold Spring Harbor Perspectives in Medicine* 1.1 (2011), a006841. doi: 10.1101/cshperspect.a006841.
- [6] N Suwantarat and A Apisarnthanarak. “Risks to healthcare workers with emerging diseases: lessons from MERS-CoV, Ebola, SARS, and avian flu”. In: *Current Opinion in Infectious Diseases* 28.4 (2015), pp. 349–361. doi: 10.1097/QCO.0000000000000183.
- [7] R Verity, LC Okell, I Dorigatti, P Winskill, C Whittaker, N Imai, G Cuomo-Dannenburg, H Thompson, PGT Walker, H Fu, A Dighe, JT Griffin, M Baguelin, S Bhatia, A Boonyasiri, A Cori, Z Cucunubá, R FitzJohn, K Gaythorpe, W Green, A Hamlet, W Hinsley, D Laydon, G Nedjati-Gilani, S Riley, S van Elsland, E Volz, H Wang, Y Wang, X Xi, CA Donnelly, AC Ghani, and NM Ferguson. “Estimates of the severity of coronavirus disease 2019: a model-based analysis”. In: *The Lancet Infectious Diseases* 20.6 (2020), pp. 669–677. doi: 10.1016/S1473-3099(20)30243-7.

- [8] J Wahlgren. “Influenza A viruses: an ecology review”. In: *Infection Ecology & Epidemiology* 1.1 (2011), p. 6004. doi: 10.3402/iee.v1i0.6004. (Visited on 06/26/2021).
- [9] J Gea-Banacloche, RT Johnson, A Basic, JA Butman, PR Murray, and AG Agrawal. “West Nile Virus: Pathogenesis and Therapeutic Options”. In: *Annals of Internal Medicine* 140.7 (2004), p. 545. doi: 10.7326/0003-4819-140-7-200404060-00015.
- [10] “Chapter 17 Pandemics: Risks, Impacts, and Mitigation”. In: *Disease Control Priorities, Third Edition (Volume 9): Improving Health and Reducing Poverty*. Ed. by DT Jamison, H Gelband, S Horton, P Jha, R Laxminarayan, CN Mock, and R Nugent. The World Bank, 2017. ISBN: 978-1-4648-0527-1.
- [11] I Julkunen, K Melén, M Nyqvist, J Pirhonen, T Sareneva, and S Matikainen. “Inflammatory responses in influenza A virus infection”. In: *Vaccine* 19 (2000), S32–S37. doi: 10.1016/S0264-410X(00)00275-9.
- [12] J Oxford and D Hockley. “Chapter 15 Orthomyxoviridae”. In: *Perspectives in Medical Virology*. Vol. 3. Elsevier, 1987, pp. 213–232. ISBN: 978-0-444-80879-0.
- [13] D Mudhakir and H Harashima. “Learning from the Viral Journey: How to Enter Cells and How to Overcome Intracellular Barriers to Reach the Nucleus”. In: *The AAPS Journal* 11.1 (2009), p. 65. doi: 10.1208/s12248-009-9080-9.
- [14] A Cann. “Chapter 2 Particles”. In: *Principles of molecular virology*. Sixth edition. Amsterdam: Elsevier/AP, Academic Press is an imprint of Elsevier, 2016. ISBN: 978-0-12-801946-7.
- [15] IA Schaap, F Eghiaian, A des Georges, and C Veigel. “Effect of Envelope Proteins on the Mechanical Properties of Influenza Virus”. In: *Journal of Biological Chemistry* 287.49 (2012), pp. 41078–41088. doi: 10.1074/jbc.M112.412726.
- [16] IA Wilson, JJ Skehel, and DC Wiley. “Structure of the haemagglutinin membrane glycoprotein of influenza virus at 3 Å resolution”. In: *Nature* 289.5796 (1981), pp. 366–373. doi: 10.1038/289366a0.
- [17] JN Varghese, WG Laver, and PM Colman. “Structure of the influenza virus glycoprotein antigen neuraminidase at 2.9 Å resolution”. In: *Nature* 303.5912 (1983), pp. 35–40. doi: 10.1038/303035a0.
- [18] RM Pielak and JJ Chou. “Influenza M2 proton channels”. In: *Biochimica et Biophysica Acta (BBA) - Biomembranes* 1808.2 (2011), pp. 522–529. doi: 10.1016/j.bbamem.2010.04.015.

- [19] A Ali, RT Avalos, E Ponimaskin, and DP Nayak. “Influenza Virus Assembly: Effect of Influenza Virus Glycoproteins on the Membrane Association of M1 Protein”. In: *Journal of Virology* 74.18 (2000), pp. 8709–8719. doi: 10.1128/JVI.74.18.8709-8719.2000.
- [20] AJ Eisfeld, G Neumann, and Y Kawaoka. “At the centre: influenza A virus ribonucleoproteins”. In: *Nature Reviews Microbiology* 13.1 (2015), pp. 28–41. doi: 10.1038/nrmicro3367.
- [21] E Area, J Martin-Benito, P Gastaminza, E Torreira, JM Valpuesta, JL Carrascosa, and J Ortín. “3D structure of the influenza virus polymerase complex: Localization of subunit domains”. In: *Proceedings of the National Academy of Sciences* 101.1 (2004), pp. 308–313. doi: 10.1073/pnas.0307127101.
- [22] E Jourdain, G Gunnarsson, J Wahlgren, N Latorre-Margalef, C Bröjer, S Sahlin, L Svensson, J Waldenström, Å Lundkvist, and B Olsen. “Influenza Virus in a Natural Host, the Mallard: Experimental Infection Data”. In: *PLoS ONE* 5.1 (2010). Ed. by J Chave, e8935. doi: 10.1371/journal.pone.0008935.
- [23] H Kida, R Yanagawa, and Y Matsuoka. “Duck influenza lacking evidence of disease signs and immune response”. In: *Infection and Immunity* 30.2 (1980), pp. 547–553. doi: 10.1128/iai.30.2.547-553.1980.
- [24] RG Webster. “Chapter 14 Antigenic Variation in Influenza Viruses”. In: *Origin and Evolution of Viruses*. Elsevier, 1999, pp. 377–390. ISBN: 978-0-12-220360-2.
- [25] S Duffy. “Why are RNA virus mutation rates so damn high?” In: *PLOS Biology* 16.8 (2018), e3000003. doi: 10.1371/journal.pbio.3000003.
- [26] JK Pfeiffer and K Kirkegaard. “Increased Fidelity Reduces Poliovirus Fitness and Virulence under Selective Pressure in Mice”. In: *PLoS Pathogens* 1.2 (2005). Ed. by M Manchester, e11. doi: 10.1371/journal.ppat.0010011.
- [27] R Belshaw, A Gardner, A Rambaut, and OG Pybus. “Pacing a small cage: mutation and RNA viruses”. In: *Trends in Ecology & Evolution* 23.4 (2008), pp. 188–193. doi: 10.1016/j.tree.2007.11.010.
- [28] M Vignuzzi and R Andino. “Closing the gap: the challenges in converging theoretical, computational, experimental and real-life studies in virus evolution”. In: *Current Opinion in Virology* 2.5 (2012), pp. 515–518. doi: 10.1016/j.coviro.2012.09.008.
- [29] J Parker. “Errors and alternatives in reading the universal genetic code”. In: *Microbiological Reviews* 53.3 (1989), pp. 273–298. doi: 10.1128/mr.53.3.273-298.1989.

- [30] MI Nelson, C Viboud, L Simonsen, RT Bennett, SB Griesemer, K St. George, J Taylor, DJ Spiro, NA Sengamalay, E Ghedin, JK Taubenberger, and EC Holmes. “Multiple Reassortment Events in the Evolutionary History of H1N1 Influenza A Virus Since 1918”. In: *PLoS Pathogens* 4.2 (2008). Ed. by Y Kawaoka, e1000012. doi: 10.1371/journal.ppat.1000012.
- [31] LL Shu, YP Lin, SM Wright, KF Shortridge, and RG Webster. “Evidence for Interspecies Transmission and Reassortment of Influenza A Viruses in Pigs in Southern China”. In: *Virology* 202.2 (1994), pp. 825–833. doi: 10.1006/viro.1994.1404.
- [32] J Steel and AC Lowen. “Influenza A Virus Reassortment”. In: *Influenza Pathogenesis and Control - Volume I*. Ed. by RW Compans and MBA Oldstone. Vol. 385. Cham: Springer International Publishing, 2014, pp. 377–401. ISBN: 978-3-319-11154-4.
- [33] SS Wong and RJ Webby. “Traditional and New Influenza Vaccines”. In: *Clinical Microbiology Reviews* 26.3 (2013), pp. 476–492. doi: 10.1128/CMR.00097-12.
- [34] IG Barr, J McCauley, N Cox, R Daniels, OG Engelhardt, K Fukuda, G Grohmann, A Hay, A Kelso, A Klimov, T Odagiri, D Smith, C Russell, M Tashiro, R Webby, J Wood, Z Ye, and W Zhang. “Epidemiological, antigenic and genetic characteristics of seasonal influenza A(H1N1), A(H3N2) and B influenza viruses: Basis for the WHO recommendation on the composition of influenza vaccines for use in the 2009–2010 Northern Hemisphere season”. In: *Vaccine* 28.5 (2010), pp. 1156–1167. doi: 10.1016/j.vaccine.2009.11.043.
- [35] CJ Wei, MC Crank, J Shiver, BS Graham, JR Mascola, and GJ Nabel. “Next-generation influenza vaccines: opportunities and challenges”. In: *Nature Reviews Drug Discovery* 19.4 (2020), pp. 239–252. doi: 10.1038/s41573-019-0056-x.
- [36] B Dadonaite, B Gilbertson, ML Knight, S Trifkovic, S Rockman, A Laederach, LE Brown, E Fodor, and DLV Bauer. “The structure of the influenza A virus genome”. In: *Nature Microbiology* 4.11 (2019), pp. 1781–1789. doi: 10.1038/s41564-019-0513-7.
- [37] PG Higgs. “RNA secondary structure: physical and computational aspects”. In: *Quarterly Reviews of Biophysics* 33.3 (2000), pp. 199–253. doi: 10.1017/S0033583500003620.
- [38] JS Kieft. “Viral IRES RNA structures and ribosome interactions”. In: *Trends in Biochemical Sciences* 33.6 (2008), pp. 274–283. doi: 10.1016/j.tibs.2008.04.007.

- [39] WN Moss, SF Priore, and DH Turner. “Identification of potential conserved RNA secondary structure throughout influenza A coding regions”. In: *RNA* 17.6 (2011), pp. 991–1011. doi: 10.1261/rna.2619511.
- [40] MJ Smola, GM Rice, S Busan, NA Siegfried, and KM Weeks. “Selective 2'-hydroxyl acylation analyzed by primer extension and mutational profiling (SHAPE-MaP) for direct, versatile and accurate RNA structure analysis”. In: *Nature Protocols* 10.11 (2015), pp. 1643–1669. doi: 10.1038/nprot.2015.103.
- [41] Anaconda Software Distribution. *Anaconda*. 2020. URL: <https://anaconda.com>.
- [42] PJ Cock, T Antao, JT Chang, BA Chapman, CJ Cox, A Dalke, I Friedberg, T Hamelryck, F Kauff, B Wilczynski, et al. “Biopython: freely available Python tools for computational molecular biology and bioinformatics”. In: *Bioinformatics* 25.11 (2009). Publisher: Oxford University Press, pp. 1422–1423.
- [43] J Huerta-Cepas, F Serra, and P Bork. “ETE 3: Reconstruction, Analysis, and Visualization of Phylogenomic Data”. In: *Molecular Biology and Evolution* 33.6 (2016), pp. 1635–1638. doi: 10.1093/molbev/msw046.
- [44] L McInnes, J Healy, and S Astels. “hdbscan: Hierarchical density based clustering”. In: *The Journal of Open Source Software* 2.11 (2017), p. 205. doi: 10.21105/joss.00205.
- [45] V Satopaa, J Albrecht, D Irwin, and B Raghavan. “Finding a "Kneedle" in a Haystack: Detecting Knee Points in System Behavior”. In: *2011 31st International Conference on Distributed Computing Systems Workshops (ICDCS Workshops)* (2011), pp. 166–171. doi: 10.1109/ICDCSW.2011.20.
- [46] K Katoh and DM Standley. “MAFFT Multiple Sequence Alignment Software Version 7: Improvements in Performance and Usability”. In: *Molecular Biology and Evolution* 30.4 (2013), pp. 772–780. doi: 10.1093/molbev/mst010.
- [47] CR Harris, KJ Millman, SJvd Walt, R Gommers, P Virtanen, D Cournapeau, E Wieser, J Taylor, S Berg, NJ Smith, R Kern, M Picus, S Hoyer, MHv Kerkwijk, M Brett, A Haldane, JFd Río, M Wiebe, P Peterson, P Gérard-Marchant, K Sheppard, T Reddy, W Weckesser, H Abbasi, C Gohlke, and TE Oliphant. “Array programming with NumPy”. In: *Nature* 585.7825 (2020), pp. 357–362. doi: 10.1038/s41586-020-2649-2.
- [48] W McKinney. “Data Structures for Statistical Computing in Python”. In: *Proceedings of the 9th Python in Science Conference*. Ed. by Svd Walt and J Millman. 2010, pp. 56–61. doi: 10.25080/Majora-92bf1922-00a.

- [49] ML Waskom. “seaborn: statistical data visualization”. In: *Journal of Open Source Software* 6.60 (2021), p. 3021. doi: 10.21105/joss.03021.
- [50] F Pedregosa, G Varoquaux, A Gramfort, V Michel, B Thirion, O Grisel, M Blondel, P Prettenhofer, R Weiss, V Dubourg, J Vanderplas, A Passos, D Cournapeau, M Brucher, M Perrot, and E Duchesnay. “Scikit-learn: Machine Learning in Python”. In: *Journal of Machine Learning Research* 12 (2011), pp. 2825–2830.
- [51] SciPy 1.0 Contributors, P Virtanen, R Gommers, TE Oliphant, M Haberland, T Reddy, D Cournapeau, E Burovski, P Peterson, W Weckesser, J Bright, SJ van der Walt, M Brett, J Wilson, KJ Millman, N Mayorov, ARJ Nelson, E Jones, R Kern, E Larson, CJ Carey, İ Polat, Y Feng, EW Moore, J VanderPlas, D Laxalde, J Perktold, R Cimrman, I Henriksen, EA Quintero, CR Harris, AM Archibald, AH Ribeiro, F Pedregosa, and P van Mulbregt. “SciPy 1.0: fundamental algorithms for scientific computing in Python”. In: *Nature Methods* 17.3 (2020), pp. 261–272. doi: 10.1038/s41592-019-0686-2.
- [52] L McInnes, J Healy, and J Melville. “UMAP: Uniform Manifold Approximation and Projection for Dimension Reduction”. In: (2020). URL: <http://arxiv.org/abs/1802.03426>.
- [53] A Viehweger, M Hoelzer, and C Brandt. “Addressing dereplication crisis: Taxonomy-free reduction of massive genome collections using embeddings of protein content”. In: (2019). doi: 10.1101/855262.
- [54] A Viehweger, S Krautwurst, DH Parks, B König, and M Marz. “An encoding of genome content for machine learning”. In: (2019). doi: 10.1101/524280.
- [55] K Pearson. “LIII. *On lines and planes of closest fit to systems of points in space*”. In: *The London, Edinburgh, and Dublin Philosophical Magazine and Journal of Science* 2.11 (1901), pp. 559–572. doi: 10.1080/14786440109462720.
- [56] LVD Maaten and GE Hinton. “Visualizing Data using t-SNE”. In: *Journal of Machine Learning Research* 9 (2008), pp. 2579–2605.
- [57] RJGB Campello, D Moulavi, A Zimek, and J Sander. “Hierarchical Density Estimates for Data Clustering, Visualization, and Outlier Detection”. In: *ACM Transactions on Knowledge Discovery from Data* 10.1 (2015), pp. 1–51. doi: 10.1145/2733381.
- [58] RJGB Campello, D Moulavi, and J Sander. “Density-Based Clustering Based on Hierarchical Density Estimates”. In: *Advances in Knowledge Discovery and Data Mining*. Ed. by J Pei, VS Tseng, L Cao, H Motoda, and G Xu. Red. by D Hutchison, T Kanade, J Kittler, JM Kleinberg, F Mattern, JC Mitchell, M Naor, O Nierstrasz,

- C Pandu Rangan, B Steffen, M Sudan, D Terzopoulos, D Tygar, MY Vardi, and G Weikum. Vol. 7819. Springer Berlin Heidelberg, 2013, pp. 160–172. ISBN: 978-3-642-37455-5.
- [59] C Malzer and M Baum. “A Hybrid Approach To Hierarchical Density-based Cluster Selection”. In: *2020 IEEE International Conference on Multisensor Fusion and Integration for Intelligent Systems (MFI)*. IEEE, 2020, pp. 223–228. doi: 10.1109/MFI49285.2020.9235263.
- [60] D Moulavi, PA Jaskowiak, RJGB Campello, A Zimek, and J Sander. “Density-Based Clustering Validation”. In: *Proceedings of the 2014 SIAM International Conference on Data Mining* (2014), pp. 839–847. doi: 10.1137/1.9781611973440.96.
- [61] M Ester, HP Kriegel, J Sander, and X Xiaowei. “A density-based algorithm for discovering clusters in large spatial databases with noise”. In: (1996). URL: <https://www.osti.gov/biblio/421283>.
- [62] E Schubert, J Sander, M Ester, HP Kriegel, and X Xu. “DBSCAN Revisited, Revisited: Why and How You Should (Still) Use DBSCAN”. In: *ACM Transactions on Database Systems* 42.3 (2017), pp. 1–21. doi: 10.1145/3068335.
- [63] E Maor. *Trigonometric delights*. Princeton science library. Princeton, NJ: Princeton University Press, 2013. ISBN: 978-0-691-15820-4.
- [64] YM Deng, N Spirason, P Iannello, L Jolley, H Lau, and IG Barr. “A simplified Sanger sequencing method for full genome sequencing of multiple subtypes of human influenza A viruses”. In: *Journal of Clinical Virology* 68 (2015), pp. 43–48. doi: 10.1016/j.jcv.2015.04.019.
- [65] “A revision of the system of nomenclature for influenza viruses: a WHO memorandum”. In: *Bulletin of the World Health Organization* 58.4 (1980), pp. 585–591. URL: <https://pubmed.ncbi.nlm.nih.gov/6969132/>.
- [66] DL Suarez. “Evolution of avian influenza viruses”. In: *Veterinary Microbiology* 74.1 (May 2000), pp. 15–27. doi: 10.1016/S0378-1135(00)00161-9.
- [67] WHO/OIE/FAO H5N1 Evolution Working Group. “Continued evolution of highly pathogenic avian influenza A (H5N1): updated nomenclature: H5N1 clade nomenclature update”. In: *Influenza and Other Respiratory Viruses* 6.1 (2012), pp. 1–5. doi: 10.1111/j.1750-2659.2011.00298.x.



---

# List of Figures

1.2.1	<i>Orthomyxoviridae</i>	6
1.6.2	Clustering methods	9
2.1.1	Preprocessing pipeline	13
2.1.2	Clustering pipeline	13
2.1.3	Postprocessing pipeline	13
2.2.4	K-mer vector creation	14
2.4.5	Hybrid clustering threshold	17
2.4.6	Chord calculation background	18
2.4.7	Mutual reachability calculation	20
2.6.8	Precalculation pipeline	21
2.6.9	Alignment pipeline	21
3.0.1	Antigen subtype frequency	24
3.0.2	Cosine distance approximation	25
3.1.3	Clustering of segment 4 with PK	29
3.1.4	Clustering tree of segment 4 with PK	32
3.2.5	Centroid guidetree of segment 4 with PK	35
3.3.6	UPGMA tree of H13/H16 with cosine distance	36
3.3.7	Relation of collection date and k-mer vector distance	37
3.4.8	Simple clustering tree of H13/H16 with cosine distance	39
3.4.9	Simple clustering tree of H13/H16 with evolutionary distance	40
3.4.10	Simple clustering tree of H13/H16 with PCA	41
3.5.11	Comparison of H13/H16 component reductions	44
3.6.12	Clustering tree of segment 4	46
3.6.13	Similarity matrix of segment 4 clusters	48
3.6.14	7-mer vector calculation involving transitions	49
A.0.1	Clustering of segment 4 with PD	67
A.0.2	Clustering of segment 4 with UD	68
A.0.3	Clustering of segment 4 with UK	69
A.0.4	Clustering tree of segment 4 with UK	70

A.0.5	Centroid guidetree of segment 4 with UK . . . . .	72
A.0.6	UPGMA tree of H13/H16 with euclidean distance . . . . .	73
A.0.7	Simple clustering tree of H13/H16 with euclidean distance . . . . .	74
A.0.8	Simple clustering tree of H13/H16 with UMAP . . . . .	75
A.0.9	Clustering of segment 1 . . . . .	77
A.0.10	Clustering tree of segment 1 . . . . .	78
A.0.11	Similarity matrix of segment 1 clusters . . . . .	79
A.0.12	Clustering of segment 2 . . . . .	80
A.0.13	Clustering tree of segment 2 . . . . .	81
A.0.14	Similarity matrix of segment 2 clusters . . . . .	82
A.0.15	Clustering of segment 3 . . . . .	83
A.0.16	Clustering tree of segment 3 . . . . .	84
A.0.17	Similarity matrix of segment 3 clusters . . . . .	85
A.0.18	Clustering of segment 4 . . . . .	86
A.0.19	Clustering of segment 5 . . . . .	87
A.0.20	Clustering tree of segment 5 . . . . .	88
A.0.21	Similarity matrix of segment 5 clusters . . . . .	89
A.0.22	Clustering of segment 6 . . . . .	90
A.0.23	Clustering tree of segment 6 . . . . .	91
A.0.24	Similarity matrix of segment 6 clusters . . . . .	92
A.0.25	Clustering of segment 7 . . . . .	93
A.0.26	Clustering tree of segment 7 . . . . .	94
A.0.27	Similarity matrix of segment 7 clusters . . . . .	95
A.0.28	Clustering of segment 8 . . . . .	96
A.0.29	Clustering tree of segment 8 . . . . .	97
A.0.30	Similarity matrix of segment 8 clusters . . . . .	98

# List of Tables

2.1.1	Pipeline tools . . . . .	11
2.1.2	Search parameter . . . . .	12
2.1.3	Summary of the clustering methods . . . . .	12
3.0.1	Explained variance by different PCA settings . . . . .	25
3.1.2	Clustering results with the Kneedle Algorithm . . . . .	27
3.1.3	Clustering results with the DBCV . . . . .	28
3.1.4	Unclassified sequences in segment 4 cluster 29 with PK . . . . .	31
3.2.5	Anomalies in segment 4 cluster 2 with PK . . . . .	33
3.2.6	Anomalies in segment 4 cluster 48 with PK . . . . .	33
A.0.1	Cluster database with PK . . . . .	65
A.0.2	Cluster database with UK . . . . .	66
A.0.3	Anomalies in segment 4 cluster 105 with UK . . . . .	71
A.0.4	Anomalies in segment 4 cluster 265 with UK . . . . .	71
A.0.5	Clustering results . . . . .	76
A.0.6	Cluster database . . . . .	76



# A Appendix

**Table A.0.1 Cluster database with PK..**

Accession	Segment	Cluster	H	Centroid	N	Strain
>CY021716	1	0	H1	False	N1	A/AA/Huston/1945
>CY020292	1	0	H1	False	N1	A/AA/Marton/1943
>CY083917	1	9	H1	False	N1	A/Aalborg/INS132/2009
>CY063613	1	9	H1	False	N1	A/Aalborg/INS133/2009
>CY073732	1	9	H1	False	N1	A/Aalborg/INS283/2009
>CY062698	1	9	H1	False	N1	A/Aarhus/INS116/2009
>CY062706	1	9	H1	False	N1	A/Aarhus/INS118/2009
>CY066942	1	9	H1	False	N1	A/Aarhus/INS236/2009
>CY066950	1	9	H1	False	N1	A/Aarhus/INS237/2009
>CY066958	1	9	H1	False	N1	A/Aarhus/INS238/2009
>CY066966	1	9	H1	False	N1	A/Aarhus/INS240/2009
>CY066974	1	9	H1	False	N1	A/Aarhus/INS241/2009
>CY066982	1	9	H1	False	N1	A/Aarhus/INS242/2009
>CY067038	1	9	H1	False	N1	A/Aarhus/INS251/2009
>CY067046	1	9	H1	False	N1	A/Aarhus/INS252/2009
>CY067054	1	9	H1	False	N1	A/Aarhus/INS253/2009
>CY067062	1	9	H1	False	N1	A/Aarhus/INS254/2009
>CY176577	1	9	H1	False	N1	A/Aarhus/INS3_653/2011
>CY176585	1	9	H1	False	N1	A/Aarhus/INS3_654/2011
>CY176593	1	9	H1	False	N1	A/Aarhus/INS3_655/2011
...	...	...	...	...	...	...

**Table A.0.2 Cluster database with UK..**

Accession	Segment	Cluster	H	Centroid	N	Strain
>CY021716	1	111	H1	False	N1	A/AA/Huston/1945
>CY020292	1	111	H1	False	N1	A/AA/Marton/1943
>CY083917	1	130	H1	False	N1	A/Aalborg/INS132/2009
>CY063613	1	106	H1	False	N1	A/Aalborg/INS133/2009
>CY073732	1	106	H1	False	N1	A/Aalborg/INS283/2009
>CY062698	1	99	H1	False	N1	A/Aarhus/INS116/2009
>CY062706	1	122	H1	False	N1	A/Aarhus/INS118/2009
>CY066942	1	106	H1	False	N1	A/Aarhus/INS236/2009
>CY066950	1	106	H1	False	N1	A/Aarhus/INS237/2009
>CY066958	1	106	H1	False	N1	A/Aarhus/INS238/2009
>CY066966	1	106	H1	False	N1	A/Aarhus/INS240/2009
>CY066974	1	99	H1	False	N1	A/Aarhus/INS241/2009
>CY066982	1	122	H1	False	N1	A/Aarhus/INS242/2009
>CY067038	1	99	H1	False	N1	A/Aarhus/INS251/2009
>CY067046	1	106	H1	False	N1	A/Aarhus/INS252/2009
>CY067054	1	122	H1	False	N1	A/Aarhus/INS253/2009
>CY067062	1	99	H1	False	N1	A/Aarhus/INS254/2009
>CY176577	1	46	H1	False	N1	A/Aarhus/INS3_653/2011
>CY176585	1	46	H1	False	N1	A/Aarhus/INS3_654/2011
>CY176593	1	46	H1	False	N1	A/Aarhus/INS3_655/2011
...	...	...	...	...	...	...

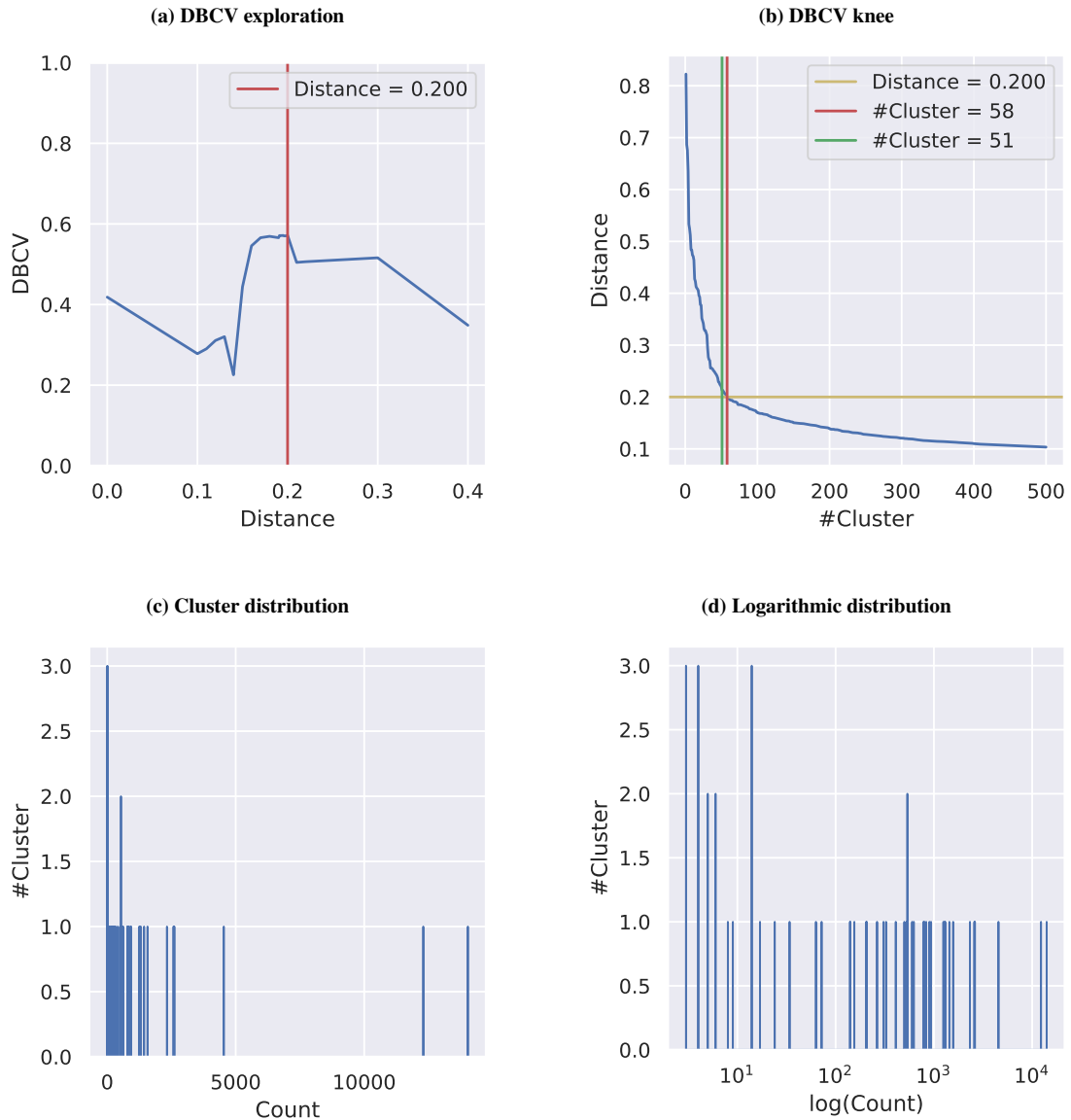


**Fig. A.0.1 Clustering of segment 4 with PD.**

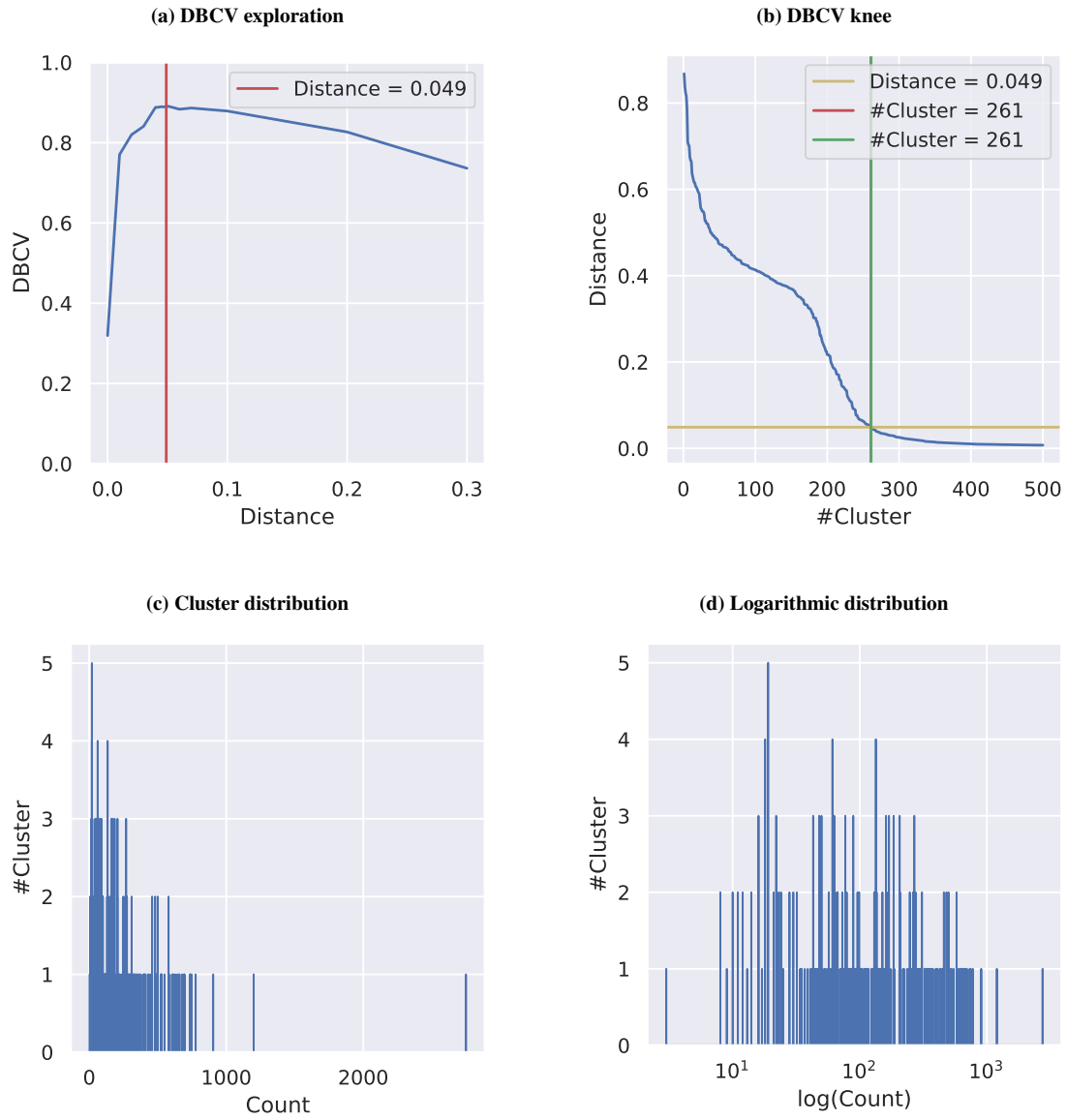


**Fig. A.0.2 Clustering of segment 4 with UD.**

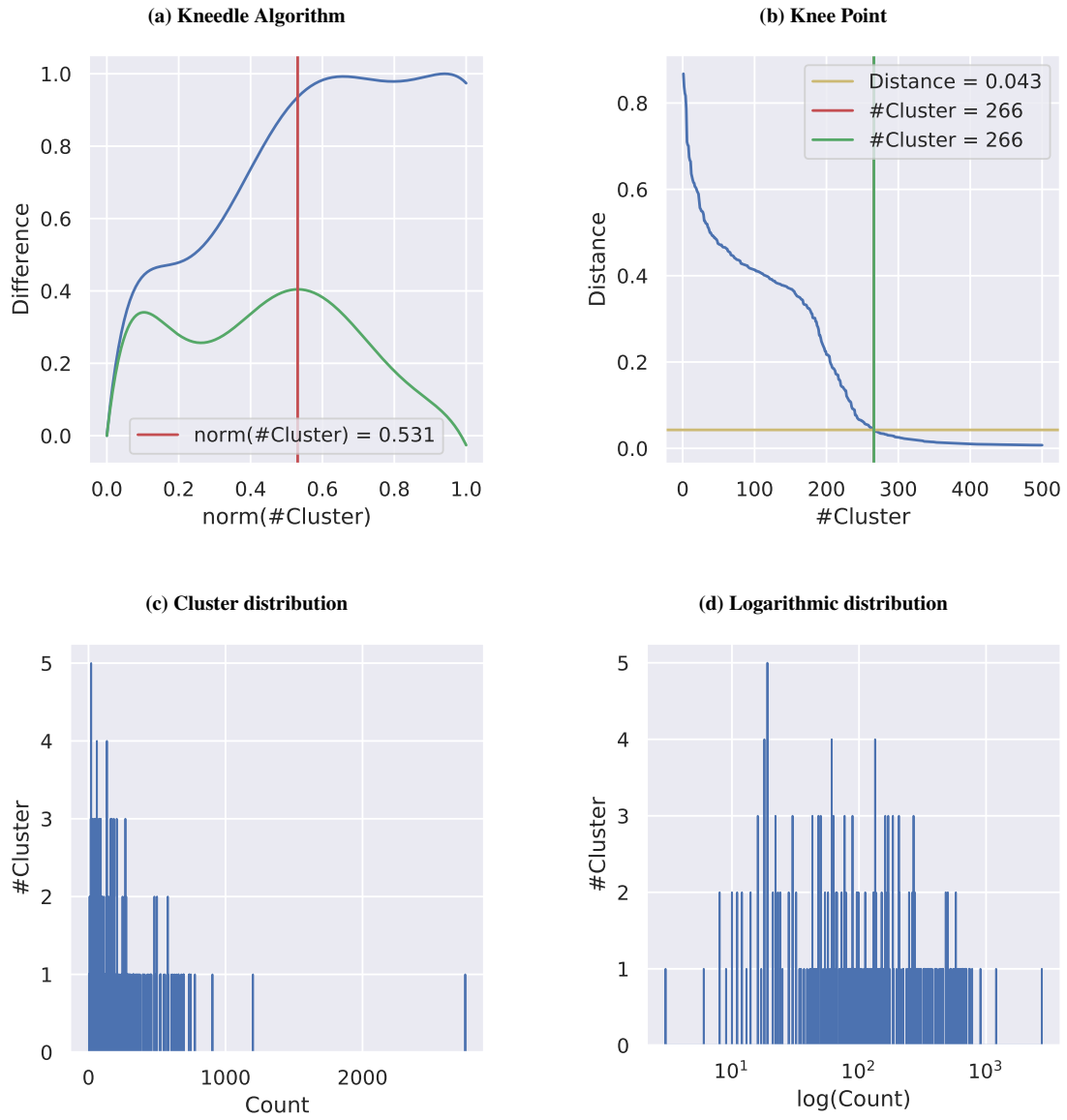


**Fig. A.0.3 Clustering of segment 4 with UK.**

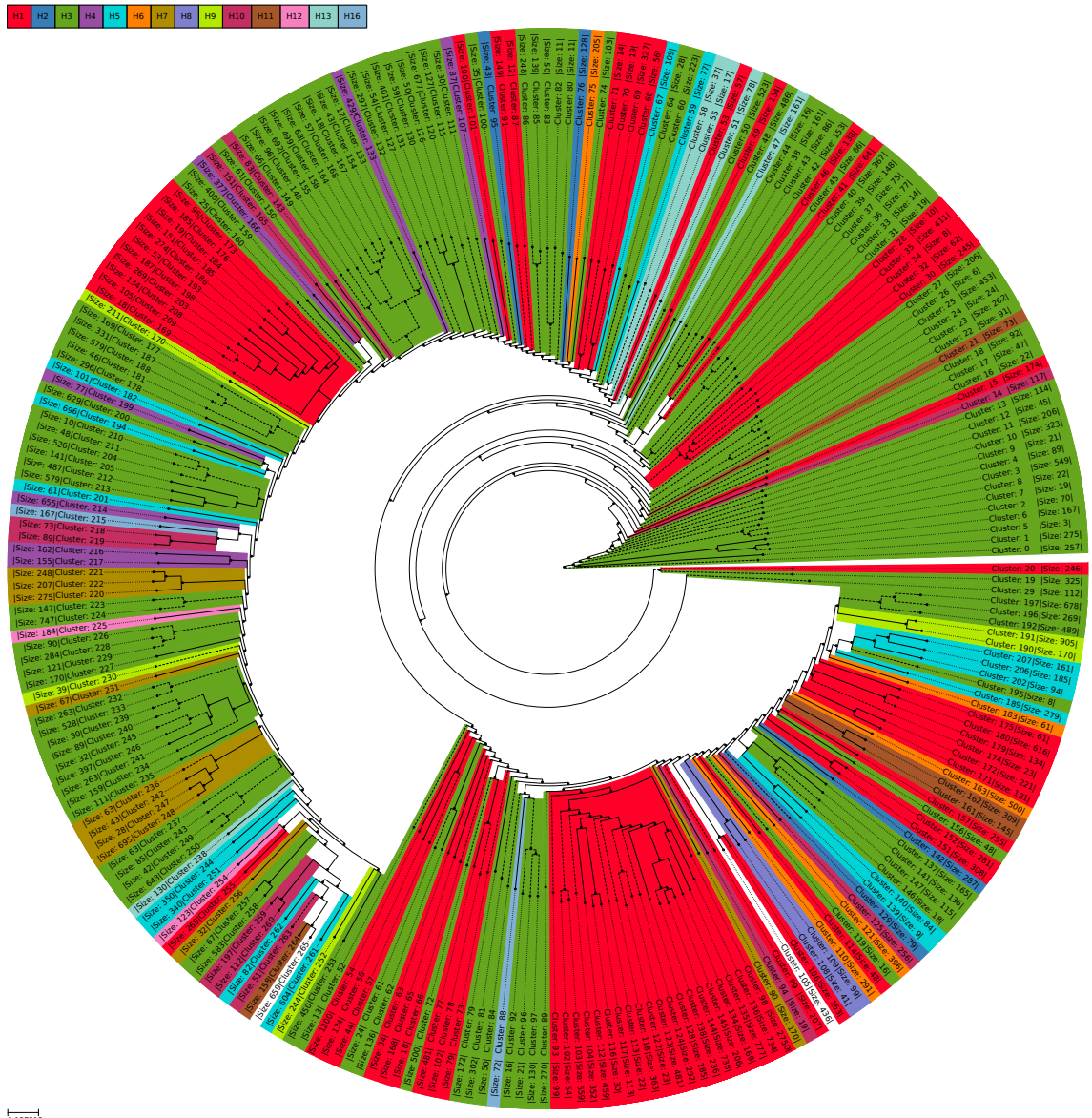


**Fig. A.0.4 Clustering tree of segment 4 with UK.**

**Table A.0.3 Anomalies in segment 4 cluster 105 with UK..**

<b>Accession</b>	<b>H1</b>	<b>H10</b>
>MK237334	0.046	0.490

**Table A.0.4 Anomalies in segment 4 cluster 265 with UK..**

<b>Accession</b>	<b>H7</b>	<b>H10</b>	<b>H12</b>
>MT406929	0.355	0.137	0.487
>MT407001	0.354	0.138	0.486
>MT407041	0.502	0.487	0.195
>GQ907286	0.491	0.480	0.181
>MF146658	0.501	0.485	0.191
>MK327718	0.458	0.457	0.530
>MK327694	0.458	0.457	0.530
>MK327702	0.458	0.457	0.530
>MK326656	0.458	0.457	0.530
>MK327734	0.458	0.457	0.530
>MK327726	0.458	0.457	0.530
>MK327686	0.458	0.457	0.530
>MK327758	0.457	0.456	0.530
>KY644423	0.459	0.456	0.530
>KJ195668	0.460	0.458	0.529
>KY644472	0.462	0.457	0.533
>KX960412	0.462	0.458	0.533
>KX960458	0.463	0.457	0.533
>KY644351	0.462	0.459	0.534
>KX960451	0.462	0.458	0.533
...	...	...	...

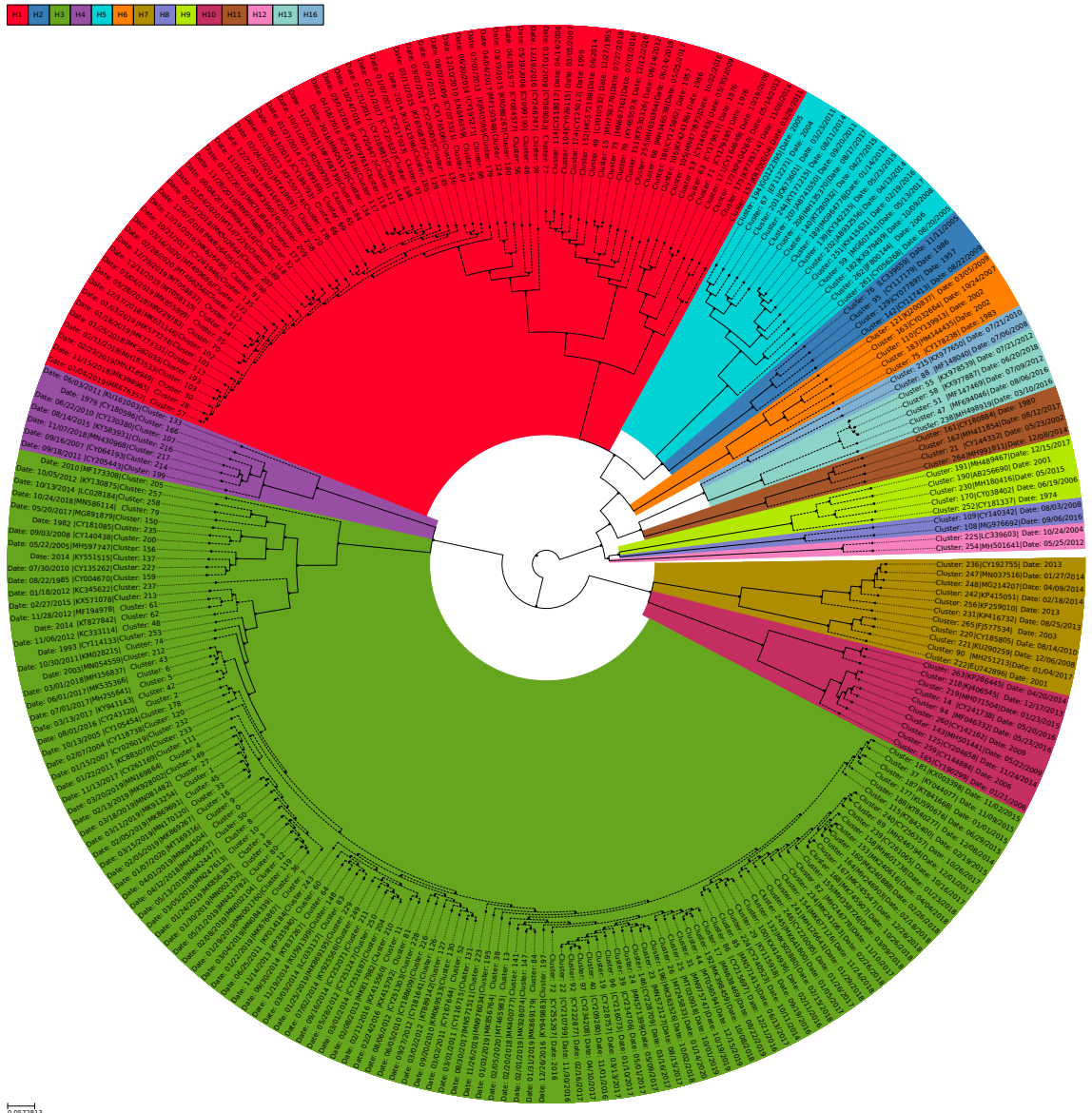


**Fig. A.0.5 Centroid guidetree of segment 4 with UK.**

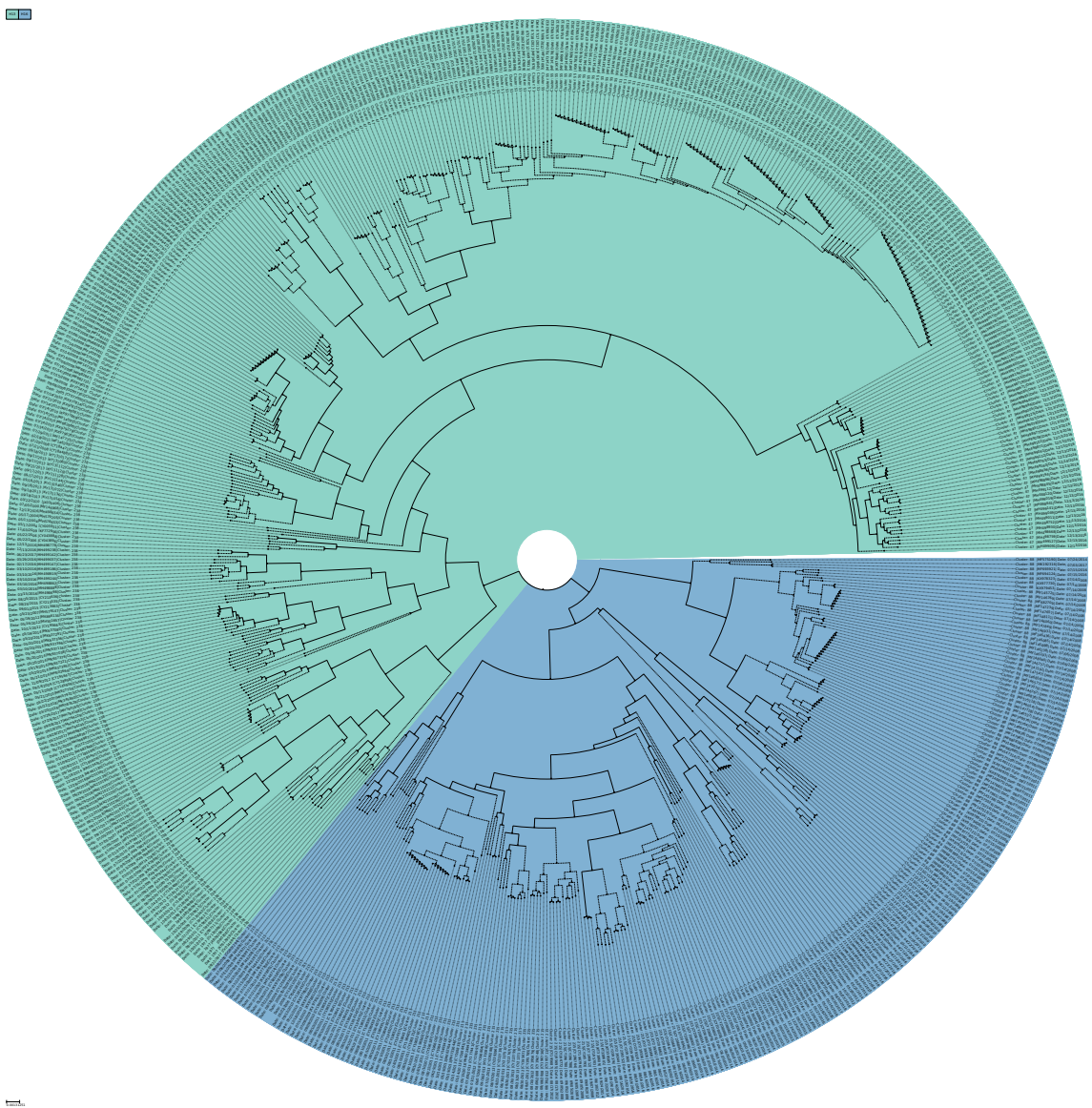


**Fig. A.0.6 UPGMA tree of H13/H16 with euclidean distance. .**

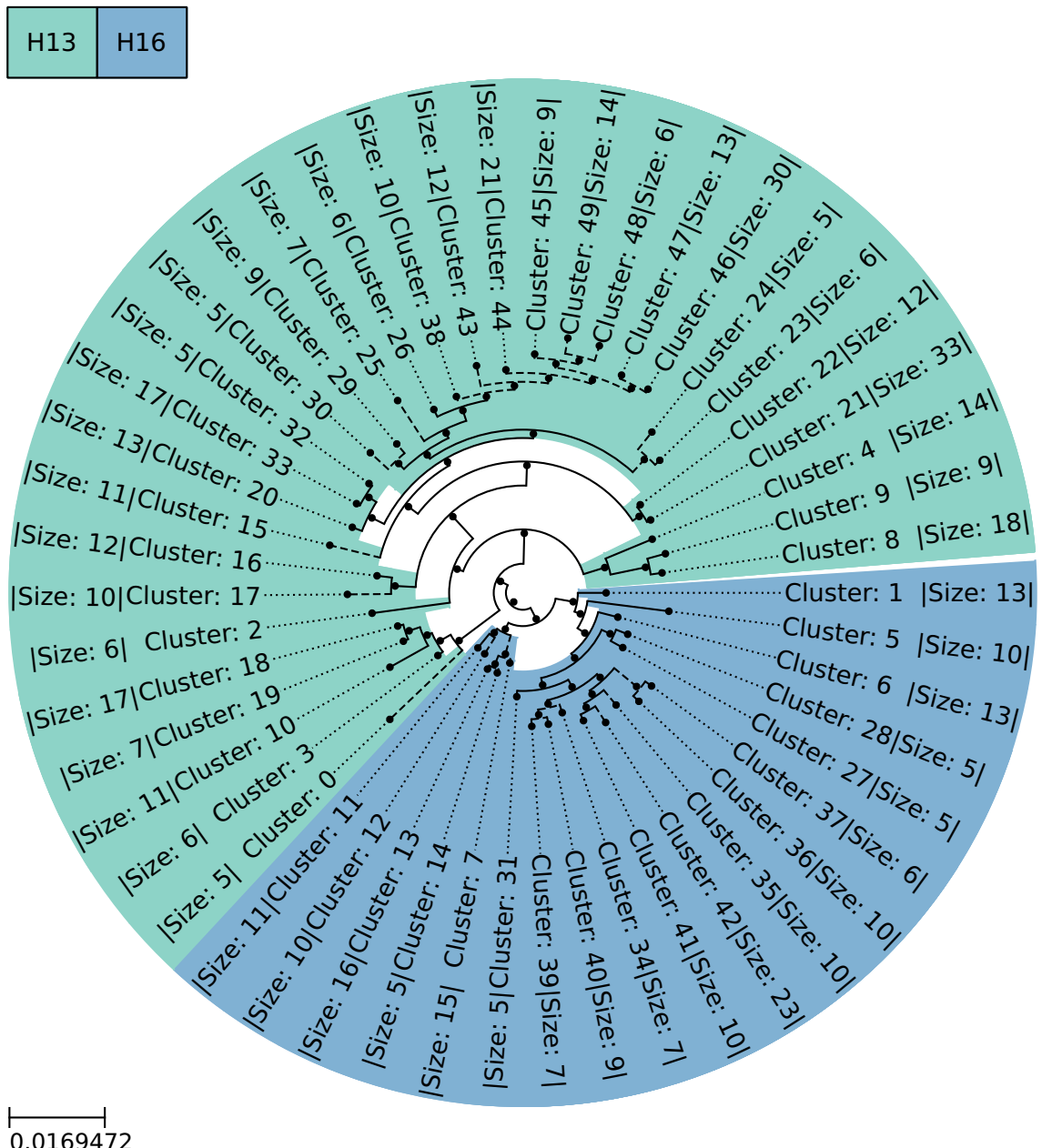
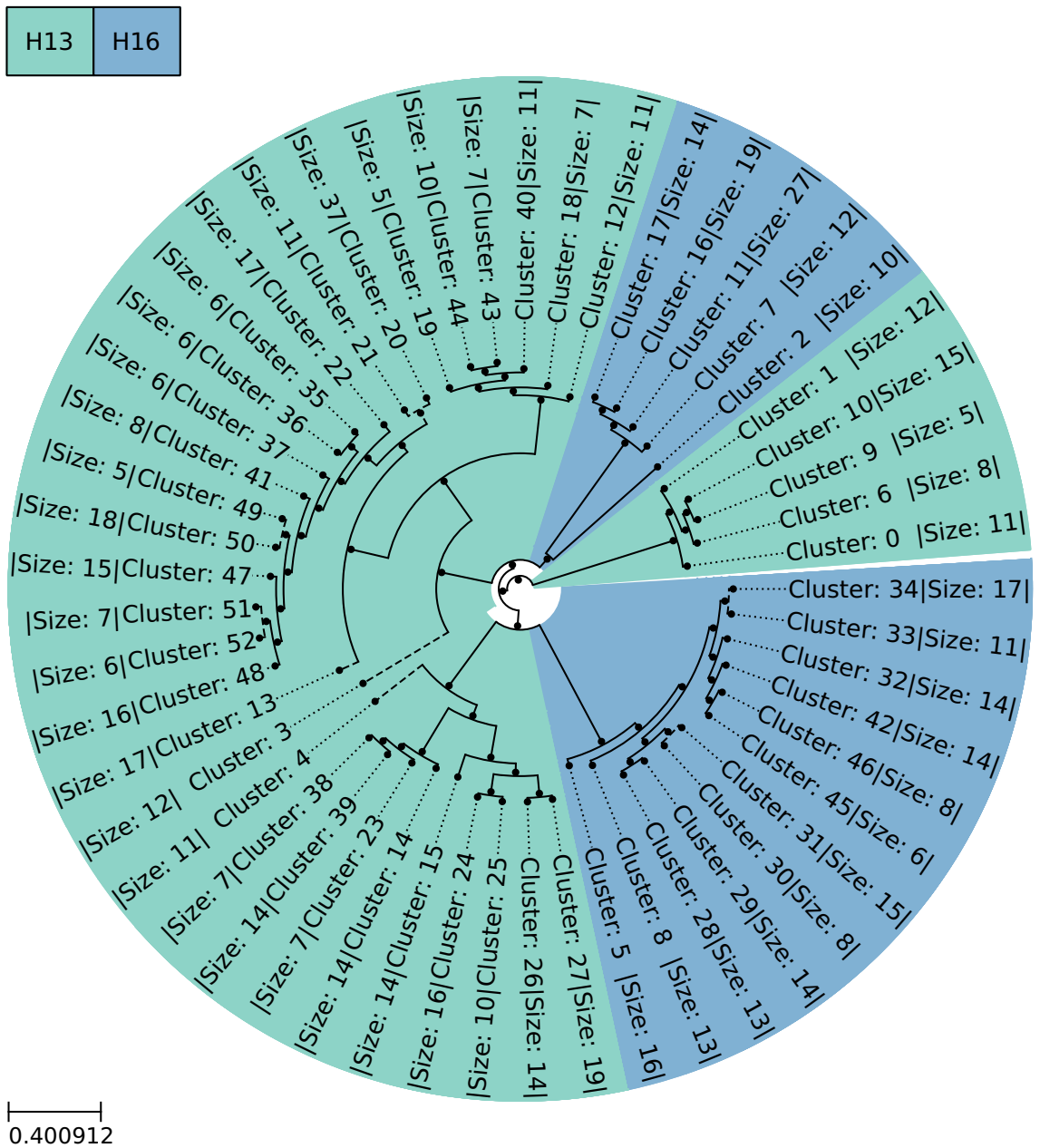


Fig. A.0.7 Simple clustering tree of H13/H16 with euclidean distance. .



**Fig. A.0.8 Simple clustering tree of H13/H16 with UMAP..**

**Table A.0.5 Clustering results.**

Segment	#Cluster			#Mixed		#Unclustered	$\varepsilon$	Var( $X$ )
	Final	Raw	Normalized	H	N			
1	28	71	0.140	19	20	29	0.345	0.811
2	28	66	0.130	17	17	23	0.375	0.798
3	29	70	0.138	18	19	28	0.402	0.816
4	57	78	0.154	1	44	11	0.251	0.793
5	26	74	0.146	22	22	19	0.362	0.837
6	40	58	0.114	28	3	17	0.293	0.803
7	30	75	0.148	16	17	28	0.454	0.858
8	24	67	0.132	16	16	23	0.409	0.860

**Table A.0.6 Cluster database..**

Accession	Segment	Cluster	H	Centroid	N	Strain
>CY021716	1	1	H1	False	N1	A/AA/Huston/1945
>CY020292	1	1	H1	False	N1	A/AA/Marton/1943
>CY083917	1	10	H1	False	N1	A/Aalborg/INS132/2009
>CY063613	1	10	H1	False	N1	A/Aalborg/INS133/2009
>CY073732	1	10	H1	False	N1	A/Aalborg/INS283/2009
>CY062698	1	10	H1	False	N1	A/Aarhus/INS116/2009
>CY062706	1	10	H1	False	N1	A/Aarhus/INS118/2009
>CY066942	1	10	H1	False	N1	A/Aarhus/INS236/2009
>CY066950	1	10	H1	False	N1	A/Aarhus/INS237/2009
>CY066958	1	10	H1	False	N1	A/Aarhus/INS238/2009
>CY066966	1	10	H1	False	N1	A/Aarhus/INS240/2009
>CY066974	1	10	H1	False	N1	A/Aarhus/INS241/2009
>CY066982	1	10	H1	False	N1	A/Aarhus/INS242/2009
>CY067038	1	10	H1	False	N1	A/Aarhus/INS251/2009
>CY067046	1	10	H1	False	N1	A/Aarhus/INS252/2009
>CY067054	1	10	H1	False	N1	A/Aarhus/INS253/2009
>CY067062	1	10	H1	False	N1	A/Aarhus/INS254/2009
>CY176577	1	10	H1	False	N1	A/Aarhus/INS3_653/2011
>CY176585	1	10	H1	False	N1	A/Aarhus/INS3_654/2011
>CY176593	1	10	H1	False	N1	A/Aarhus/INS3_655/2011
...	...	...	...	...	...	...

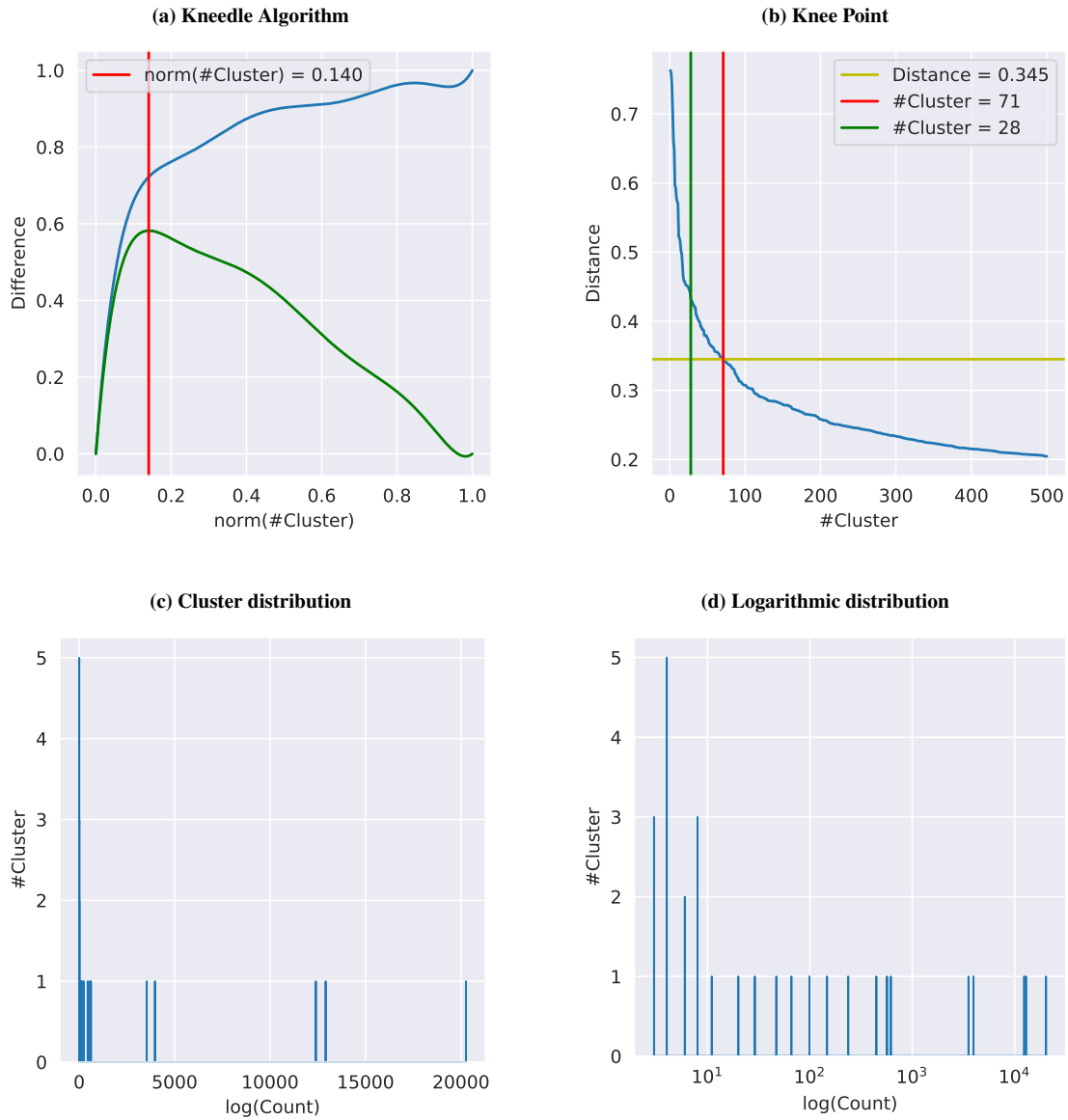


**Fig. A.0.9 Clustering of segment 1.**

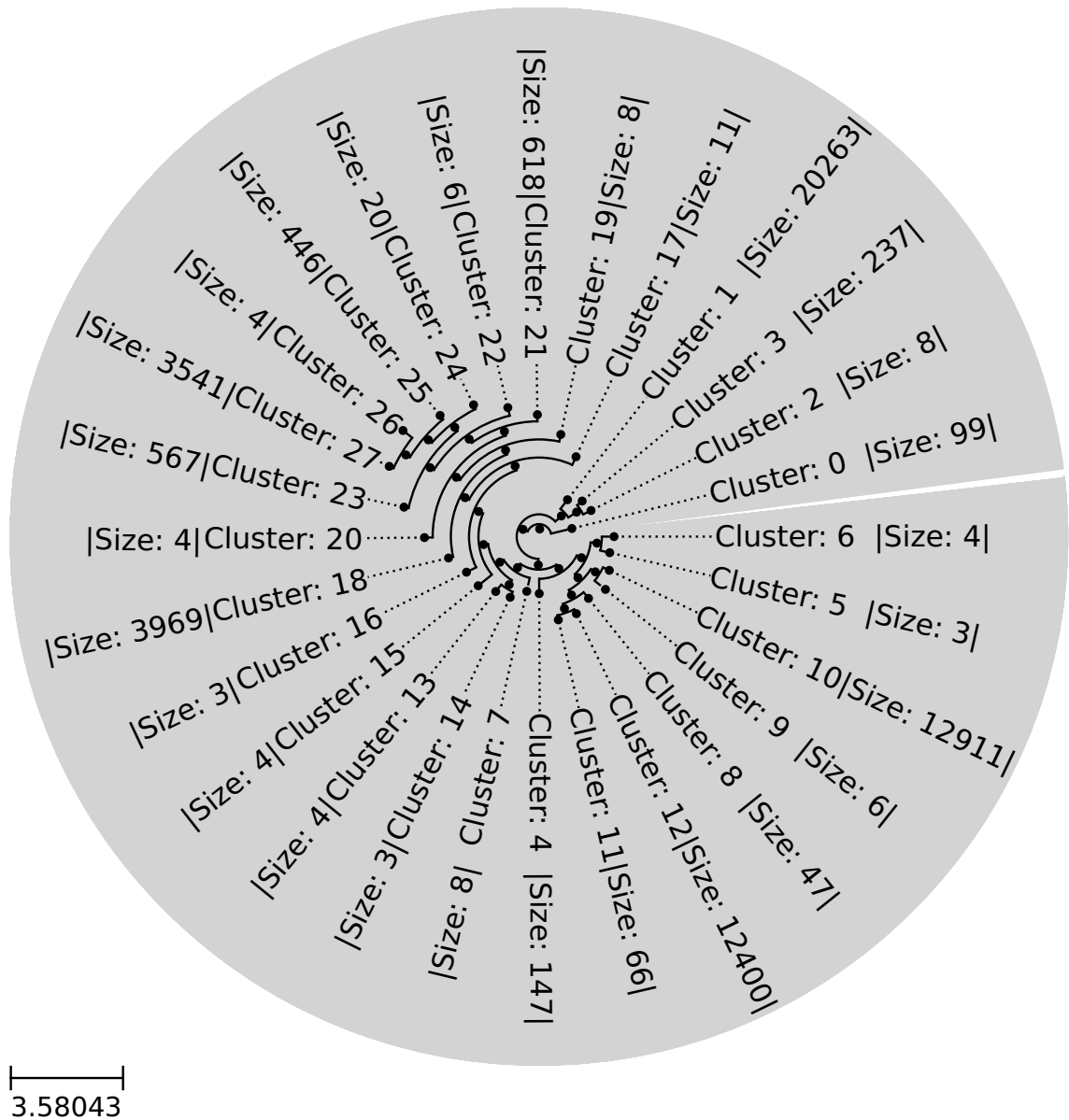


**Fig. A.0.10 Clustering tree of segment 1.**

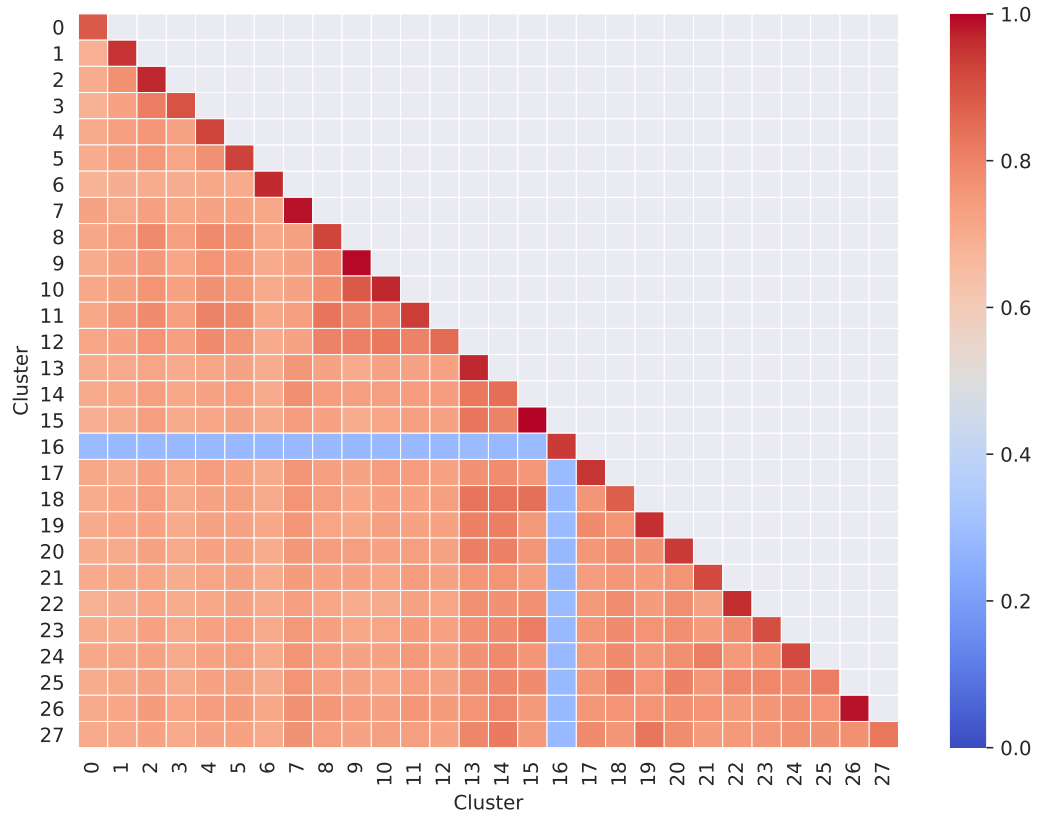


**Fig. A.0.11 Similarity matrix of segment 1 clusters.**

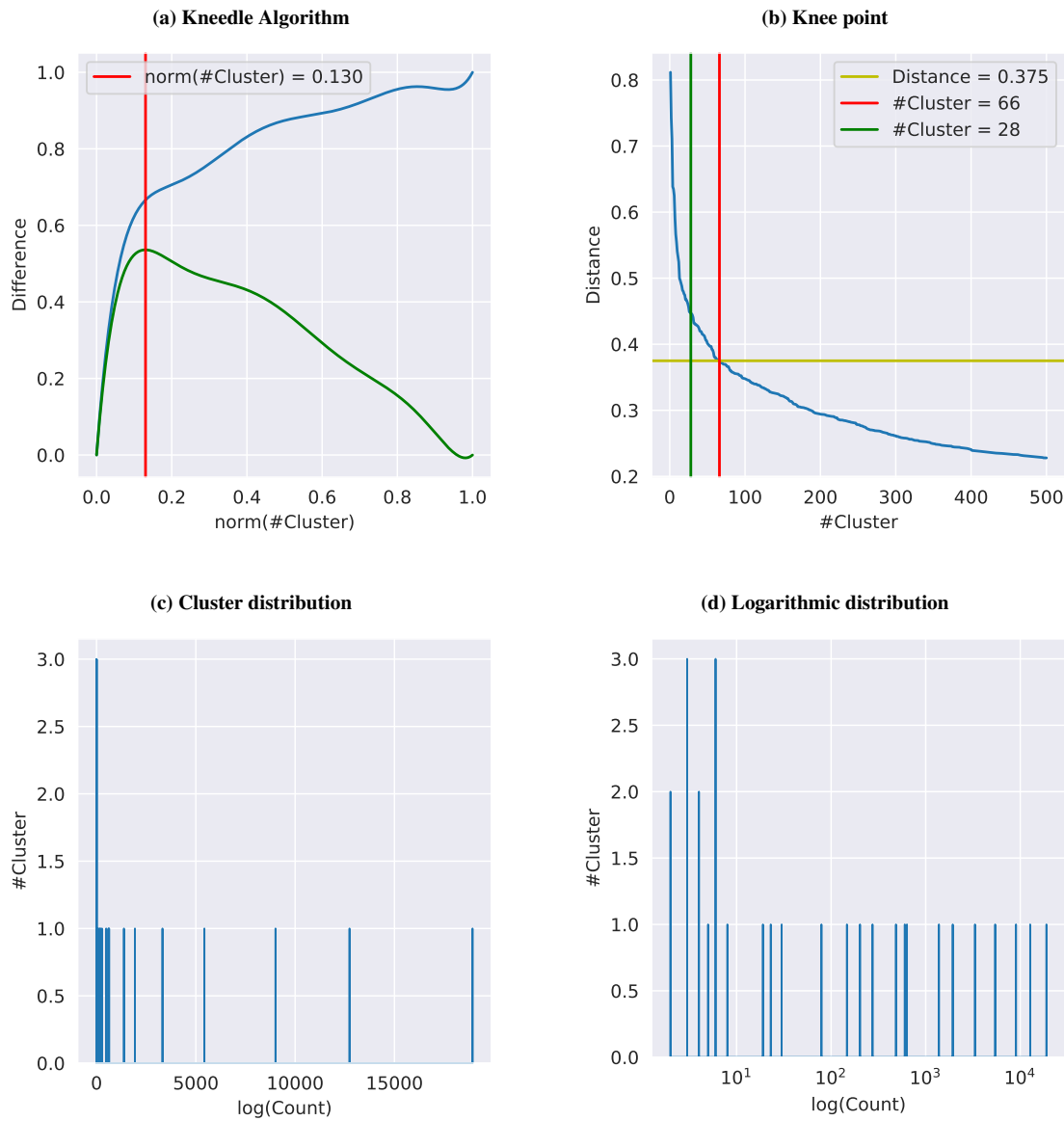


**Fig. A.0.12 Clustering of segment 2.**

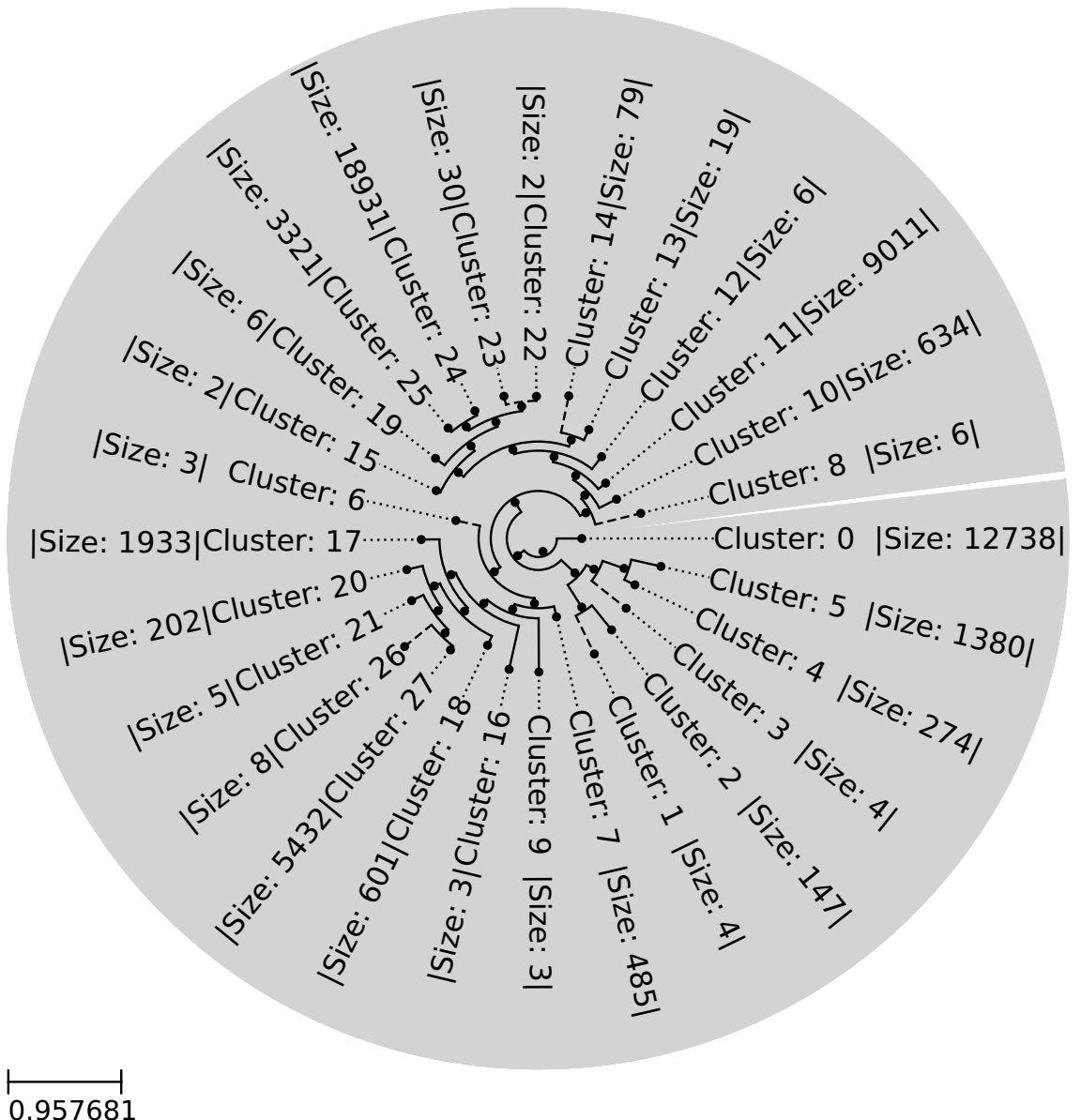


**Fig. A.0.13 Clustering tree of segment 2.**

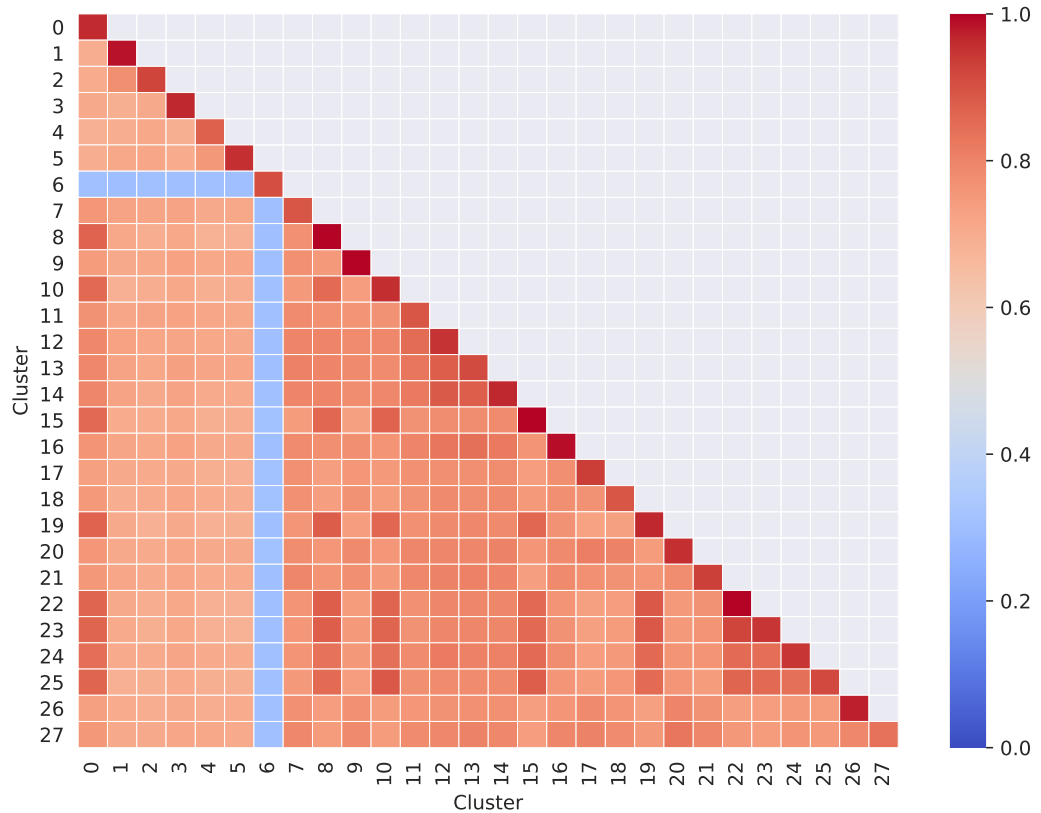


**Fig. A.0.14 Similarity matrix of segment 2 clusters.**

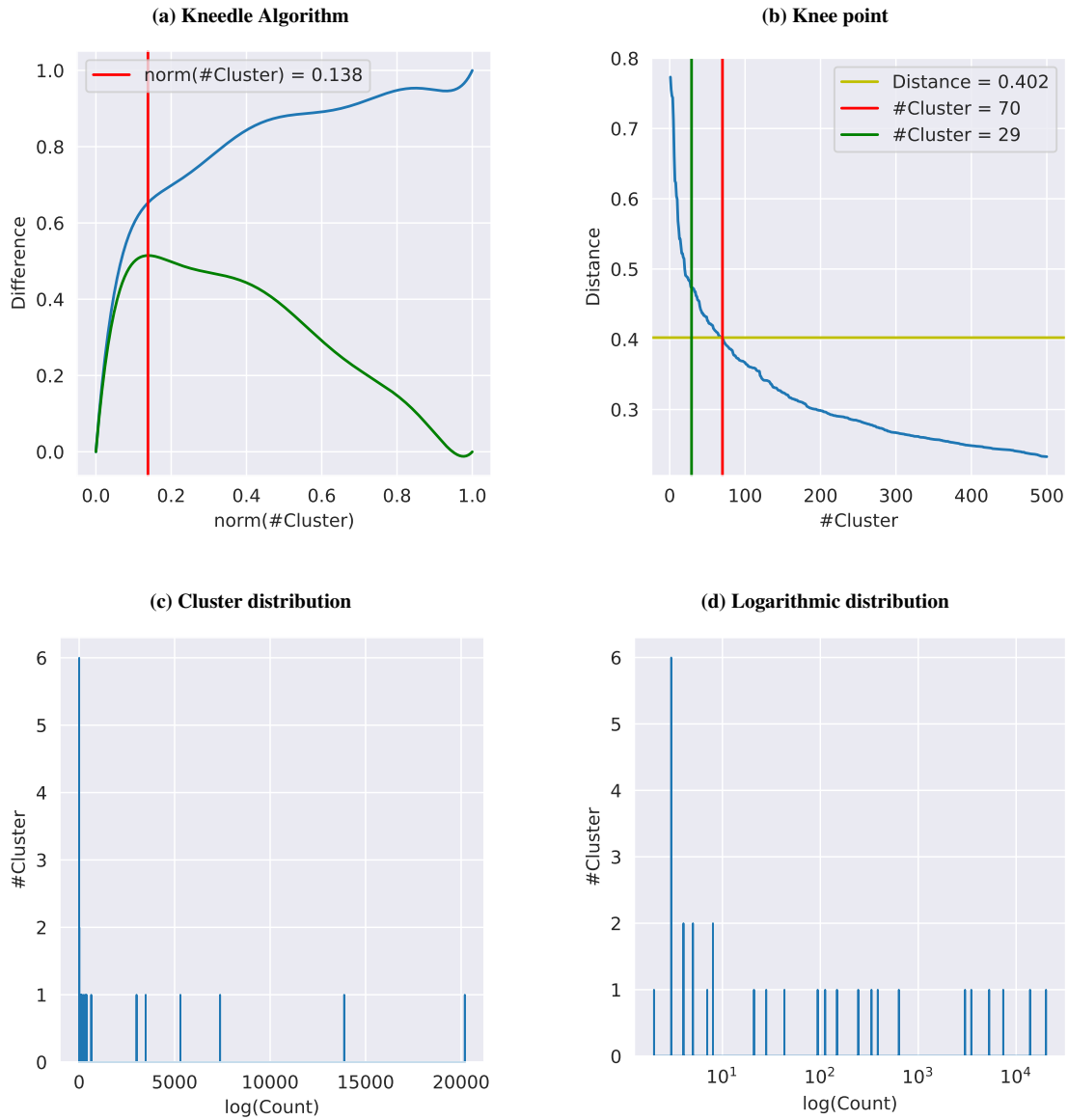


**Fig. A.0.15 Clustering of segment 3.**

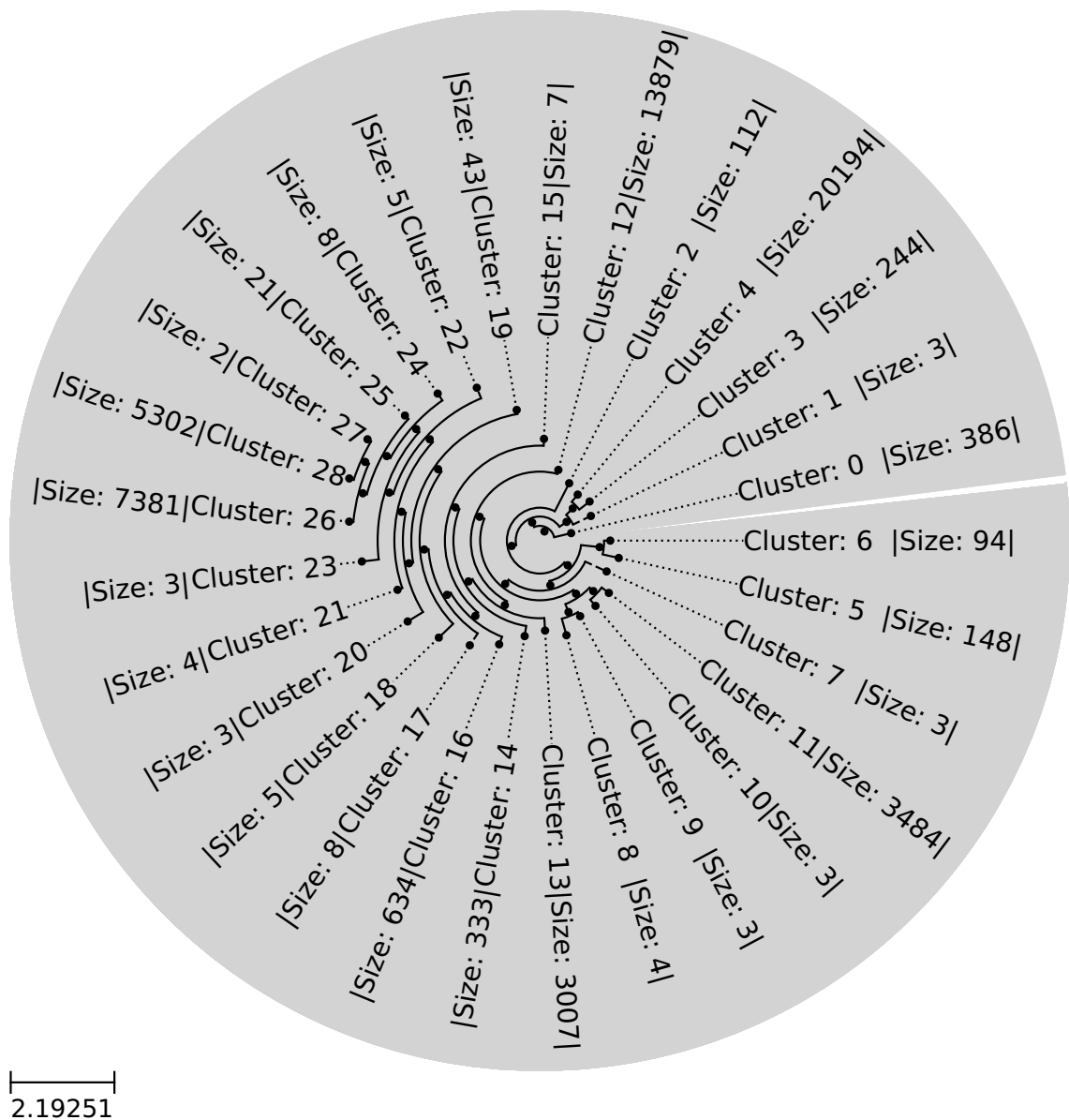
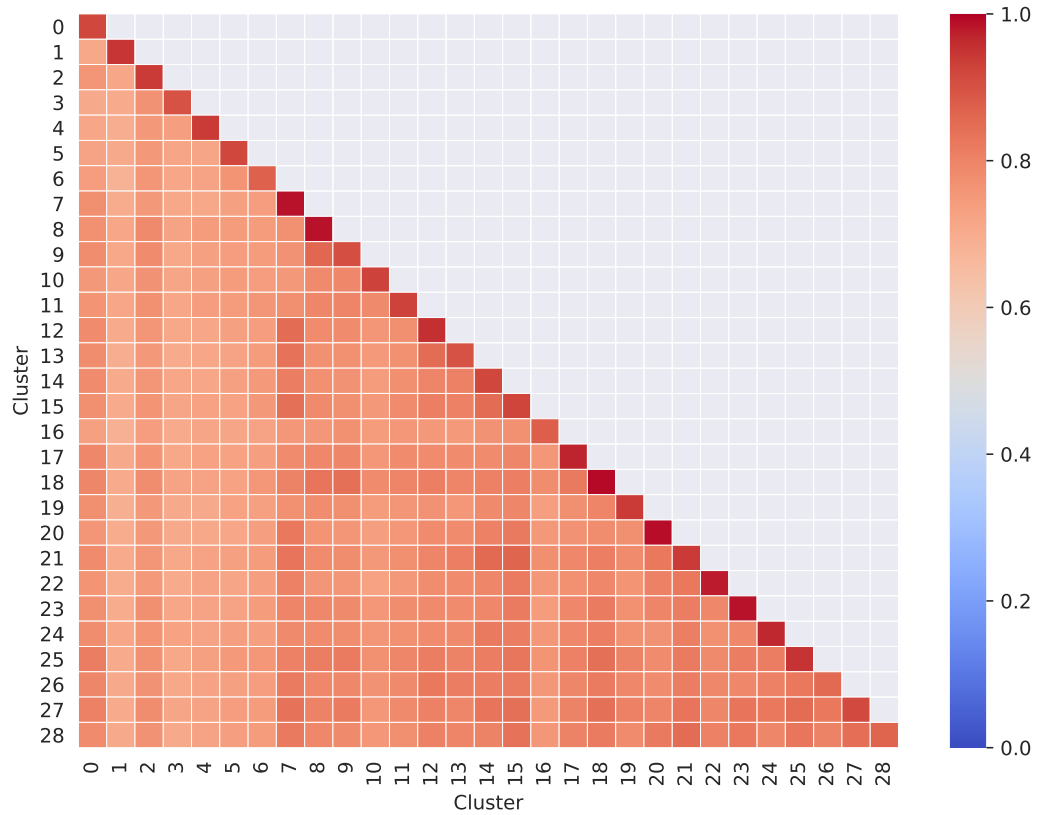
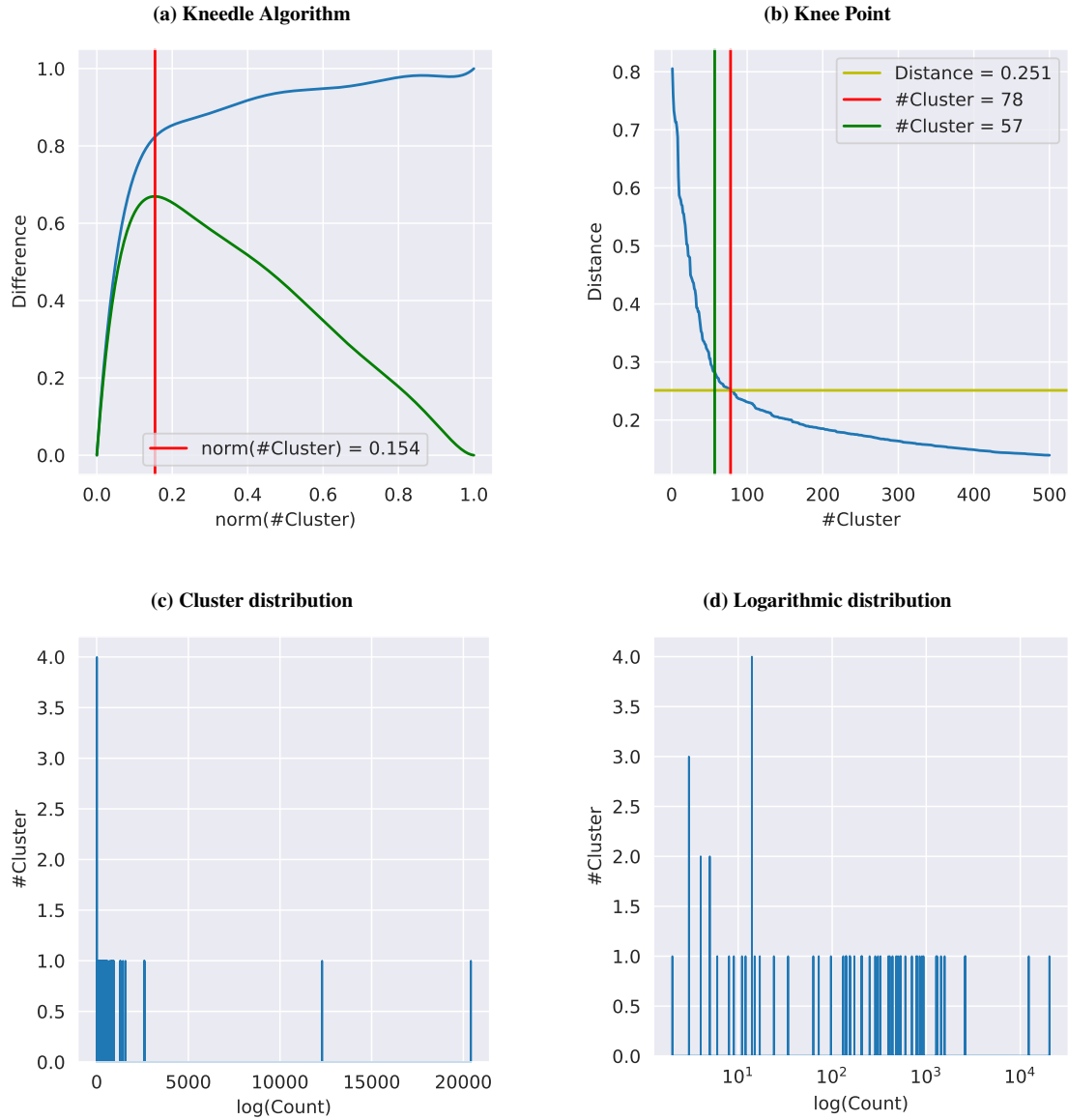


Fig. A.0.16 Clustering tree of segment 3.



**Fig. A.0.17 Similarity matrix of segment 3 clusters.**



**Fig. A.0.18 Clustering of segment 4.**

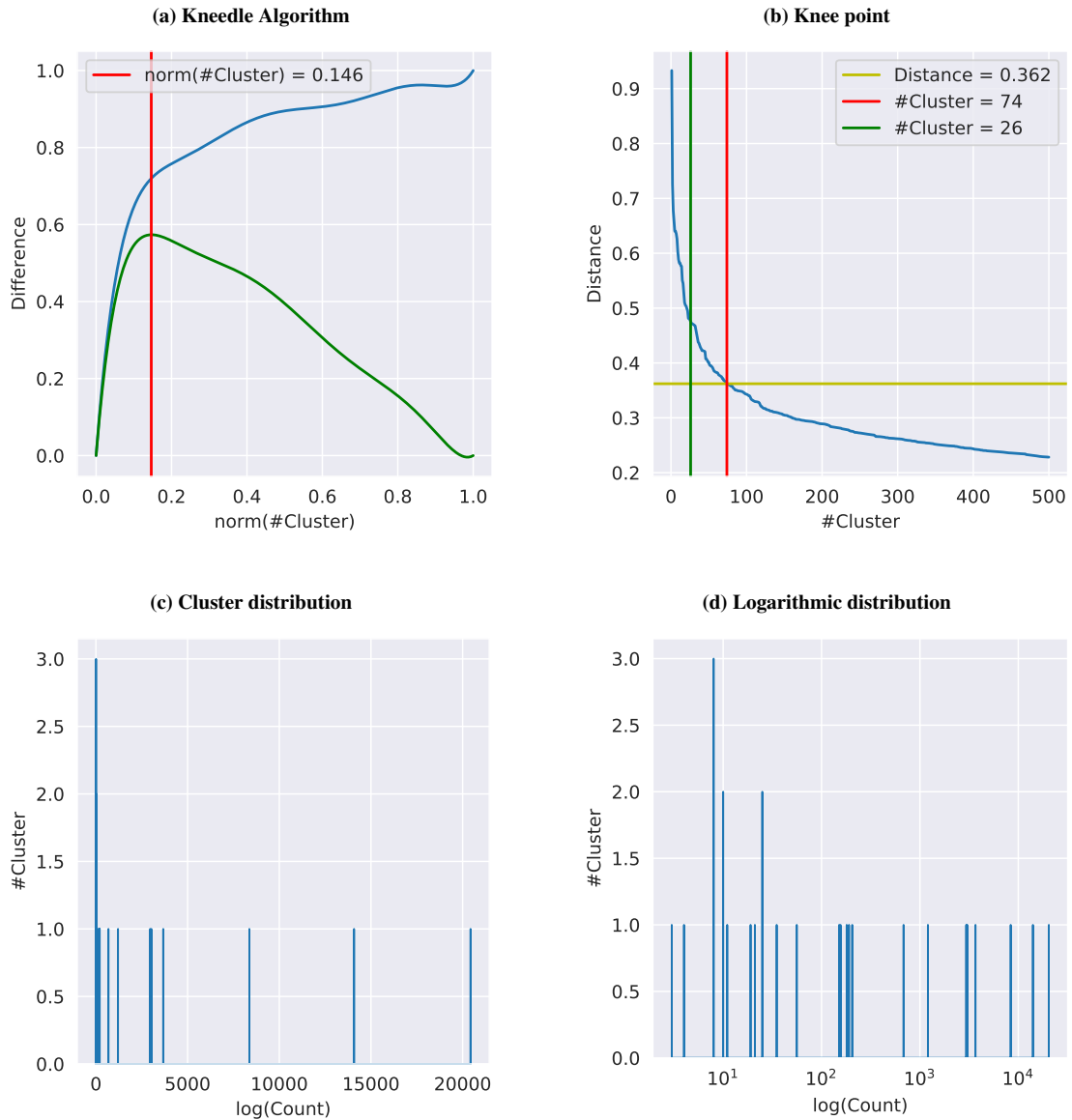


**Fig. A.0.19 Clustering of segment 5.**

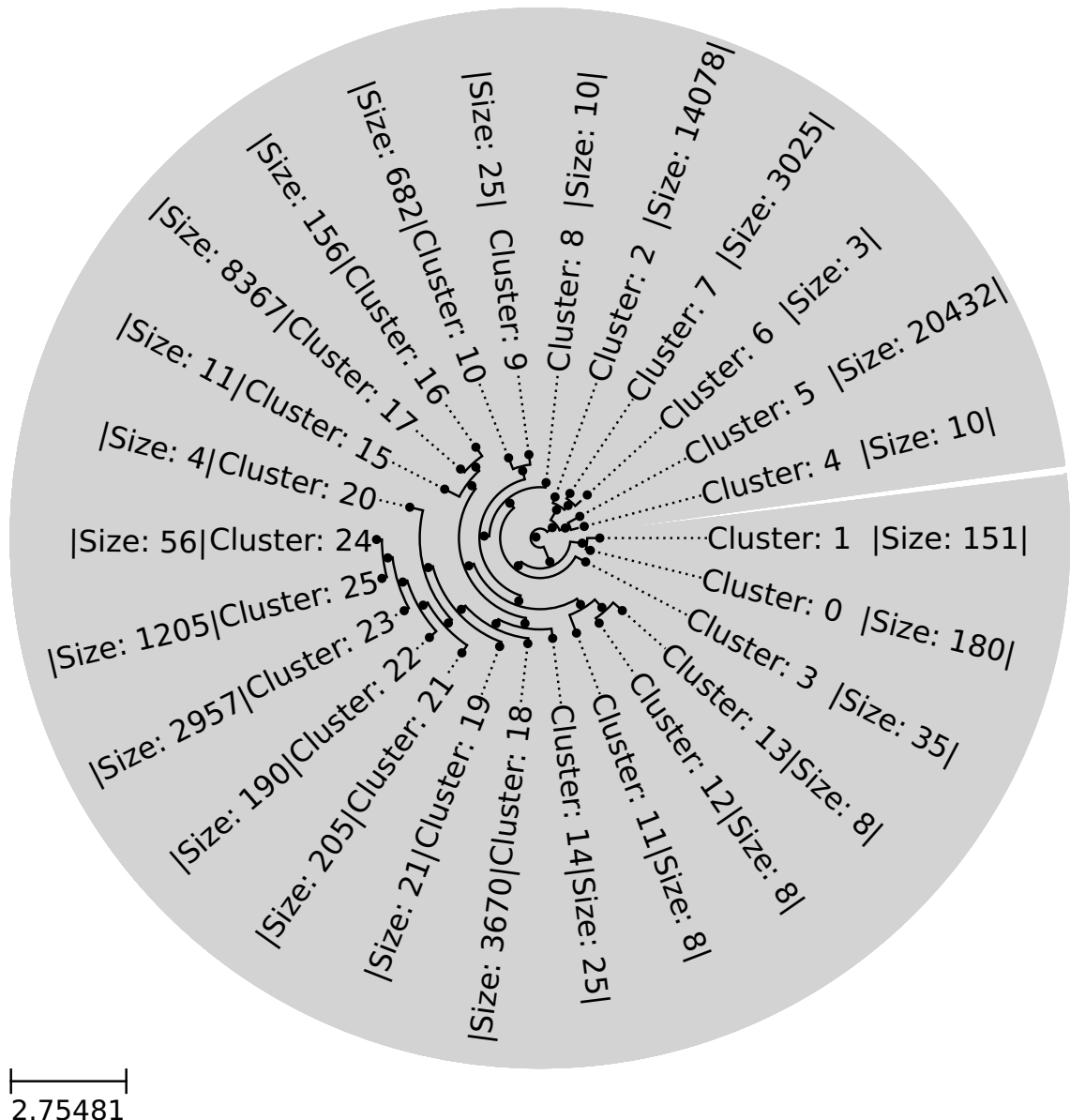


**Fig. A.0.20 Clustering tree of segment 5.**

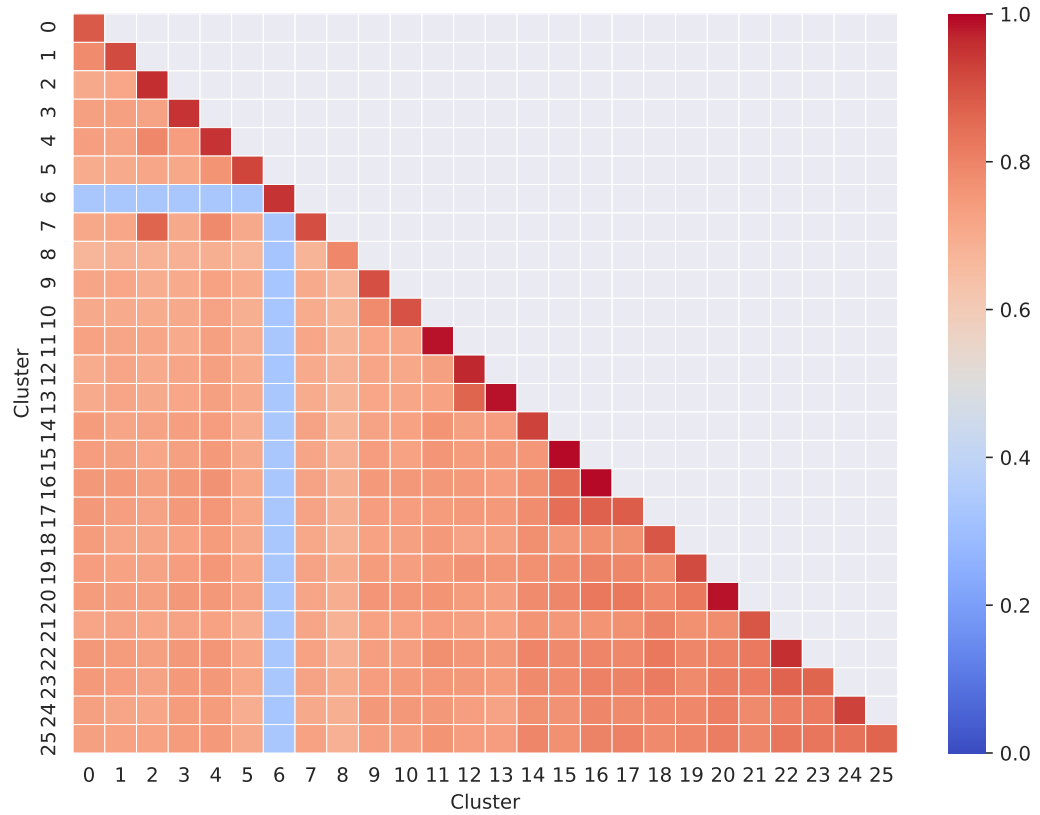


**Fig. A.0.21 Similarity matrix of segment 5 clusters.**

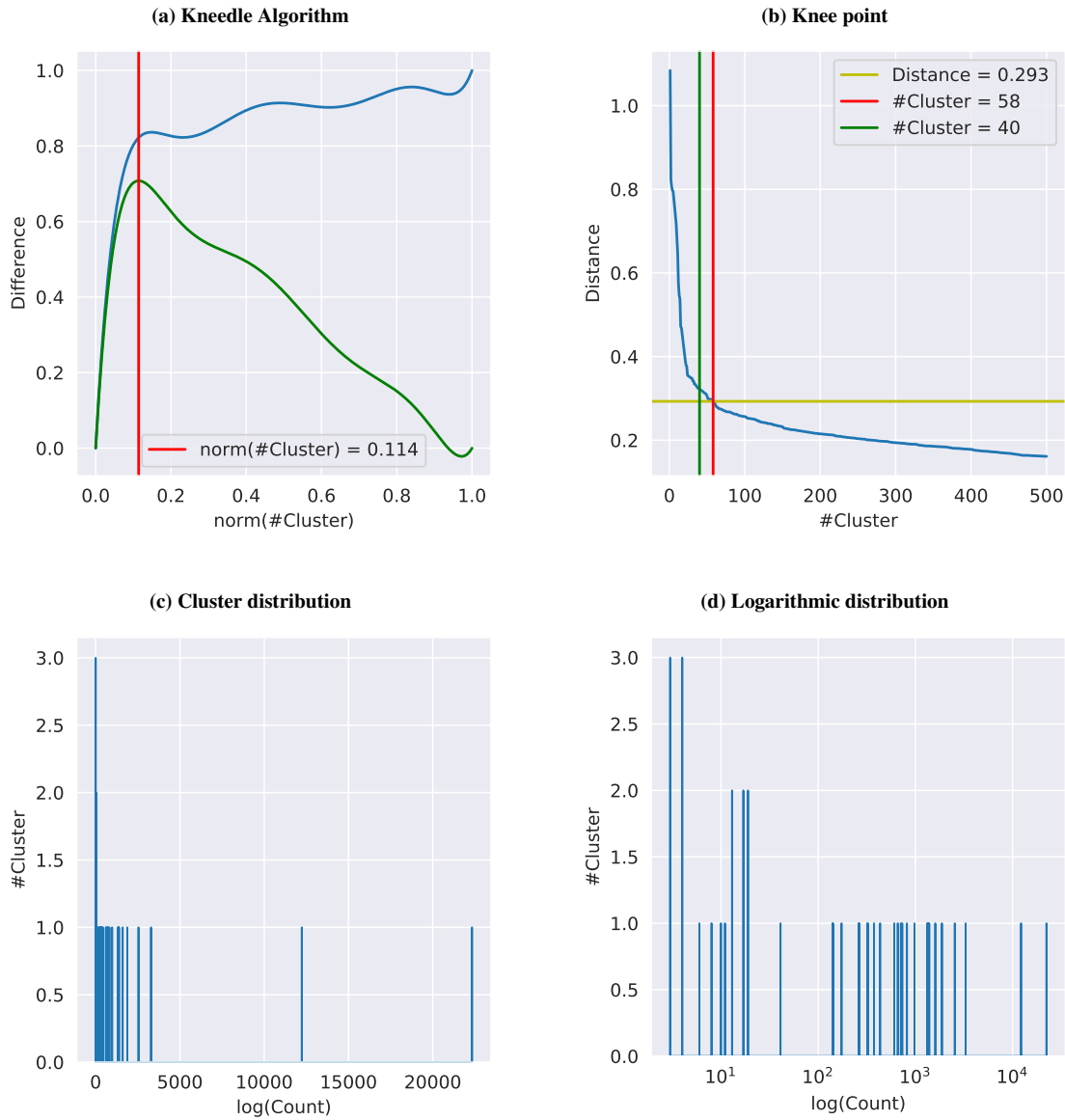


**Fig. A.0.22 Clustering of segment 6.**

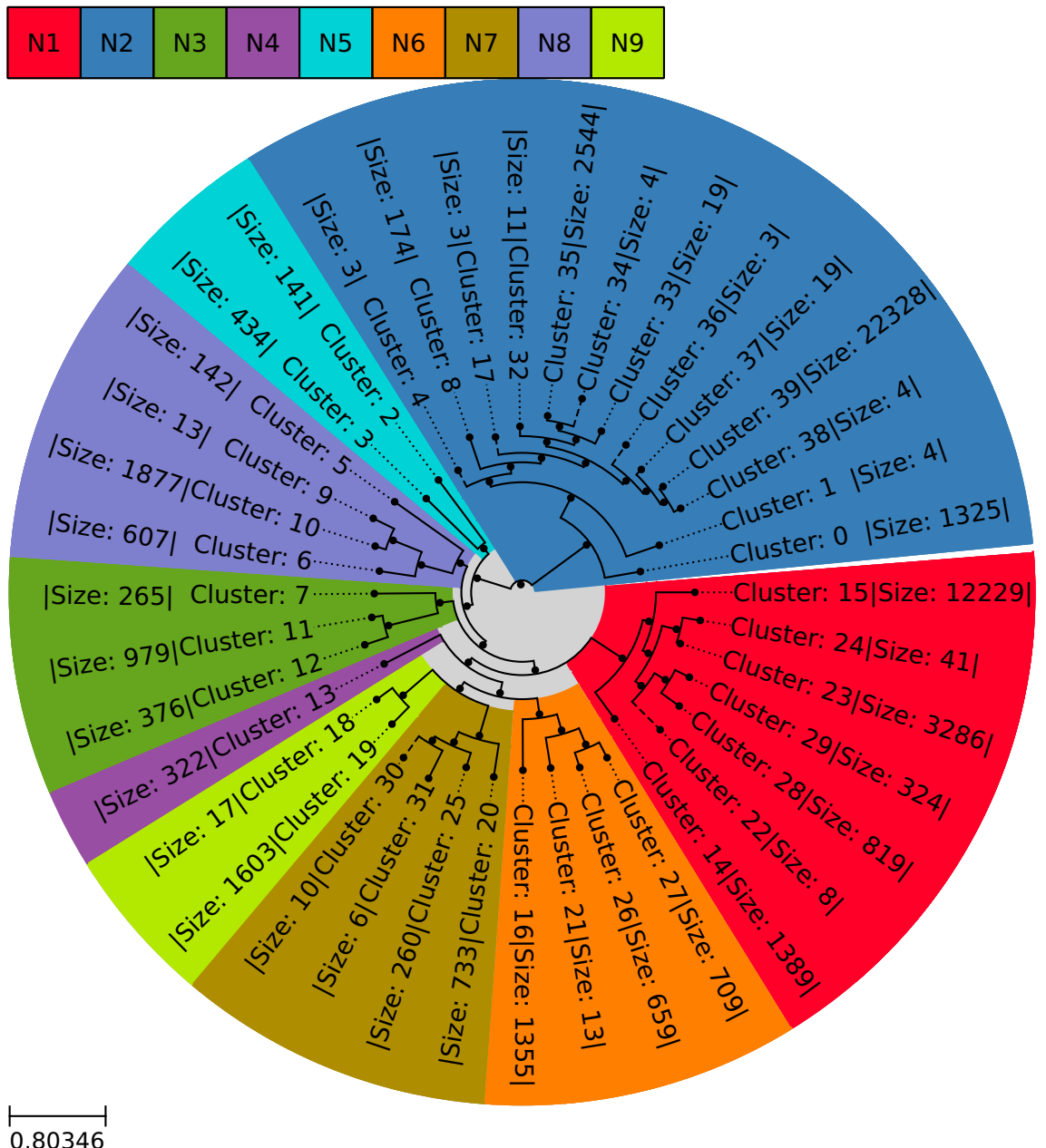
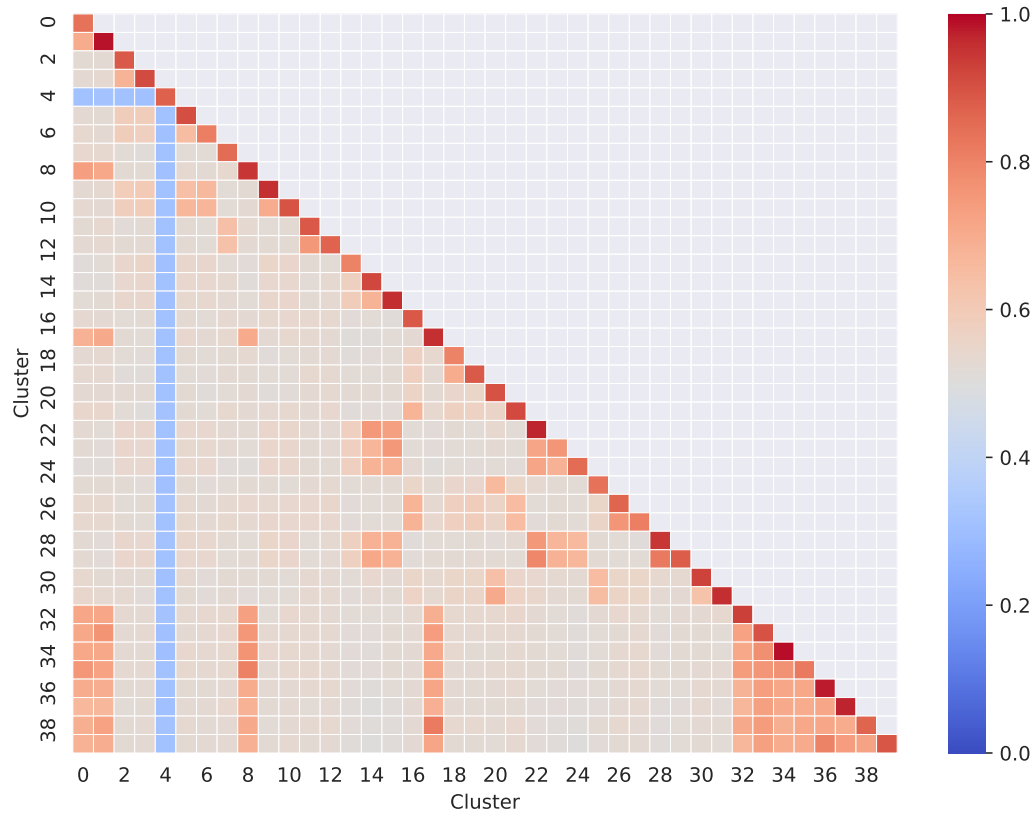
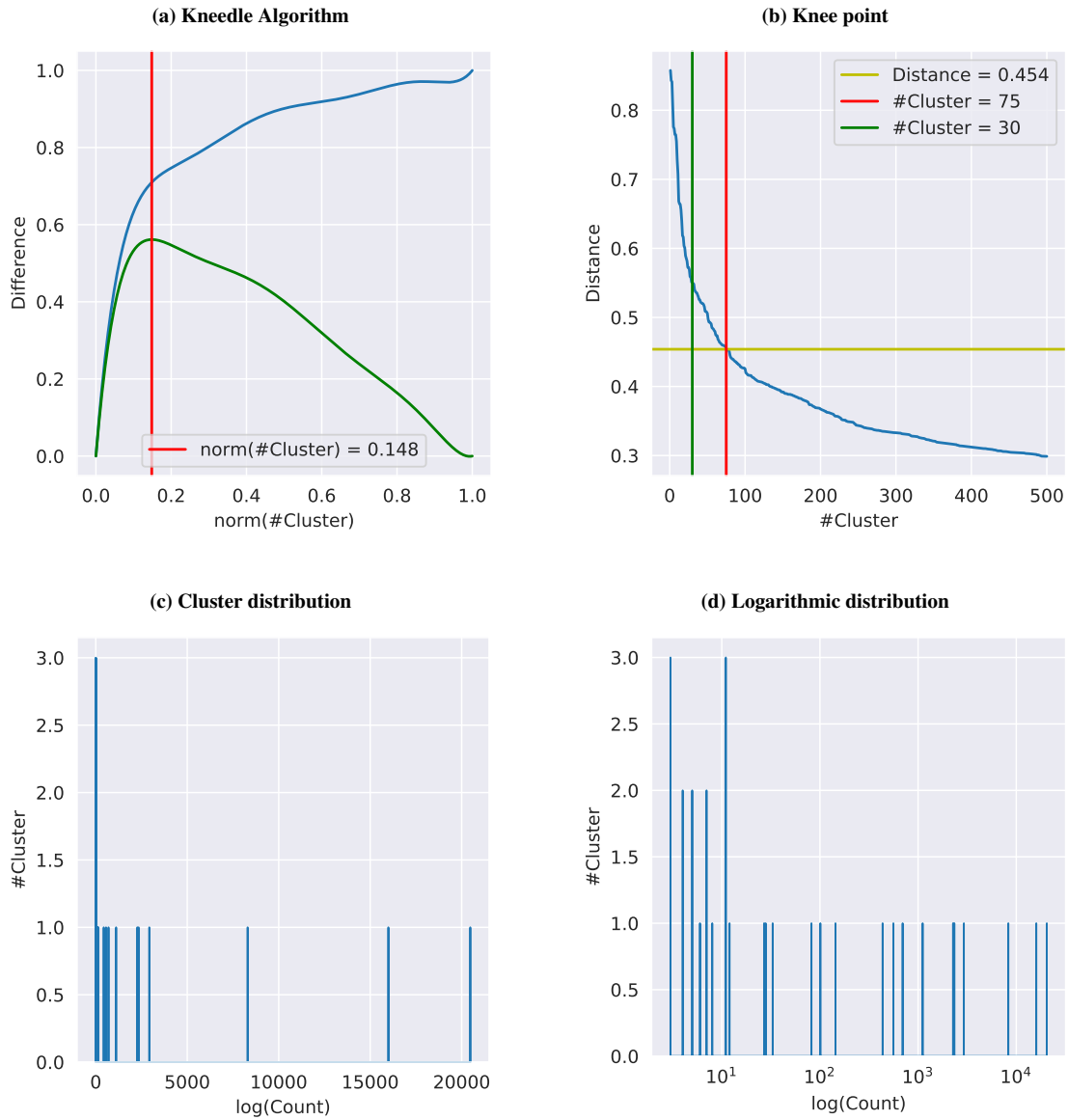


Fig. A.0.23 Clustering tree of segment 6.



**Fig. A.0.24 Similarity matrix of segment 6 clusters.**



**Fig. A.0.25 Clustering of segment 7.**

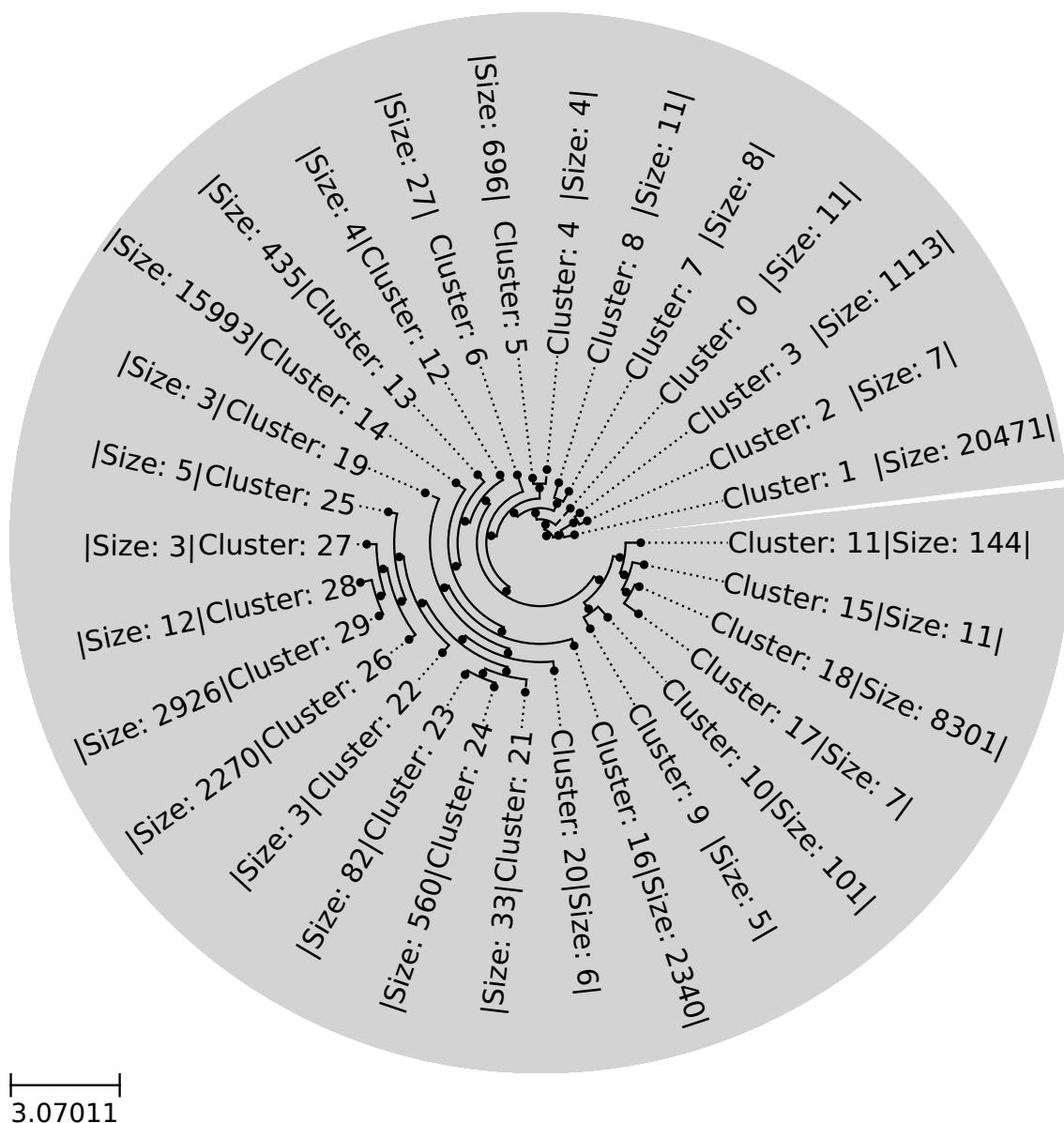


**Fig. A.0.26 Clustering tree of segment 7.**

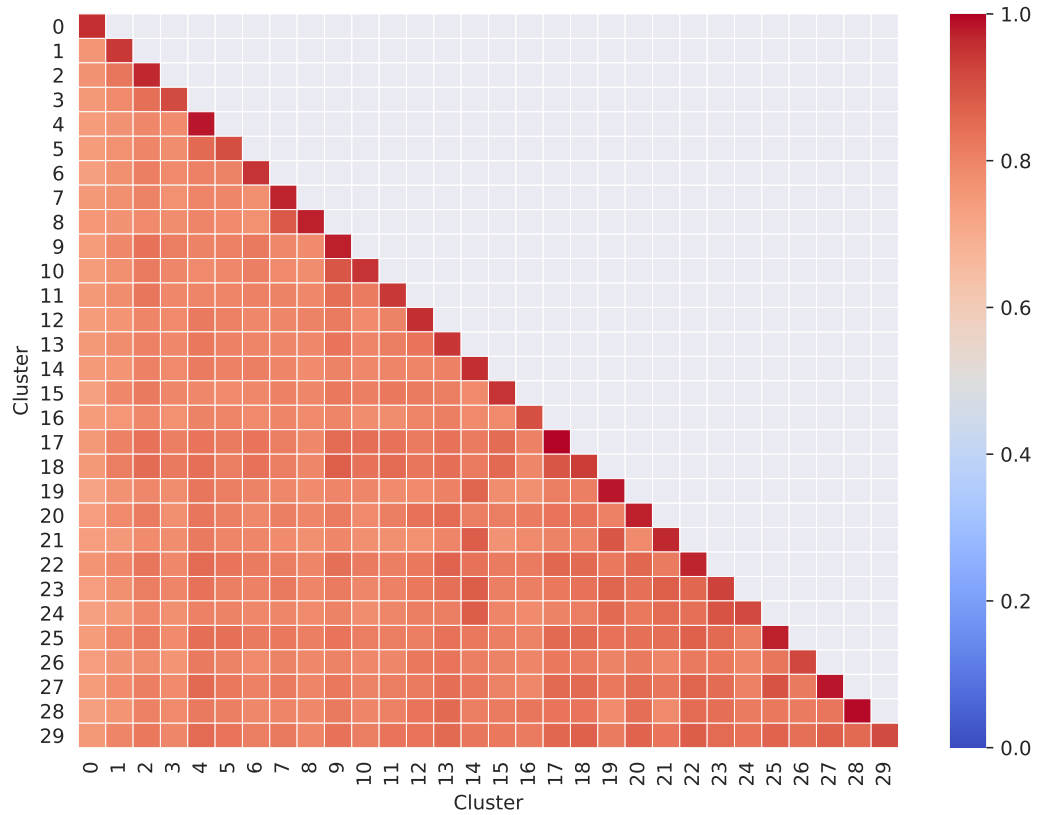


**Fig. A.0.27 Similarity matrix of segment 7 clusters.**

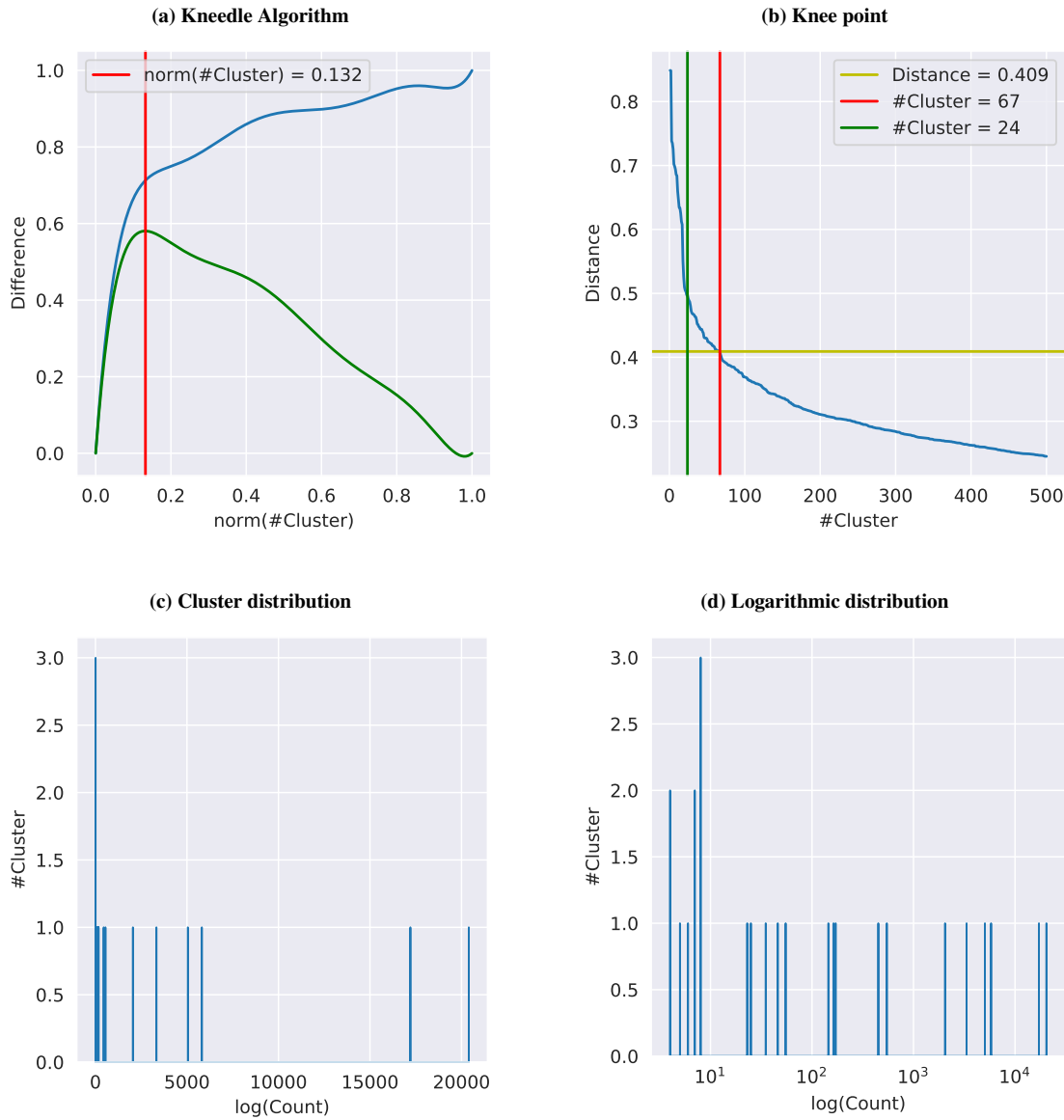


**Fig. A.0.28 Clustering of segment 8.**

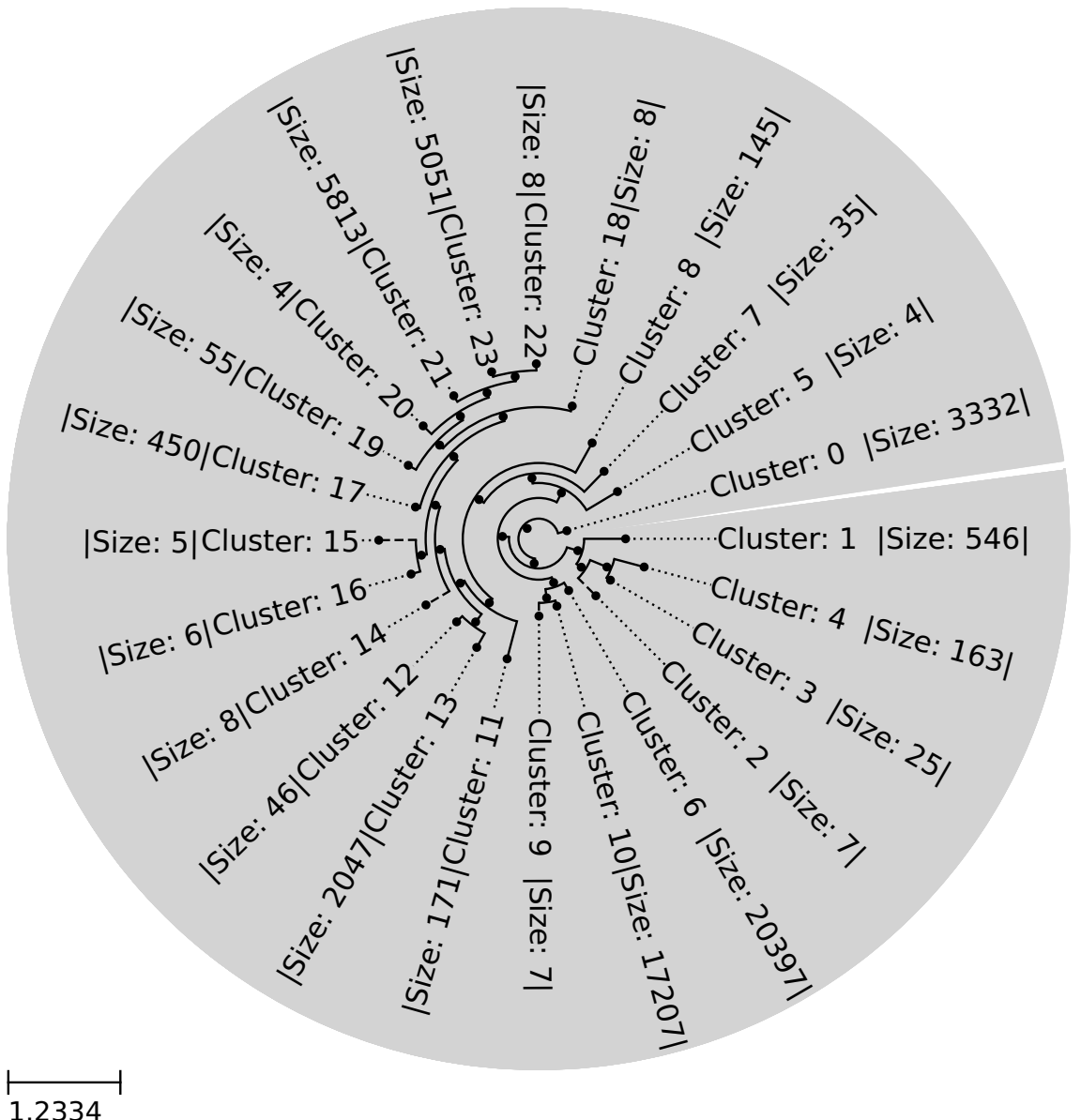
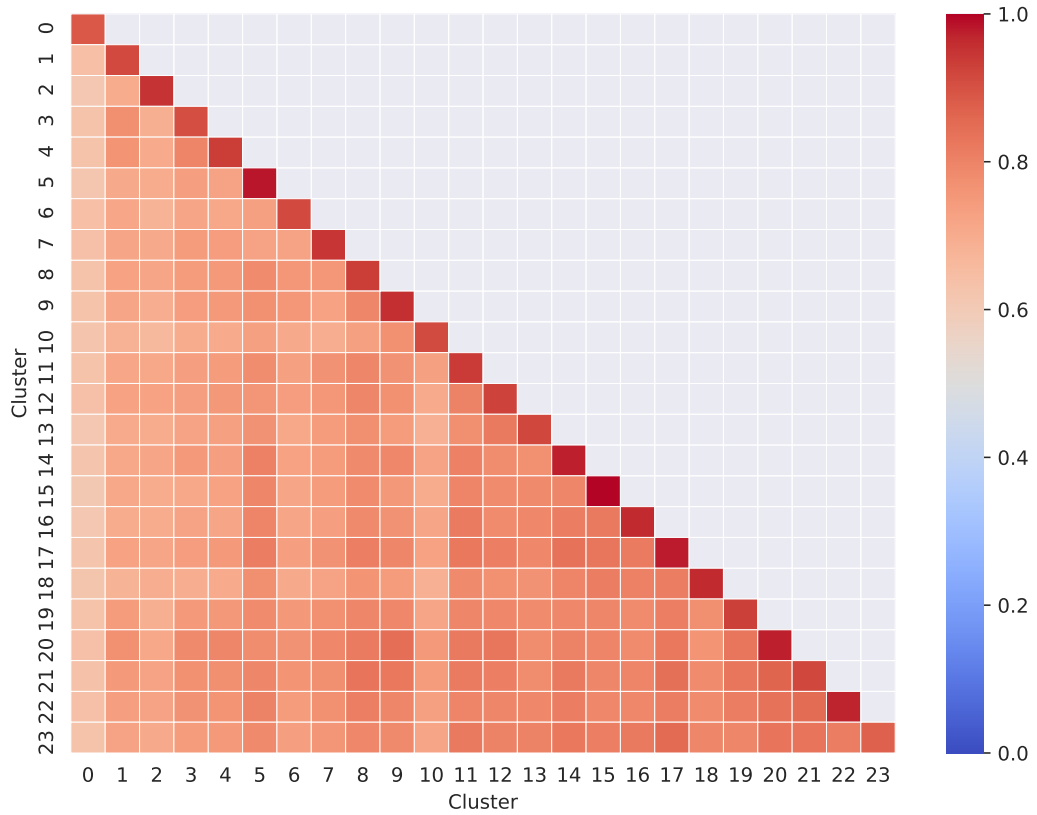


Fig. A.0.29 Clustering tree of segment 8.



**Fig. A.0.30** Similarity matrix of segment 8 clusters.

# **Declaration of Originality**

Ich erkläre, dass ich die vorliegende Arbeit selbstständig und nur unter Verwendung der angegebenen Quellen und Hilfsmittel angefertigt habe.

Seitens des Verfassers bestehen (keine) Einwände die vorliegende Masterarbeit für die öffentliche Benutzung im Universitätsarchiv zur Verfügung zu stellen.

Jena, den 14.07.2021

---

Alexander henoch